ASSESSMENT OF REACTOR VESSEL INTEGRITY (ARVI)

CO-ORDINATOR

Prof. B.R. Sehgal
KTH, Royal Institute of Technology
Division of Nuclear Power Safety
Drottning Kristinas V.33A
100 44 Stockholm, SWEDEN
Tel.: + 46 8 790 9252
Fax.: + 46 8 790 9197
E-mail: Sehgal@ne.kth.se

LIST OF PARTNERS

Royal Institute of Technology, Stockholm, Sweden
Fortum Engineering, Finland
CEA/DRN (Grenoble) , France
VTT Energy, Finland
Framatome, France
IKE (University Stuttgart), Germany
University of California Santa Barbara, USA
Nuclear Research Institute Rez (NRI), Czech Republic
Electric Power Research Institute Budapest (VEIKI), Hungary

CONTRACT N°: FIKS-CT1999-00011

EC Contribution:	ECU 700 000 €
Partners Contribution:	ECU
Starting Date:	December 1999
Duration:	36 months

CONTENTS

LIST OF ABBREVIATIONS AND SYMBOLS

HF	Heat Flux
WP	Work Package
SE	Seminars
ECTS	European Credit Transfer System
LPT	Linear Position Transducers
PT	Pressure transducers
PV	Pressure Vessel
RPV	Reactor Pressure Vessel
TC	Thermocouples
CHF	Critical Heat Flux
ECC	Emergency Core Cooling
ECCM	Effective Conductivity – Convectivity Method
IVMR	In Vessel Melt Retention
KTH	Kungliga Tekniska Högskolan (Royal Institute of Technology) Stockholm, Sweden
LOCA	Loss of Coolant Accident
SAM	Severe Accident Management

EXECUTIVE SUMMARY

The ARVI (Assessment of Reactor Vessel Integrity) project involved a total of 9 organizations from Europe and USA. The objective of the ARVI project was to resolve the safety issues that remained unresolved for the melt vessel interaction phase of the in-vessel progression of a severe accident. The top level objectives were to provide the data and the models to assess (a) the feasibility of promulgating the in-vessel melt retention (IVMR) scheme in current and future plants or in its absence;(b) the time available before vessel failure in which emergency accident management measures could terminate the accident within the vessel. The second level objectives were to determine (1) the mode and location of vessel failure, (2) the melt discharged to the containment (3) the effectiveness of the gap cooling, (4) the critical heat flux for external cooling of the lower head, (5) the effects of melt stratification and (6) to apply the data and models for design of IVMR for some specific plants. The work consisted of experiments and analysis development. The modeling activities in the area of structural analyses were focused on the support of EC-FOREVER experiments as well as on the exploitation of the data obtained from those experiments for modeling of creep deformation and the validation of the industry structural codes. Work was also performed for extension of melt natural convection analyses to consideration of stratification, and mixing (in the CFD codes). Other modeling activities were for (1) gap cooling CHF, (2) lower head dynamic loading due to steam explosion inside and (3) simple models for system code. Finally, the methodology and data could be applied to design of IVMR severe accident management scheme for VVER-440/213 plants. The work was broken up into five packages. They were divided into many tasks, which were performed by different partners. The work consisted of experiments and analysis development. The major experimental project was EC-FOREVER in which data was obtained on melt pool natural convection and lower head creep failure and rupture. The EC-FOREVER experiments were the first in the world in which vessels, containing heated melt, and the lower head wall maintained at prototypic accident conditions, were ruptured. Additional tests were made in which the melt pool was flooded with water to determine the potential for in-vessel coolability. The results obtained from the experiments were related to the following main issues, (1) the effectiveness of gap cooling, (2) multiaxial creep laws for different vessel steels, (3) effects of penetrations, (4) mode and location of lower head failure and (5) data for validation of computer codes. Two other experimental projects were also conducted. One was the COPO experiments, which was concerned with the effects of stratification and metal layer on the thermal loads on the lower head wall during melt pool convection. The second experimental project was conducted at ULPU facility, which provided data and correlations of CHF due to the external cooling of the lower head. The modelling activities in the area of structural analyses focused on supporting the EC-FOREVER experiments. These were exploited to validate the industrial structural codes. Work on the melt pool turbulent natural convection analyses through Computational Fluid Dynamics was performed, which essentially determined the stratification and mixing process. Other modelling activities were on the (1) gap cooling model for CHF, (2) simple models for system code. Finally, the methodology and data have been applied to design of IVMR severe accident management scheme for VVER-440/213 plants.

A. OBJECTIVES AND SCOPE

The top level objective of the ARVI project was to resolve all the remaining issues that were unresolved for the melt vessel interaction during the late phase of the in-vessel progression of a severe accident, resulting in accurate assessments about (a) the feasibility of promulgating the in- vessel melt retention (IVMR) scheme in a plant or in its absence;(b) the time available before vessel failure in which emergency accident management measures may terminate the accident within the vessel. The second level objectives were (1) to determine the mode and location of vessel failure, (2) to determine the effects of melt stratification, (3) to determine the effectiveness of the gap and external cooling, and (4) to apply the data and models for design of IVMR for some specific plants.

In WP1 a series of 6 experiments were achieved. The objectives of the EC-FOREVER tests were to obtain multi-axial creep deformation and vessel failure mode data for the prototypical vessel geometry (scaled 1:10), under prototypical thermal and pressure loading conditions and to investigate the gap cooling.

The purpose of the COPO-experiments within the ARVI was to contribute in understanding of the heat transfer phenomena of a stratified corium pool, towards thermal analyses for the in-vessel retention of molten corium (IVMR).

The objective of the specific BALI experiment was to study the focusing-effect phenomenon while employing a simulant fluid, and to validate the existing correlations.

The primary objective of the UCSB contribution to the ARVI project was to study the limit of coolability from a reactor vessel to coolant in the in-vessel retention (IVR) scheme, and to examine potentials to enhance critical heat fluxes (CHF), so to allow the use of IVR scheme for severe accident management in high-power reactors.

In the WP3.1 an axisymmetric Finite Element (FE) model was developed based on the multi-purpose code ANSYS/ Multiphysics. Using the Computational Fluid Dynamics (CFD) module FLOTRAN the melt pool convection was simulated. The transient structural mechanical calculations were then performed applying a creep model, which takes into account the large temperature, stress and strain variations.

The objective of the PASULA code analyses was to assist the FOREVER pressure vessel deformation and rupture experiments by pre-test and post-test calculations. The PASULA code was used to support design and analysis of experiments with penetrations.

In WP4.1 . The objective was to derive a CHF model to interpret and unify several experiments which have been performed recently to investigate corium coolability in gaps formed between oxidic corium and a metallic vessel.

The WP4.2 aimed to assess the TOLBIAC code with COPO experiments P20 and P21 and study the influence of heat transfer coefficients and interfacial shear stress between the two stratified liquids without crust at the interface.

The objective of WP4.3 was the development and application of simplified, fast running models for the corium behaviour in the core and the lower plenum which can be used in a core melt code like KESS or a system code like ATHLET-CD.

Finally, the objective of WP5 was to develop the in-vessel melt retention (IVMR) scheme for VVER-440 reactors for the case of a severe accident, more specifically for the VVER-440/213 plant type operating in Paks (Hungary) and Dukovany (Czech Republic). The objectives included also a short assessment of mechanical loading and preliminary analysis of technical feasibility of the IVMR strategy.

B. WORK PROGRAMME

B.1 Experimental Program on Vessel Creep, Vessel Failure and Gap Cooling (EC-FOREVER experiments)

This task was performed by Royal Institute of Technology, Stockholm, Sweden.

The EC-FOREVER (European Commission's failure of reactor vessel retention) facility employs a $1/10^{th}$ scale (400 mm diameter) carbon steel vessel, constructed, welded, and heat-treated according to the vessel manufacture code. The experiment is performed by pouring a binary oxide melt into the vessel at 1200°C, heating the melt with a heater to maintain it at 1100 to 1200°C, then, pressurizing the vessel wall to 25 bars pressure with Argon gas. The vessel wall temperature is maintained at 800 to 1000° to experience creep and eventually fail.

The following experiments were performed.

(1) Creep and rupture of a vessel $1/10^{th}$ scale with lower head made from French carbon steel, which has been fully characterized in the REVISA Project of the fourth framework program. The high-temperature oxide melt is prepared in a SiC-crucible placed in a 50kW induction furnace, which is, then, poured into the test section. The melt will be maintained at ~1200°C, and the vessel wall at ~1000°C by adding ~ 40KW power to the melt through a heater inserted in the melt. Specified over-pressurization is supplied with an inert gas supplied, after the vessel temperature has achieved steady-state conditions. The pressure inside vessel will be maintained at 20-25 bars. The melt will be ejected on vessel failure.

(2) Repeat of experiment No.1, with less amount of melt.

(3) Creep and failure of a vessel with the same French carbon steel lower head, which contains scaled penetrations representative of a French PWR, at the same test conditions.

(4) Creep and rupture of a vessel made with the American carbon steel employed by the LHF Project, conducted by the Sandia National Laboratory which is being characterised in the OECD LHF Project, under the auspices of the OECD, at the same environmental conditions as in Experiment No.1. The data obtained in experiments 4 will be compared with, those obtained in the U.S. LHF and the OECD LHF projects.

(5) Addition of melt into a $1/10^{th}$ scale vessel; maintaining heating and convection of the melt in the vessel, with pressure maintained at 25 bars. After ≈ 10% creep has been obtained, and potentially a gap has developed, add water at the top surface of the melt pool. Observe vessel wall temperature to ascertain if the water penetrates the gap and cools the vessel wall.

(6) Another gap cooling test as defined in the test No 5, with measurement of the heat flux at top surface through condensation of the steam produced.

The above EC-FOREVER experiments have provided first data in the World of convection of a high-temperature heated melt pool in spherical geometry. Such data can be employed for validation of the natural circulation heat transfer correlations for uniform pools used in the evaluation of the vessel thermal loads. These data will complement those measured earlier in the RASPLAV, BALI, COPO, ACOPO, UCLA and SIMECO facilities.

The data measured for the creep of the French and the American vessel carbon steel, which are well characterized, will be compared to those obtained in the RUPTHER, and in the LHF and OLHF programs. It will serve as validation benchmarks for the methods developed in U.S.A (based on the Abacus code) and those developed in Europe.

B. 2 Experimental Program on Stratified Melt Pool Convection and Vessel External Cooling

WP 2 consist of two Tasks as described below:

B. 2.1 COPO and metal layer experiments

This task was performed by Fortum Nuclear Services, Finland and CEA/DRN (Grenoble), France.

The COPO facility of Fortum Nuclear Services is a half-scale slice facility employing salted water as the fluid simulating the melt. The facility achieves Ra` values of 10^{15}-10^{16}. It had performed experiments with crusted boundary conditions and later performed tests on stratified pools.

The objective of the tests on the COPO facility are to confirm the results obtained on the SIMECO facility during the MVI Project and afterwards, for experiments on the effects of the stratification. If physically possible the effects of the metal layer, on the vessel thermal loadings will also be investigated.

Two experiments were carried out. Both experiments started with a stratified configuration without an intermediate plate, which has been used in the previous stratified-pool COPO experiments. In the both experiments, as in all previous COPO tests, the heavier oxidic layer of a corium pool is simulated with a water-zincsulfate solution. The upper, lighter oxidic layer is simulated with pure water. This arrangement allow a direct comparison to previous COPO experiments with an intermediate plate between the layers. However, depending on the findings of pretest assessments done before the experiments, it is decided to use - instead of pure water - some other liquid in the upper layer (e.g. some light aqueous solution of an organic substance) in order to prevent premature breakup of the stratification. The Rayleigh number had been varied between the two experiments. The experiments had obtained data on the heat transfer from a stratified pool as well as on possible breakup of the stratification.

To study the effect of a metallic layer on top of oxidic pool, some specific tests were performed at BALI facility independently from oxidic pool assuming the existence of a stable crust between oxidic and metallic phases. In the frame of this project, their results will be available for code validation.

B. 2.2 ULPU Experiments

This task was performed by the University of California Santa Barbara, US.

The ULPU facility is a full size facility in which critical heat fluxes are measured. The vessel wall is prototypic steel and the heat fluxes imposed are varied along the angle from 0 to 90^{o}. A convection loop of full height is established. Previously data was obtained for the AP-600 geometry and conditions. Additional data for CHF, on a full scale PWR vessel wall mock-up and a physics-based model for CHF on a large scale downward facing heated surface were obtained. Five tests were performed with different power shapes, to achieve critical heat fluxes. The power shapes model the heat flux distributions of (1) a homogenous pool, (2) a stratified pool, (3) pool with a

metal layer, (4) stratified pool with a metal layer, and (5) uncertainties in the distributions. In addition, effects of the penetrations are simulated as closely as possible. In this new ULPU test series, visualization is provided to observe the flow patterns under conditions approaching CHF and at CHF by high-speed movie. The phase distribution data of two-phase boundary layers in upper region are provided.

B.3 Analysis Development and Validation on Vessel Structural Loadings, Creep and Failure

WP.3 consists of four tasks as described below.

B. 3.1 Coupled Thermal Hydraulic and Creep Analysis

This task was performed by Royal Institute of Technology, Stockholm, Sweden.

with the MVITA code, which had coupled the thermal analysis of melt pool convection with a creep model. The creep model uses creep law from literature. The MVITA code was employed for pre- and post-test analyses of the EC-FOREVER experiments.

B. 3.2 PASULA Code Analyses and Validation

This task was performed by the VTT Energy, Finland.

PASULA code was enhanced during the MVI Project incorporating features which make it efficient for lower head structural and creep analysis. The code can calculate large creep deformation. Future development was needed for 3-D analyses in non-symmetrical cases. First multi-axial creep laws for the steel employed in the EC-FOREVER experiments were determined. Second, pre- and post-experiment analyses of some of the EC-FOREVER experiments had been performed. Failure criteria based on different stress and strain states were developed further and tested against experimental data.

B. 3.3 SYSTUS+ Code Validation

This task was performed by Framatome, France.

The SYSTUS+ code is a structural analysis code used by the nuclear industry. It is able to calculate large creep deformations. This code was validated against the EC-FOREVER data. The objective was to verify different creep models and to identify that (or those) which provide good agreement between the measurements and the predictions.

B. 3.4 Lower Head Dynamic Loading

This task was performed by University of California Santa Barbara, US.

If the lower head can not survive the in-vessel steam explosion loads, in-vessel melt retention becomes moot. Therefore, some corium relocation scenarios are assumed in consultation with work performed by other investigators in EU Projects on core melt progression. Steam explosion yields are calculated and the spatial-dynamic loading on the lower head are calculated. Structural calculations were performed to estimate the challenge to the integrity of lower head. Steam explosion loads on the locations of the penetrations were provided for analysis of the structural response of the penetrations.

B.4 Analysis Development and Validation on Gap Cooling

WP.4 consists of three tasks as described below.

B. 4.1 CHF Modeling in Gaps

This task was performed by CEA/DRN (Grenoble), France.

A model for critical heat flux (CHF) in narrow gaps, based on counter current flooding limited (CCFL) flow, is derived. The model was validated against data obtained in various geometries (flat plate, curved), at different pressures and with different fluids. The model is also tested against the data measured in the EC-FOREVER gap cooling test. The correlation derived was applied to prototypic accident condition and the limitations on achieving lower head wall coolability with gap cooling has identified.

B. 4.2 TOLBIAC Code Development and Validation

This task was performed by CEA/DRN (Grenoble), France.

The TOLBIAC code simulates the behavior of a corium pool within a structure. It has three field equation in 2-D cylindrical or rectangular geometry. The 3 fields are the metallic material, oxidic material and the gas. The modeling includes crust formation and wall ablation. The code can model the development of stratification and/or layer inversion due to density differences. This code was validated against data obtained in the COPO facility in this project. Heat transfer and inter-layer shear relationships were the focus.

B. 4.3 Application of MVI and ARVI data and models in system code

This task was performed by IKE (University Stuttgart), Germany.

The models and data developed in the ARVI and MVI Projects were assessed for incorporation in a system code KESS and KESS+ATHLET codes or a risk assessment code. Calculations were performed for typical scenarios.

B.5 Design of in-vessel melt retention scheme for VVER-440/213 plant.

This task was performed by NRI (Nuclear Research Inst.Rez), CZ and VEIKI, HU.

The purpose of this task is to provide a preliminary design of the IVMR SAM scheme for the VVER 440S located in Eastern Europe. The data and the validated methodology developed in the MVI Project and in this work were employed.

C. WORK PERFORMED AND RESULTS

C.1 Experimental program on vessel creep, gap cooling and vessel failure (EC-FOREVER experiments)

C.1.1 The FOREVER Experimental Program

The idea of FOREVER experimental program is to simulate the prototypic severe accident scenario of melt pool convection in the accident management scenario of vessel de-pressurization, *i.e.*, the vessel pressure is maintained at ~25 bar. The vessel is at $1/10^{th}$ scale *i.e.* its outer diameter of the vessel is ~400 mm and wall thickness is ~15 mm. Some experiments were designed to perform with eight Inconel-600 penetrations, which were welded in the lower head of the vessel spanning from $15\text{-}55^0$ from the bottom of the vessel. In those tests, penetrations had dimensions of ~3.8 mm diameter and a height of ~ 65 mm. In this programme, it was decided to use the American (previously tested by SNL in their LHF and OLHF programmes) and

the French (supplied by FRAMATOME) reactor steels for the lower head of FOREVER experiments. It was planned to use the German Steel in upper cylindrical part for the FOREVER experiments, which was welded to either American steel and French steel. Material used for lower head has much greater strength at high temperature than the material used for upper cylindrical part. Characteristics of these materials can be found in Ref. [1].
The scaling considerations for the FOREVER tests can be summarized as follows:

(i) 1:10 linear in geometry, *(ii)* 1:1 in heat flux, *(iii)* 1:10 in vessel wall temperature difference, *(iv)* 1:1 in hoop stress, and *(v)* 1:10 in thermal stress.
Thus, it can be identified that with the chosen vessel geometry and test conditions membrane stresses are modelled exactly while the thermal stresses are not.
More importantly, in the FOREVER tests the temperature peaks at 60-80^0, while stress distributions peak in the region of 45-60^0, which is similar to prototypic reactor accident scenario. This is the major difference between the FOREVER and the Sandia LHF experiments (Ref. [2]).
The OLHF tests (Ref. [3]) employ a larger temperature drop across the vessel wall than in the FOREVER test and achieve a closer simulation of the thermal stress, although their heat flux and temperature distributions are non-prototypic.
First four experiments were named as: EC-FOREVER-1, -2, -3, -3B respectively. The experiments observed the timing, the mode and the location of failure of lower head. EC-FOREVER-3 and EC-FOREVER-3B investigated the effects of penetration on these parameters. Those experiments employed a lower head made of 16MND5-French reactor steel.
In EC-FOREVER-1 & -3, the melt volumes were above the hemispherical part of the vessel, which resulted in an early vessel failure around the weld line *i.e.* between the hemispherical and the cylindrical parts of the RPV.
In all the experiments, pressure was ~25 bar, but heat input and melt volume differed from the experiment to experiment. The melt volumes in those seven experiments are different and were around 13 litres. Heat inputs, in these experiments was around 38 kW except for the gap cooling experiment in which it was decreased to 28 kW. Under these conditions, vessel with penetration failed after ~4.5 hours (equivalent time) pressurisation.
Maximum failure strain is obtained from the experiment (EC-FOREVER-3B) on a lower head vessel (made of French reactor steel) with penetrations. However lower head vessel (French reactor steel) without penetrations failed with a maximum failure strain of ~13.5 % after ~3 hours (equivalent time) of pressurisation, and failure occurred at angle ~70^0 from the bottom of the vessel.
Though the angle of failure was similar in the both cases, failure time was increased considerably in the EC-FOREVER-3B compared to the EC-FOREVER-2 experiments. Reason had been attributed to lower external wall temperature due to penetration in EC-FOREVER-3B test compared to the EC-FOREVER-2 test.
As mentioned earlier, FOREVER programme was designed to perform experiment with vessel steel made of the American steel. Experiment on the American steel was achieved in EC-FOREVER-4 experiment.

C.1.2 Experimental procedure

A melt of an oxidic mixture: 30% CaO + 70% B_2O_3 (by weight) undergoes convection in the lower head due to the heat input by a specially designed heater

(KANTHAL©SUPER, made of Molybdenum Silicate) distributed evenly inside the melt. In the experiment, heat input was maintained at a value such that, melt pool temperature attained a maximum value of ~1300^{o}C. The binary oxide melt has properties similar to those of UO_2 + ZrO_2. In the experiments, there is no external or internal cooling of the lower head. Properties of $CaO+B_2O_3$ are available in Ref. [4]. The lower head loses heat primarily by radiation and to some extent by convection. Melt pool and vessel wall temperature are measured by thermocouples (TCs) and the vessel wall displacements are measured by linear displacement transducers. Temperatures and displacements were measured on the opposite sides of the vessel to determine the uniformity of the spatial distributions. A pressure control valve was used to maintain the pressure in the vessel at a desired value during the experiment. Test vessel with its instrumentation and the induction furnace was kept inside the containment for the sake of human safety, (figure1). In all the tests, the vessel was pre-heated to about 400^{o}C to avoid thermal shock. This also prevented thermal shock to the heating element. The hot oxide melt, prepared in a SiC crucible in the induction furnace, and poured into the vessel through a funnel. After pouring the melt, the vessel opening was closed quickly and the vessel was made leak tight. Care must be taken to switch on the internal heater immediately after pouring the melt, otherwise hot melt may cool down, form a crust and damage the heater element. Heater power was increased to deliver the desired power level and to maintain the oxide melt. Time was allowed to establish a steady state convection of melt inside the vessel. After the steady state temperature conditions were reached, pressure was applied to the vessel employing a balloon of argon gas. Heater power input and vessel pressure were kept constant during the experiment and experiment was continued till the vessel failure or to the time of water injection in the gap cooling experiments. The containment temperature was kept below 50^{o}C by employing ventilation, in order to assure the proper operation of the instrumentation. It was necessary, because various instruments may not work properly at the higher temperature. Also special fans were employed to cool the displacement transducers as they received heat due to radiation from the vessel. It was important to maintain the temperature required for proper operation of the instrumentation.

C.1.3 Experimental results on Vessel Creep, Vessel Failure and Gap Cooling

C.1.3.1 EC-FOREVER-1 experiment

EC-FOREVER-1 experiment focused on the vessel (with out penetrations) failure, in the absence of any cooling of the vessel wall. In this test, the vessel wall was heated up to1300K, and pressurized to 28 bars. The melt was delivered in two portions due to the limited size of the crucible (15 litres). After the first pouring, which fills the hemispherical part of the vessel, heater power was raised up to 38 kW. The steady state data for melt pool convection and thermal expansion of the vessel was obtained in the meanwhile before the second pouring was done. A total melt volume of 20 litres occupying the hemispherical lower head as well as up to 5 cm of the cylindrical upper part, with a heat generation of 38 kW provided the thermal loading on the vessel wall. The steady-state condition was reached, and the multiaxial creep deformations of the vessel were measured till the failure was achieved. The amount of melt in this test was increased to avoid a possible heater failure as it occurred in the previous FOREVER-C2 test. This failure occurred because of the heater uncovery due to the volume expansion of the vessel and subsequent melt level

drop. The increase in melt volume above the location of the welding led to higher temperature field than in the previous experiment. Vessel failure was achieved at a lower creep strain of about 6 %. The failure site was located just above the welding joint and it was looking upwards. The EC-FOREVER-1 test was performed on March 17, 2000. The distinguishable feature of this test in comparison to the LHF tests (performed at SNL, USA) is the high temperature conditions in the vessel ~1000^{o}C as compared to ~ 800^{o}C in all the LHF tests and medium pressure, prototypic, loadings (28 bars) as compared to 50-100 bars in all the LHF tests.

C.1.3.2 EC-FOREVER-2 experiment

EC-FOREVER-2 experiment focussed on the vessel failure, in the absence of any cooling of the vessel wall and was performed on November 2, 2000. In this test the melt level was kept below the welding joint. Hence, the heater was redesigned so that it is not uncovered during the process of vessel expansion. The pressure was also reduced to 25 bars so as to avoid any prompt plastic deformation at high temperature. The power level was kept the same, equal to 38 kW. The vessel failure was achieved at a failure strain of about 13 %. The average creep strain rate observed was about 3.5 % h^{-1}, and maximum creep strain rate, before failure was about 8% h^{-1}, and the failure site was located at angle of 73^{o} from bottom or at about 5 cm from the welding and it was looking upwards like a fish mouth, (Figure 2). The circumferential length of the site was about 1/5th of the total circumference. Only about 1/3rd of the total melt volume got discharged and the rest of the melt was contained in the vessel when it got depressurised. The comparison of various results with the pre-test calculations of ANSYS was quite good (Ref. [5]), in terms of the wall temperature profiles, wall thickness profiles, failure angle and failure strain. The failure time obtained was shorter in the experiment than in the calculations, by about 1/2 hour.

C.1.3.3 EC-FOREVER-3 and –3(B) tests

EC-FOREVER-3 and –3(B) were conducted respectively on 22nd May and 26th July 2001. EC-FOREVER-3(B) experiment was a repeat of the EC-FOREVER-3 test. It simulates the late stages of in-vessel melt progression of nuclear reactor severe accident scenario. Vessel lower part was made of 16MND5-French reactor steel while upper cylindrical part was made of 15Mo-German Steel. The EC-FOREVER-3 and –3B experiments include eight Iconel-600 penetrations in the lower head of the vessel. The previous FOREVER experiments do not employ penetrations. So, the main objectives of both experiments were to investigate the creep failure of a 1:10th scale reactor pressure vessel with penetration under the combined thermal and pressure loading, in absence of any external cooling. Detailed descriptions of the penetrations, vessel dimension, test facilities and its experimental procedure can be seen in Ref. [6]. The conditions for the EC-FOREVER-3 test can be summarised as: (1) Melt Volume ~14 litres, (2) Power generation in the melt ~38 kW, (3) maximum recorded temperature in the melt pool ~1400^{o}C, (4) maximum external wall temperature ~910^{o}C, (5) internal pressure load ~2.5 MPa while the test conditions for EC-FOREVER-3(B) test can be summarised as: (1) Melt Volume ~12.3 litres, (2) Power generation in the melt ~38 kW, (3) maximum recorded temperature in the melt pool ~1300^{o}C, (4) maximum external wall temperature ~900^{o}C, (5) internal pressure load ~2.5 MPa. Experimental conditions are more or less same in both the experiments. These two experiments mainly differ in the melt volume. In EC-FOREVER-3 melt volume was unexpectedly higher than the volume of the lower head of scaled reactor

vessel. As a result of which the vessel failed in an unexpected location i.e. at the welding. We rectified the melt volume in EC-FOREVER-3(B) by measuring the vessel lower head using water. Deviation from theoretical volume of ~14 litres was probably due to the manufacturing tolerance during head forging process of the vessel lower head. The maximum displacement in EC-FOREVER-3(B) is ~32 mm and this occurs around ~46^{o} from the bottom of the vessel. It should be mentioned here that this is slightly greater than that in the previous EC-FOREVER-2 test and significantly greater than that in the EC-FOREVER-3 experiment. General creep behaviour is similar as in the EC-FOREVER-2 test. The displacements are more or less axi-symmetric except near failure region. Failure occurred at an angle of ~70^{o} from the bottom of the vessel. Significant amount of melt was discharged from the vessel lower head. Vessel wall thickness in most of the region does not change appreciably except near failure site where thickness is reduced by 33% of its initial value. Overall maximum temperature is lower by ~40^{o}C compared to EC-FOREVER-2 but it is quite similar to EC-FOREVER-3 experiments. Thus it may be concluded from these experiments that it probably due to effects of penetrations as reported in Ref. [6]. Also it should be mentioned here that temperature has a direct role in the lower head failure time. Since external wall temperature was lower by ~40^{o}C, failure time was increased by ~1.5 hours. If penetrations decrease the wall temperature and increase the failure time, then it is a significant difference. Vessel during failure is shown in Figure 3. Failure is like a fish mouth and it covers 17% of the circumference.

C.1.3.4 EC-FOREVER-4 Experiment

The EC-FOREVER-4 experiment was performed successfully on 14th Feb. 2002. The facility employed a 1/10th scaled lower head (hemispherical in shape and made of SA533B, American reactor steel) of 400 mm outer diameter and 15 mm wall thickness. Figure 4 shows the displacement of vessel on the various angular locations on the right side along with the histories of pressurisation and heat input. The same on the left side are shown in Figure 5. It can be seen that the maximum displacement at failure was ~27 mm and it was measured between the angles 45-60^{o}. The occurrence of the location of maximum displacement is consistent with previous observation reported in EC-FOREVER-1, -2, -3 and -3(B). This corresponds to ~13.5% strain at failure. This is more or less similar to the French Reactor steel used in the previous EC-FOREVER experiments. Shape of the failure was like a fish mouth (figure 6). Comparing with previous EC-FOREVER experiments, the failure was quite large and failure shape and area resemble more like that in the SNL test with American reactor steel. It is interesting to note that vessel wall creep near the failure site and its thickness is much lower than that the other EC-FOREVER experiments which were performed with the lower head made of 16MND5 French reactor steel.

C.1.3.5 EC-FOREVER-5 Experiment

The EC-FOREVER-5 experiment was performed on 18th June. 2002. About 12 litres of binary oxide melt was used. After the melt pouring process, heater power was switched on. Initially heater power was raised to 26 kW and after the melt pool established steady state, a pressure load of 2.5 MPa was applied in the vessel. Since the heater power was too low, creep was very slow. So, it was decided to raise the heater power to 30 kW. One clear difference in this experiment is that heat input was lower than in previous experiments. The reason behind this was that we wanted a crust to form in the lower head along the wall so that there could be a gap formation

(between vessel wall and crust) during the creeping process of the vessel. After ~12 hours of creep, we observed 5% creep in the vessel and then water was poured into the vessel to study the GAP cooling. Heater was on while we poured the water. After ~30 minutes of water pouring, heater became inoperative and heat input to the melt was stopped. The histories of external wall temperatures are shown in Figure 7 and 8. From these figures it can be seen that during the steady sate of experiment (before water pouring) maximum external wall was ~875^{o}C, which occurred at an angle around 70^{o} from the bottom of the vessel. The occurrence of maximum temperature is consistent with the previous EC-FOREVER experiments performed. After pouring the water, wall temperature went down in ~3 hours. It is interesting to see, that wall temperature at angle 90^{o} drop almost immediately. But as we go below 90^{o}, we found cooling rate was slow. This signifies that there was no gap created between the wall and the crust, which did not allow the fast cooling to occur in the other part of the vessel.

During the EC-FOREVER-5 experiment extensive data on combined natural convection thermal loads, cooling of vessel and multiaxial creep deformation of a 1:10 scale vessel under prototypic conditions were obtained. Maximum external wall temperature, under which experiment was performed, was ~875^{o}C at 73^{o} from the bottom of the vessel. This is lower than the previous EC-FOREVER experiments performed earlier. This was done intentionally to form a crust near wall of the vessel, so that during the creep process of the vessel, there will be a GAP created between the vessel wall and the crust. However no Gap was found in the experiment. Except in the top part, cooling rate in the other part was very slow. From results, it was concluded that possibility of GAP cooling mechanism seems to be remote, however cooling does occur due to some ingression of water in the melt pool.

C.1.3.6 EC-FOREVER-6 experiment

EC-FOREVER-6 experiment, in addition to the gap cooling, aimed to determine the heat flux through the surface of the corium when cooled by an overlying water pool. In FOREVER-6 the corium was simulated by oxidic mixture, which was heated by embedded heater inside to a temperature over 1000^{o}C. After steady melt pool convection was established, water was injected into the melt vessel to form a pool over the melt. Heat transfer from the corium to the water pool generates steam, which is condensed and collected to determine the heat transfer rate. This provides information regarding the ability to cool the molten core and the likelihood of retaining it within the reactor pressure vessel. In this experiment, internal cooling was achieved by injecting water on the melt upper surface. Two big water tanks in series were used to condense the generated steam. There was no external cooling except for heat loss from outer surface of vessel by radiation and natural convection to air. One flow meter was used to measure the flow of steam at exit. Two pressure transducers were used to measure the pressure in the vessel and near flowmeter, during the experiment. Two thermocouples were installed in the first condensing tank and one thermocouple was installed in the second condensing tank. The dimensions of steam flow path, condensing tank capacity and water injection rate were selected based on pre test analysis done using RELAP code. Pressure and temperature values had been maintained for such duration of time that a minimum of 5mm creep was observed before injecting water. Pressure relief test was done one day before the experiment, to see the relief time and modify loss coefficients in RELAP code, so that it can be used for the post test analysis with confidence. This test data

was used to set up the loss coefficients in the loop. Heater power input and vessel pressure were kept constant till the time when sufficient creep in vessel was observed and then water was injected into vessel. Both gas pressurisation, heater power were stopped and the three valves leading out from vessel were opened. Table I gives the event sequence of transient after water pouring.

C.1.3.6.1 Experimental results and calculations

The experimental data of condensing tank temperature, steam flow rate at exit, pressure near the flow meter and the pressure near pressure vessel are presented in Figure 9. For better understanding of the problem, the data selected is only for the initial 300 seconds, i.e. for the first two water injections, as it will be just an exponential cooling followed by this. The raw experimental data contained lot of noise, which was to be eliminated. The noise elimination is done by use of noise filter option from MATLAB software. Figure 9 shows both filtered data and non-filtered data of four important parameters, which were required for heat flux (heat which is being removed as the melt cools) calculations. From Figure 9(b) it was found that it took around 11 seconds from the time of valve opening to the time of water getting in contact with melt (which can be observed as the pressure peaks up). By the time water was in contact with the melt surface, the pressure in the vessel was about 7 bar, as the depressurization has been there for more than 11 seconds. As water came in contact with the melt surface, it was turbulent boiling with heated corium particle ejection. The initial steam generation rate peaked up, and then came down drastically as the quantity of water added increased, thus cooling the upper surface of melt and forming a layer of crust. Hence now the heat liberated will be used in raising temperature of water (sensible heat). Posttest examination has showed that, the melt crust has grown from the crucible walls to the center and forms a solid crust at the center, submerged in water. The upper surface was always maintained wet by supplying sufficient water so that there won't be complete evaporation from the melt surface.

C.1.3.6.2 Modelling and Nodalisation

FOREVER experimental set up is modeled as shown in Figure 10. Before proceeding with nodalisation, it is to be noted that the vessel part of the problem is divided into two parts. One, that contains melt volume and water on top (Part B of figure 10) and second one that contains rest of the set up (Part A of Figure 10). Calculations regarding the part B are done separately and the effect of this on the part A is considered in terms of the forced steam generation rate at a given state into part A. This can be done in RELAP by using time dependent volume and time dependent junction option (Volume- 505 and Junction- 150). The part A of the set up is modeled in RELAP as shown in Figure 10. The vessel is modeled as single volume (Volume-506) and the three pipes are connected using vertical junctions to the vessel. The pipes have three on-off valves in-between to initiate the pressure relief (discharge) scenario. These three pipes are connected to one large diameter pipe with cross-junctions. This large diameter pipe in turn is connected in series connection of pipes of larger diameter and smaller diameter in order to have sufficient pressure drop near flow meter. The length of each pipe and expansion ratio required for proper pressure drop is estimated from pre-test analysis done using RELAP. The condensing tank at the exit is modeled as outlet boundary using time dependant volume (Volume- 104). The table II gives geometrical details of model. Compared to the experimental set up, the measuring points in our model will be Pressure in 4^{th} volume of pipe 507

(Representing pressure of vessel), Pressure in 1st volume of pipe 103 (Representing pressure near flow meter), flow in 1st junction of pipe 103 (representing flow meter reading) and heat flow rate at junction 157 (representing the heat gone to condensing tank). The experimental value of this heat flow is calculated from the rate of temperature rise (Figure 9-a) of total condensing tank mass of 146 kg. We had the above four data from the experiment. The data, which was required to be calculated, was the steam generation rate at inlet, which will give same output at above mentioned measuring points. We had done many trials by changing flow rate and state of steam generated till we got a result, which nearly matched the experimental data. Figure 11 represents both experimental data and the code output. The data in Figure 11-c is not matching because we had some problem with the pressure transducer near the flow meter, and hence we could not compare it with this result as the experimental data itself was not reliable.

C.1.3.6.3 Heat flux calculations

The cooling rate of corium is difficult to predict analytically because of large uncertainties in the morphology. What we have adopted is a simplified approach, where the energy required to raise the system pressure is combined to the energy going out of the system to find the net energy supplied to system (i.e. the net cooling rate). By using this approach, the result of steam generation rate inside the vessel, which was obtained from RELAP code, is shown in Figure 12-a. We can see the sudden spike in steam generation rate at the time when water came in contact with the melt surface. This maximum steam generation rate is around 0.11 kg/s, which decreases drastically to very low value, as more and more subcooled water is getting added. After some time this rate again peaks up as water injection is stopped and the water in vessel gets heated up and the heat from melt is used to generate the steam (latent heat). The second drop observed is due to the second addition of water and the process after this follows the same as mentioned above. Figure 12-b represents the latent heat removal rate in vessel, which corresponds to the steam generation rate at a given state. The maximum latent heat removal rate is around 1.8 MW/m^2. Figure 12-c and -d represent the cumulative mass and latent heat generated. If one forms a triangle ABC from two peaks A and B (Figure 12-a), then on integrating over this area yields 3.6 MJ. This can be justified with the sensible heat required to raise temperature of water of 5 kg mass from 20°C to saturation at 7 bar, i.e. 3.15 MJ. Hence total energy liberated in initial 100 seconds is around 11.15 MJ (with latent heat of 8.0 MJ). To cross check the above heat balance and to find initial maximum heat flux, consider second part of the problem i.e. part B as shown in Figure 10 (The melt part of the core). More detailed view of this part as required for the calculation is shown in Figure 13. All the temperatures, T represent thermocouples located at different locations in the vessel. T-29 to T-33 are the melt centerline (center of vessel) temperatures at different heights as shown in Figure 13. These heights represent the initial state, as vessel expands, the height with respect to thermocouple locations change. At any given time, the height of melt volume h is calculated from;

$$Melt\ Volume = \frac{\pi h}{6}\left(6 h r_0 - 2 h^2\right)$$

$$Where,\ r_0 = Radius\ of\ Vessel$$

With this equation, the initial height of the melt volume was 166 mm (corresponding to melt volume 11.0 litres). Due to lateral expansion of 2 mm and vertical expansion of 14 mm, the melt level was dropped to 151 mm. Now if we consider 1 cm thick layer of melt from this dropped layer (which was the situation just before pouring of water), then T-30 will represent the average temperature of this layer. If we consider two more 1cm layers below this layer, then T-31 and T-32 will represent the average temperature of these layers respectively. Now at different heights h , the radius of the melt layer is calculated from, $r_h = 2hr_0 - h^2$. Taking each layer as 1 cm thick circular disc of radius r_h , the mass of each layer is found, and is represented in figure 13.

Period of our interest for initial calculation is 100 seconds *i.e.*, after the second injection of water takes place. Consider the temperature variation of centerline thermocouples for initial few seconds (Figure 14). The initial dropping rate of T-30 is 20 K/s, T-31 is 5 K/s and T-32 is 1.5K/s. Considering the 100 seconds data, the total energy liberated is calculated as;

$$Energy\ of\ Layer\ n\ after\ time\ t = Q_n = m_n\left(Cp_l(T_i - T_{ls}) + h_{fusion} + Cp_s(T_{ls} - T_t)\right)$$

$$Where,\ m_n\ is\ Mass\ of\ layer\ n\ (see\ figure\ 5)$$

$$Cp_l = 2.2\,kJ/kg.K\ and\ Cp_s = 1.53\,kJ/kg.K\ are\ liquid\ and\ solid\ specific\ heats.$$

$$T_i\ and\ T_t\ are\ initial\ temperature\ and\ temperature\ at\ time\ t$$

$$h_{fusion}\ is\ latent\ heat\ of\ fusion = 460\frac{kJ}{kg}$$

$$Q = Q_1 + Q_2 + Q_3 = 8151.1\,kJ\ (for\ initial\ 100\,s)$$

$$Q_{total} = Q + Q_{conduction} = 8151.1\,kJ + 14.0\,kW \times 100\,s = 9551.0\,kJ$$

This total energy is corresponding to the latent heat liberated as calculated earlier. The formation of cracks and porous structures (as it is seen after post test visualization of vessel) as the corium solidifies can enhance cooling beyond what one would predict for an impermeable solid. If we consider the solid upper surface area of melt then with the initial 100 s data, the average heat flux obtained is 0.867 MW/m^2 (from part A we obtain average heat flux of 1.0 MW/m^2). If we extrapolate the plot shown in figure 12-b then, the critical heat flux at the point of water and melt contact is coming around 2 MW/m^2. It is to be noted that this value corresponds to the value quoted in Critical heat flux table for pressure of 7 bar and near saturation condition (Ref. [7]). For initial 100 seconds data, the average mass flux is around 0.38 kg/m^2.s, which matches to the data reported by (Ref. [8]).

C.2 Experimental Program on Stratified Melt Pool Convection and Vessel External Cooling

C.2.1 COPO and melt layer experiments

C.2.1.1 Background

The purpose of the COPO-experiments within the ARVI was to contribute in understanding of the heat transfer phenomena of a stratified corium pool. In thermal analyses for in-vessel retention of molten corium (IVR) it has been typically assumed that, in the final state, the molten pool in the lower plenum of the reactor pressure

vessel (RPV) is stratified into two layers. A heavier, molten oxidic layer is assumed at the bottom and a lighter, molten metallic layer on the top. On the other hand, experiments carried out within the OECD RASPLAV project with corium initially containing Zr, ZrO_2 and UO_2 revealed a tendency of the corium to stratify into uranium and zirconium rich layers. The phenomenon was observed in the tests including some unoxidised zirconium (so-called C-22 corium) and some amount of carbon. There was no steel present in these experiments. It is not entirely clear, yet, how the stratification found in RASPLAV would change the picture of a real corium pool in the lower head of a RPV. Nevertheless, it is of crucial importance to understand the impact of stratification on the heat flow distribution from the corium pool. For a metallic layer on top of an oxidic pool, the main concern is the so-called focussing effect, which may cause excessive thermal loads on the reactor pressure vessel wall at the metallic layer. On the other hand, a question that is not fully answered yet is whether the stratification mechanism found in RASPLAV could reduce the heat transfer upwards from the UO_2 rich layer in which most of the decay power is anticipated to be produced. This would then reduce the focusing effect due to the molten metallic layer, but at the same time increase the thermal loads at the vessel wall adjacent to the oxide. The impact of stratification on the molten pool heat transfer has been previously studied in the SIMECO experiments at Royal Institute of Technology (RIT) in Stockholm. Stratified SIMECO experiments have been carried out using stable and unstable stratified miscible pairs of liquids (water - salt water), with immiscible liquid pairs (water - paraffin oil) and with binary liquids showing a miscibility gap. The modified Rayleigh number was in the range of 10^{13} - 10^{14} , i.e. somewhat lower than in reactor applications. It was found out that the presence of the interface between the layers significantly reduces the upward / downward power split assuming that the decay power is generated in the lower layer. Stratified pool experiments have been carried out previously with Fortum's COPO II facility, too. In those experiments the lower, heat generating layer was simulated with a water - zinc sulfate solution and the upper layer with distilled water. The layers were separated with a thin intermediate plate made of aluminium. The main objective of those tests was to study the focusing effect caused by a possible metallic layer on top of a molten oxidic pool. The present experiments carried out within the ARVI project were continuation of the earlier COPO II stratified pool experiments. In the new experiments, the upper layer was simulated with paraffin oil instead of distilled water as previously. As the water layer and the paraffin oil layer are immiscible, no intermediate plate between the two layers was needed. The objective of the new tests was to complement the experimental data base from the earlier COPO tests and from the smaller scale SIMECO tests in helping to understand the effect of stratification on the heat flux distribution from the pool, without a solid boundary between the layers, in particular.

C.2.1.2 COPO facility

The COPO II facility (Figure 15) is designed for studying the heat transfer behaviour of a molten corium pool using simulant fluids. It is a two-dimensional slice of the lower head of reactor pressure vessel in a linear scale 1:2. The heat generating corium is simulated with a water - zinc sulphate solution with direct joule heating. In the tests within the ARVI-project, a non-heat generating upper layer of paraffin oil was located on top of the lower layer. A distinctive feature in COPO II is the cooling arrangement, which is based on circulation of liquid nitrogen on the outside of the

pool boundaries. The facility consists of a semicircular, 94 mm wide test section bounded at its periphery and at the top by 100 mm thick aluminium cooling units and at the lateral sides by insulated plywood walls. The semicircular test section contains the volumetrically heated fluid and the possible upper layer. The liquid nitrogen is circulated at the backside of the aluminium cooling units. Because of the low temperature (-196°C) of the liquid nitrogen, the inner surfaces of the cooling units will be frozen, thus ensuring isothermal boundary conditions for the pool. The heat fluxes from the test section into the liquid nitrogen are obtained by measuring the temperature gradients in the cooling units. The decision to use water-zinc sulphate solution and paraffin oil as the pair of immiscible liquids in the COPO tests was made based on preliminary studies. A pretest facility in a smaller scale than COPO was set up to confirm the technical feasibility of the water-zinc sulphate / paraffin oil approach before attempting the large scale COPO II experiment. The pretests with the facility demonstrated the feasibility of the pair. Based on visual observations, sharp boundaries were formed between the liquids as well as between the paraffin oil and the frozen crust. An advantage of water – paraffin oil pair was that the same pair was used previously at the smaller scale SIMECO experiments at RIT, Stockholm. A disadvatage of paraffin oil as well of any other type of oil is that the definition of the fluid properties, which are needed for calculating the dimensionless Ra', Pr and Nu numbers, may not be straightforward. It was decided to specifically measure the properties, in particular the viscosity, as a function of temperature for the oil used in the actual experiments.

C.2.1.3 Experiments

Two stratified pool experiments with the COPO II facility were carried out within the ARVI project. The location of the boundary between the layers was varied between the two experiments. The total height of the pool was kept the same in both cases. In the test P20, the effective height of the heated layer was 553 mm and the height of the paraffin oil layer 381 mm. The thickness of ice at the bottom of the pool is excluded from the height. In the other experiment, P21, the heights of the two layers were 700 mm and 238 mm. For P21, the test included a part with adiabatic (P21.1) and with cooled upper surface (P21.2). For P20 all the boundaries were cooled. During the experiment, in order to achieve the desired steady state, the power input was controlled to adjust and keep the average temperature of the upper part of the heated layer was at a predefined value For example in test P20, the maximum temperature of the volumetrically heated layer was about 74°C and the maximum temperature of the paraffin oil layer was about 35°C. The main results are summarised in Table III. For comparison, the data from previous esperiments P9 and P10 are shown, too. The test P10 was geometrically similar to the test P20, but instead of paraffin oil, distilled water was used in the upper layer and the layers were separated with a thin, electrically insulated aluminium sheet. Correspondingly, the test P9 was similar to the test P21. The heat flux profiles of the tests are shown in Figures 16 through 20. It can be seen that the paraffin oil significantly reduces the heat flux to the upper surface and to the upper part of the curved boundary. Comparing to the previous stratified COPO experiments in which distilled water was used in the upper layer and in which the two layers were separated by a solid sheet of metal, the presentation of the results in dimensionless form is more difficult in the present case. The main reasons are the facts that the exact boundary temperature between the two layers cannot be accurately measured and that the freezing point of

the paraffin oil (i.e. the boundary temperature for the convective heat transfer) is not well defined. In the full report of the COPO tests an interpretation of the results in terms of Nusselt numbers is presented. The water – paraffin oil boundary temperature was estimated by calculating it backwards from the lower layer heat transfer data of the lower layer and using correlation that had been found to comply well with the data from the earlier COPO experiments. The assumed freezing point was varied from the measured pour point of -9°C down to -40°C. It was found that for the upper surface the Nusselt numbers calculated this way were is reasonable agreement with the well-known Globe and Dropkin correlation. In particular, when a low value (-40°C) was assumed for the effective freezing point, the agreement was good. On the other hand, for the heat transfer to side boundary of the paraffin oil, the Nusselt numbers calculated in a similar way were found to be significantly higher than in previous stratified COPO experiments with distilled water.

C.2.1 BALI-metal layer experimental program

The BALI experiment aimed to study the focusing-effect phenomenon while employing a simulant fluid, and to validate the existing correlations. A facility of 2D rectangular test section with varying heights at full scale was designed and water was employed as simulant fluid. The pool was heated from below to simulate heat flux coming from oxidic pool, cooled on lateral wall with uniform temperature condition (ice crust formation) and on upper boundary with a plastic heat exchanger to simulate radiative heat transfer. An analytical model, based on the description of large convection cells in the rectangular cavity was developed and validated against the data from BALI rectangular test section experiments (Ref. [9]).

For sidewall heat transfer, a good agreement is observed (figure 21) with Chawla & Chan (1982), (Ref. [10] correlations, for laminar or turbulent flow regime depending on Rayleigh number value. Transition is observed for Grashof number about 10^{+9}

- Laminar flow regime (average value)

$$\overline{Nu_H} = 0.677\,\mathrm{Pr}^{1/4}\left(\frac{20}{21}+\mathrm{Pr}\right)^{-1/4} Ra_H{}^{1/4}$$

- Turbulent flow regime (average value)

$$\overline{Nu_H} = \frac{0.16}{\left[1+\left(0.492/\mathrm{Pr}\right)^{9/16}\right]^{16/27}} Ra_H{}^{1/3}$$

For bottom or top surfaces, the heat transfer mechanism is similar to Rayleigh-Bénard convection and we observed (figure 22) that experimental results are well correlated by the Globe-Dropkin (1959) correlation (Ref. [11]). The original correlation established for a cell heated from below and cooled only by the top has been modified to consider heat transfer from bottom plate to the bulk, and from bulk to upper plate. From Globe-Dropkin correlation valid up to $Ra \sim 10^{+9}$, $Nu_{RB} = 0.069 Ra^{0.333} Pr^{0.074}$, we obtain the following expression (Ra based on H/2 and ΔT between bulk and top or bottom surface):

$$Nu_{up\ or\ dn} = 0.174 Ra^{0.333} Pr^{0.074}$$

From the sidewall, upward and downward correlations we calculate from a zero dimension approach a concentration factor defined as the ratio between lateral heat

flux and injected bottom heat flux. The comparison with experimental results (figure. 23) shows that the concentration factor is well predicted by classical correlations for heights greater than 20 cm. For lower heights, this approach slightly overestimates the experimental results. This trend is consistent with the increase of horizontal radial thermal gradient in the pool and with the convective flow structure. For the chosen reactor bounding case (radiative upward heat transfer with surrounding temperature equal to 1700K, and metallic layer emissivity about 0.43) , concentration factors are still greater than 3 in 2D geometry for metallic layer height lower than 40 cm. For uniform cooling from above, focusing disappears. For reactor application, the concentration factors have to be transposed to 3D geometry on the basis of a zero dimension approach, or on the basis of a more detailed physical model described in the thesis of C. Villermaux (1999), (Ref. [12]). From a zero dimension approach, calculated heat flux concentration factor for reactor geometry and for the selected reactor bounding case is about 2 for a 40 cm thick metallic layer (factor 1.5 between 2D and 3D geometry). Such a concentration factor leads to an elevated lateral heat flux about 1.6 MW/m², which is considered for in vessel retention as a maximum value regarding critical heat flux limits and residual vessel wall thickness. The deliverable D2.1.2 (Ref. [9]) corresponding to the Work Package 2.1 was issued in July 2001.

C.2.2 ULPU Experiments

In this work, the research approach is based on CHF experiments performed on a full-length large-scale ULPU facility and aided by a basic understanding derived from fundamentals-oriented experiments on small-scale BETA facility, both at UCSB-Center for Risk Studies and safety (CRSS). The ULPU-2000 facility is illustrated in Figure 24, and an overall view of it is shown in Figure 25. It is a full-length representation of a reactor lower head as well as of the whole flow path between the reactor vessel and reflecting thermal insulation, all the way to the top venting openings. The width of the slice defined by the "Heater Blocks" is 15cm, and the blocks are thick enough (7 cm) to simulate the large thermal inertia of the lower head. These copper blocks are heated by imbedded cartridge heaters that are individually controlled to create any heat flux shape at will, with a maximum local flux capability of ~2 MW/m^2 and a maximum total power of 500 kW. We use a similarity rule that matches the local quality (that is, the integral of upstream power) to map any reactor power shape to an ULPU power shape for testing the critical heat flux—this mapping changes with the position being tested. This approach allows us to achieve an effective full-scale simulation of the reactor axisymmetric geometry, by the ULPU slice geometry. The "riser" simulates the full length of the reactor vessel to the top flange (~6 m), and is made with 15.2 cm in diameter pyrex glass that allows visualization. The glass is industrial strength, rated at 60 psig, so that operating at some moderately increased pressure level is feasible. The Configuration III baffle shown in figure 24 was to simulate the AP600 thermal insulation configuration, which constitutes the reference point of the present work. In search for improving the technology, we looked into the effect of the flow path that allows water to circulate around the lower head and up towards the top of the reactor vessel. From previous visualizations in ULPU-2000 Configuration III, we noticed that near the edge of the lower head the two-phase boundary layer exhibited a violently pulsatile behavior with some tendency to "shoot out" the flow, in a centrifugal-like fashion, and we thought

that a streamlining of the flow path might improve performance. The ULPU test facility was modified to include a curved baffle, as illustrated in Figure 26. The upper end of this baffle is hinged at a fixed point that allows a smooth transition into the riser. The lower end, on the other hand, is attached to a positioning mechanism that allows vertical placement in 1/2-inch intervals from a minimum of 2 inches, to a maximum of 9 inches. As shown, the radius of curvature of the baffle is the same as that of the vessel. The distance of the lower tip of the baffle from the vertical boundary just across it is 9 inches.Scoping experiments were conducted in this Configuration IV in October 2000. The preliminary results showed a consistent improvement over the whole arc, with potential gains of over 25%. Subsequently, we have completed a series of 28 determinations of simulated burnout heat fluxes in the ULPU-2000 Configuration IV facility. The results confirm preliminary indications taken prior to commencing this work, that streamlining the flow path around the lower head, and enhancing convection is beneficial to performance. In fact, the improvement was so great that in many locations we reached the power capability of the facility without observing burnout. Still, we have sufficient data to observe key trends (Figure 27), and proceed intelligently towards further optimizing the design.

Lower Region. Over this whole region the effect of increased convection in Configuration IV was to bring CHF up to the power capability limit of the lower block – 940 kW/m^2 to ~850 kW/m^2, almost linearly, as we move from position 0° to 30°, which is gradually reduced to just a few percent at 30° for the large gap (9”). The smaller gaps, $2\frac{1}{2}$” and 5” would be expected to show continuing enhancement, along the flow path, but the 940 kW/m^2 limit of the facility did not allow us at this time to distinguish trends. Nevertheless, based on these data we can put a clear lower bound of 900 kW/m^2 over this whole lower region, and this is very comfortable for the kinds of thermal loads expected in AP1000.

Middle Region. Here, we see a very significant increase of CHF due to the presence of the Configuration IV baffle as well. In this heat block (30° to 60°), the heat flux limit is 1410 kW/m^2, and this was reached under the 2½”-gap configuration. We can also see that all other gap dimensions (5”, 7”, 9”) produced essentially the same CHF of ~1200 kW/m^2. Note that in Configuration III the CHF in this region varies from ~900 to ~1100 kW/m^2, so enhancement is relatively small. This is because convection in this region, in Configuration III, is already quite strong, so rather small gaps are required to significantly improve upon it.

Upper Region. The behavior in the upper region is characterized well by performance at two positions — 75° to 80° and ~90°. In the 75° to 80° region, we reached the facility heat flux limit (third block) of 1880 kW/m^2, and the data show an optimal gap of 5”, for which the limit was reached without observing burnout. Both a larger and a smaller gap produced burnouts at somewhat smaller fluxes — 1786 kW/m^2 for 9”, while with 2½ ” we could only reach 1786 kW/m^2 because the run was interrupted with a burnout occurring in the downstream position. Clearly with a very small gap, in the upper positions we may be starving the liquid flow, and this suggests a design where side slots on the insulation (baffle) would allow water to enter along the path as needed by the pressure differential. In the 90° position, on the other hand, we observe a decrease of CHF to ~1600 kW/m^2, which is essentially the Configuration III value. This is also very relevant to high-power reactors, where higher thermal loads are expected at the uppermost region. Further studies are

underway to explore the mechanisms and solution to alleviate this problem and accommodate fluxes of ~2 MW/m^2, to provide a comfortable margin to the need of AP1000.
Interestingly, analysis of CHF results from the small-scale BETA experiments indicate that the surface morphology, aging, and chemistry are of paramount importance to the burnout mechanisms. Notably, CHF was found to increase, linearly, with the increase of nucleation site density – the latter parameter can be affected by water chemistry and surface treatment, and this open a new opportunity to the enhancement of the coolability limit.

C.3 Analysis Development and Validation on Vessel Structural Loadings, Creep and Failure

C.3.1 Coupled thermal hydraulic and creep analysis

C.3.1.1 CFD analysis of natural convection and heat transfer

For the evaluation of the temperature field within the vessel wall the CFD-module FLOTRAN® is employed. A 2D-axisymmetric model is developed for the vessel wall and the melt pool region. A homogenous melt pool is assumed inside the vessel with the surface level set 10 mm below the welding joint between hemisphere and cylinder in case of EC-2. A homogenous volumetric heat source is assumed which is applied to the volume where the heater elements are to be found. The model has 3 material zones: vessel wall / steel, liquid oxidic melt and crust. A typical temperature field of the melt with internal heat sources is given in Fig 28. The hot focus area in the vessel wall is clearly visible. Fig.29 shows the temperatures of the vessel inside and outside surfaces calculated at a heat generation rate of Q=38 kW compared to the measured temperatures in the EC-2- and EC-4-experiments, after reaching thermal steady-state. Due to the melt convection inside, the hottest region of the vessel wall is the upper part of the hemisphere just below the surface of the melt. The local temperature differences over the vessel wall correspond to the local heat flux across the wall. The maximum heat flux is about 120 kW/m^2 and the calculated maximum temperature difference is around 80 K. The measured temperatures on the outside show lower values than calculated because the thermo-couples are mounted on the wall and cannot measure exactly at the wall surface, but qualitatively the agreement between experiment and calculation is very good. The measured temperatures on the inside wall were several hundred degrees higher than calculated. This may be due to the thin boundary layer of the melt at the wall. Additionally some of the thermocouple tubes lost their wall contact and may have been close to the heater rods. It was decided not to relay on these measurements for comparison. But due to the integral character of the FOREVER-experiment the calculated temperature field is assessed, again indirectly, by the mechanical response of the vessel to the pressure load, which will be discussed later.

C.3.1.2 Structural analysis model for the vessel creep

The material damage due to significant creep and plastic strains is modeled by a damage measure D that is incrementally accumulated at the end of a time step or substep. D=0 means “no damage“, which is the initial value for all elements. The creep and plasticity strain components are calculated separately according to the experimentally found material behavior (Ref. [13]). The damage behavior was

considered in dependence on the triaxiality of the stress tensor according to Lemaitre (Ref. [14]). The damage increment is calculated for each element by averaging its nodal equivalent creep strains. If the element damage reaches the value of D=1, the element no longer contributes to the wall strength. The implementation of this model is described in (Ref. [15]). A sufficient number of elements across the wall thickness is necessary to model the changing material properties and the body load due to the temperature field derived from the CFD analysis. To save computational time, regions of lower temperatures were meshed with a lower density. Because of the large spatial and temporal temperature and stress changes within the vessel wall an advanced approach for the numerical creep modeling has been developed. Usually creep is described by analytical formulas (creep laws) with a number of free coefficients. The coefficients are used to adapt the creep laws to the data obtained in creep tests performed at constant load and temperature. However, it is difficult to achieve a satisfying adjustment for a wide range of temperatures and stresses with only one set of coefficients. Therefore a supplementary tool for the ANSYS® code has been developed which allows to independently describe the creep behavior of a material for different stress and temperature levels by means of a creep data base. Moreover, the damage is calculated as described above. The Digital® Fortran Compiler (Rev. 6.1A) was used for programming and for generating the customized ANSYS-executable on a Windows/NT® platform (Ref. [15]). The creep database was generated using the analysis of the measured data performed by Ref. [13]. Due to the uncertainties of the creep fracture strains measured in the uniaxial tests the creep fracture strain was set to 60% for temperatures above 600°C. The plasticity of the material is modeled by using the multilinear isotropic hardening option of ANSYS® (Ref. [16]). The plastic fracture strain is evaluated from the last point of the stress-strain curve. With these values the damage increment can be calculated.

C.3.1.3 Results of the pre-test calculation

Figure 30 presents on the left the temperature field in the vessel wall taken from the CFD-calculation with a power input of 38 kW and on the right the equivalent local creep strain after 1 h in the calculation with a pressure load of p=25 bar. The high temperatures in the focus region are clearly visible and, therefore, it is plausible that the maximum creep strain is obtained there, too. Figure 31 shows the local creep strain and the accumulated damage at the predicted failure time (4:05 h after pressurization). The horizontal lines indicate the initial welding line. As indicated the most damaged element is on the vessel outside, some 60 mm below the welding line. This corresponds very well to the failure position observed in the experiment EC-2, where a horizontal crack of some 150 mm length was created about 50 mm below the welding line (Figure 32). Melt level drop due to vessel expansion is an additional information the experimentators asked for is the actual melt drop during the experiment, because after a certain decrease the heater could be partially uncovered and this can cause a failure of the heater. Therefore, a post processing routine was written to get information about the volume expansion of the vessel, i.e. the melt level drop against time. Again it was found that it is useful to have a correlation to an item that can be measured on-line and is insensitive to different loading scenarios or sequences and therefore, independent of time. From the calculations it was found that the relationship between melt drop and bottom displacement is nearly independent from the starting pressure or a temperature offset.

C.3.1.4 Metallographic observations

Metallographic examinations of samples taken from different positions of the vessel wall were performed in order to detect experiment-induced microstructural changes. Additionally, annealing experiments with subsequent microstructural investigations, microhardness measurements, ion microprobe analysis and scanning electron microscopy with energy dispersive X-ray analysis of selected samples were also carried out (Ref. [17]). The result of the metallographic examination is a two-dimensional profile of the microstructure over the wall thickness and along the height position. Regions of microstructural appearances that are correlated to special transformation temperatures or environmental effects could be defined. In this way the region of highest thermal loads could be identified and the axial and radial thermal gradient could be demonstrated. The investigations revealed that creep pores are formed at highly loaded positions. They indicate remarkable creep damage. Furthermore, the metallographic examination also identifies interactions between the environment and vessel material, which are not very relevant for the vessel response during the test. There is hardly a reaction between the oxidic melt and the vessel wall. Figure 32 shows a cross sectional view over the vessel wall just above the final crack position in EC-FOREVER-2. On the left side, i.e. vessel inside, nearly no creep pores are found. Towards the outside the number of pores increases significantly and finally the coalescence of the growing pores is clearly oriented horizontally and small cracks are formed. Qualitatively the agreement between the microscopically observed damage distribution and the calculated damage parameter “D“ (Figure 31) is quite good.

C.3.1.5 Calculations for the penetration test EC-FOREVER-3

All prior sections deal with the 2D-FE-model which represents a simplification, but has been proofed as a quite powerful tool for the desired analysis.
For the experiments EC-3a and EC-3b it was necessary to develop a 3D-model, because the axisymmetry was lost by the introduction of the penetrations, which were located at different polar and circumferential positions. A 15°-slice of the vessel was modeled assuming symmetry conditions at the cutting planes. The penetration and its welding were made of INCONEL 600. The material properties for the INCONEL were taken from Ref.18. The temperature field was not evaluated by a 3D-CFD-calculation, but taking the temperatures for the vessel inside from the 2D-CFD-run as internal boundary condition and applying the same external boundary conditions was a suitable way to calculate the 3D-temperature field for the wall and penetration. The final mechanical run was rather difficult due to convergence problems caused by the different materials and their thermal expansion coefficients and due to contact problems of the penetration rod against the vessel bore where they were not welded. But even for the highest penetration rod position it became clear that the vessel will not fail at the penetration or its welding, because it is still clearly below the hot focus temperature region. Figure 33 shows the damage distribution after 3200 s creep induced by a pressure of 25 bar. The region of the damage maximum is in the vessel wall clearly above the penetration. This result was validated by the resulting failure in EC-3b, where the vessel failed similar to EC-2. Therefore no further investigations were made in 3D-FEM-calculations.

C.3.2 PASULA code analyses and validation

C.3.2.1 The PASULA computer code

PASULA computing package has been developed for a variety of structural analysis and heat conduction capabilities. During work the FEM codes related to structural analysis were developed further. Especially capabilities for three-dimensional analyses were developed including mesh generators for penetration analyses having different materials and capability for crack opening analysis and discharge of contents. The conditions are beyond the normal application area of most commercial structural mechanics codes. Highly non-linear phenomena cause difficulties for the FEM solution. Most of the pressure vessel analyses in severe accidents have concentrated to estimate the time to rupture of the vessel. However, simulation of crack initiation and growth is also important for estimating corium discharge from the vessel in plant scale. Efficient visualisation programmes have been developed to support the PASULA code for showing deformations, stress and temperature distributions etc.

C.3.2.2 Continuum mechanics for large deformation

Due to high nonlinearities and time dependent temperature distributions the calculation is advanced by taking finite time increments. The basic unknown are the incremental displacements of the nodes. Due to nonlinearities the displacements are determined by iteration. The stress and strain states are considered in integration points of finite elements. A fairly general procedure, independent of material behaviour, for calculating finite deformation and stress state was developed for a finite element analysis. In this procedure, the change of stress and strain state during a time increment is considered in a co-ordinate system aligned in the directions of principal stretches caused by deformation during the time increment (Figure 34). This has the advantage that originally a rectangular material element at the start of deformation is still rectangular after the deformation. The details of the method is presented in (Ref. [19]).

C.3.2.3 Constitutive modelling of reactor pressure vessel steels

It was found that uniaxial tensile, relaxation and creep tests within the temperature and time range of interest can be satisfactorily described by a single inelastic deformation rate model of strain hardening type ($d\varepsilon_{ie}/dt$ is inelastic strain rate)

$$\frac{d\varepsilon_{ie}}{dt} = A_T \varepsilon_{ie}^{s} \left(\frac{\sigma_{vM}}{\sigma_{ref}} \right)^{r} . \qquad (1)$$

The parameters A_T, s and r are assumed to depend only on temperature. They are determined separately from axial tensile, relaxation and creep experiments giving approximately the same values for the parameters A_T, s and r. The inelastic strain ε_{ie} is natural (logarithmic) and von Mises stress σ_{vM} is determined by using true stress components. In axial testing σ_{vM} is equal to the axial true stress. True stress and natural strain values need to be used in creep modelling, since these quantities are consistent with stress and strain measures used in large strain analysis. Reference stress σ_{ref} is used to make the term in parenthesis dimensionless. In the strain hardening type model (1) there is no specific separation of plasticity and creep, since they are both caused by similar physical processes. The parameter A_T depends strongly on temperature. The parameter s (a typical value $s \approx -0.2 \ldots -0.4$ for steels) takes strain hardening into ac-

count. The parameter r (a typical value $r \approx 3.4...4.0$ for steels) is related to the stress. The basic model (1) does not follow the measured curve at greater strain than about 0.1 at low temperatures in the ferritic phase at lower temperatures (below $\approx 700C^{o}$). That is why an additional term was introduced into the model as described in (Ref [19]).

C.3.2.4 Failure criterion

In literature different criteria for creep failure have been presented. Most of these are developed for long term load (months or years) at low temperatures (below $600^{o}C$) and deformations are small. Now the duration of load is quite short (hours), temperatures very high ($1000^{o}C$) and strains are large. At high temperatures the materials behave in a ductile way. Thus a strain-based failure criterion is more versatile than stress-based criterion. Most of the strains before fracture are caused by primary stresses due to the pressure load in a spherical or cylindrical vessel. Primary stresses, which do not relax, cause essentially a two-dimensional stress state. Secondary stresses caused by thermal gradients relax at high temperatures. Secondary stresses cause fairly small strains compared with the strains needed for a fracture at high temperatures. The ratio of the hydrostatic stress to the von Mises equivalent stress is a versatile quantity for characterising the triaxiality of the stress state. In a spherical RPV and in the membrane stress state caused by a pressure load, the stress state characterising triaxiality factor is 2/3. In a cylindrical pressurised vessel the triaxiality factor is $1/\sqrt{3}$ 0.577 (in uniaxial testing the triaxiality factor is 1/3 when neglecting the triaxiality in the necking area). Cumulative effective strain ε_{ie} in Equation (1) can be used as a failure measure for estimating rupture. The cumulative strain can be thought to describe the internal damage of the material. The critical value of the cumulative strain can be determined by simulating small scale RPV experiments by FEM. Investigation of different experiments has demonstrated that critical effective strain of magnitude 0.3-0.6 depends on the sulphur content (MnS_2) in the metal.

C.3.2.5 Pre-test axisymmetric penetration analysis

Preliminary analyses of the EC-Forever-3 penetration experiment were performed during 2001. This experiment incorporated eight scaled Inconel-600 penetrations placed from 15^{o} to 55^{o} angle from the bottom of the vessel. The objective of the pre-test calculations was to support the penetration scaling and test conduction. Penetration scaling analyses were performed with an axisymmetric model, which enabled calculation of a large number of parametric cases. Results of the calculations were reported in (Ref. [20]). An axisymmetric model was constructed around an individual penetration (Figure 35), assuming perpendicular orientation against the vessel wall. The idealised geometry described the pressure load quite well. The thermal field varies from vessel bottom to the side, having a peak in the sidewall. Due to this asymmetry, the axisymmetric geometry did not give correct thermal loads for penetrations high in the wall.

The axisymmetric model was applied to study the effect of penetration size. Scales 1:1 and 1:10 (vessel scaling) were studied penetration location. Angles 50^{o}, 55^{o} and 60^{o} were studied. The analyses showed that the effect of the small penetration is very local. The failure takes place on the hottest area of the vessel wall and not necessarily at penetration. This is further influenced by the fact that Inconel-600 creeps less than

16MND5 which partly compensates the weakness caused by the cylindrical initial crack between the penetration and the vessel wall. It was recommended to put at least one penetration close to the hottest wall area. A penetration may fail by growth of the cylindrical crack, which opens during loading. Depending on the fracture toughness properties of Inconel-600 and 16MND5 the penetration may separate circumferentially from the vessel wall. When a crack starts to grow the circumferential stress state is relaxed and crack arrest takes place. The crack opening causes fluid leakage and internal pressure decrease.

C.3.2.6 Post-test 3D penetration analysis

Post-test analyses of FOREVER-3(B) penetration test by three-dimensional FEM model were performed during 2002. Results of the calculations were reported in (Ref. [21]). For 3D analysis a special mesh generator, which optimises the mesh, was developed. Generation is a difficult task, since the penetration locating close to the hottest area is in a very oblique orientation in the vessel wall. A problem related to mesh generation is to keep computing time moderate. Another difficulty is caused by the fact that there are two different materials (base material 16MND5 and Inconel-600). The boundary between the base material and weld material did not follow element edges, but the material type in the model was determined according to the location of an integration (Gauss) point. This also reduces the number of elements and computing time. The element mesh needs not to be dense, since at high temperature the secondary stress peaks are relaxed and the stress field is rather smooth. The spherical part of the vessel was made of the French RPV steel 16MND5. The upper cylindrical part was made of German steel 15Mo3. Since the inelastic strain rate properties of 15Mo3 were not characterised, the cylindrical part was modelled to be of 16MND5. Inaccuracy caused by this assumption is not significant, because the temperatures and hence deformations were fairly low in the cylindrical part. The measured initial wall thickness was taken into account in generating the element mesh. Measured temperatures were interpolated to nodes. Figure 36 shows that greatest effective cumulative strains occur above the penetration on the hottest area, where the failure took place. Conclusions from the penetration analyses are:

- A penetration disturbs the global stress field in the vessel wall only over a very small area.
- Inconel-600 creeps less than RPV steels.
- The preliminary analysis showed that a penetration failure is possible only, if it locates on the hottest area. Otherwise the failure takes place on the hottest area without penetration.
- Temperature is the most important failure controlling parameter. Inelastic deformation rate is very sensitive to temperature and a fairly small change in temperature changes significantly the deformations and strains.

C.3.2.7 Crack opening analysis

In connection of 3D analysis the simulation of crack initiation and growth has been developed (Ref. [21]). In this method the through-thickness crack opening is increased according to local failure of the vessel wall. In case of ideal gas content the pressure inside the vessel is decreased according to the leak flow calculated from adiabatic equation for ideal gases. The vessel was filled by glass type material, whose

initial temperature was about 1300 K. The melt was a binary mixture of 30wt% CaO and 70wt% B_2O_3 with the resulting density of about 2500 kg/m^3. The discharge of the glass flow first and Argon flow were modeled. Pressure decrease was calculated by taking small time increments by assuming the pressure and temperature as spatially constant far from the opening during a time increment. Figure 37 shows post-test photograph and calculated crack opening. Leak opening analysis gave realistic results for leak area and crack length. A crack is initiated in the hottest area and the crack grows to the direction, in which the temperature gradient is smallest. This direction was now circumferential.

C.3.2.8 Post-test analysis the EC-FOREVER-4 experiment

The objective of this work was to perform post-test calculations for the FOREVER-4 experiment using a vessel to evaluate deformations at different phases of the experiment and to estimate failure location. Results of the calculations was reported in (Ref. [22]). The spherical part of the vessel was made of the U.S. steel SA533B1. The upper cylindrical part was made of German steel 15Mo3. Since the inelastic strain rate properties of 15Mo3 were not characterised, the cylindrical part was modelled to be of SA533B1. Inaccuracy caused by this assumption is not significant, because the temperatures and hence deformations are fairly low in the cylindrical part. The calculations were made using an axisymmetric FEM model. Calculated displacements became much lower than measured displacements when measured temperatures were applied. Therefore it was suspected that the measured temperatures were lower than the actual wall temperatures. A correction to measured temperatures was needed to calculate the observed vessel behaviour. Different corrections were tried based e.g. on ANSYS code steady state temperature analysis. By applying corrected temperatures much better agreement was obtained.

C.3.3 SYSTUS+ Code Validation

During the year 2001, Framatome conducted the Post-Test analysis of the EC-FOREVER 2 experiment realised at the Royal Institute of Technology, Stockholm. The simulations were made using the Finite Element programme SYSTUS. The aim is to study the multiaxial creep deformation behaviour of a nuclear reactor vessel lower head under severe accident conditions with core melt-down using 1/10 scale reactor vessel model experiments. The numerical simulation proposed here consists first in reproducing the thermal history of the vessel, and then to compute the mechanical history using a coupled creep-damage material model. This model has been implanted in the SYSTUS code. The material model parameters for the French steel 16MND5 have already been determined from 500°C to 1300°C. These will be simply recalled and used in this analysis without going into the details of their determination.

Numerical simulation of the EC FOREVER-2 test turned out to be particularly delicate due to several reasons :

From the experimental point of view :

- The temperature measurements on the internal surface are not exactly at the wall surface,
- Due to the problems during the test, the heating took place in two steps, the first having already led to some creep of the vessel,

- There are some uncertainties on the upper level of corium.

From the numerical point of view, following problems can be listed :

- Thermal option in SYSTUS code does not permit to realise the convection calculation in the corium,
- There is an important coupling between the thermal and mechanical analyses due to significant deformation (creep) of the bottom head; corium level changes during the test,
- It is not certain that there is a nominal stationary state of operation.
- Creep parameters were calibrated on uniaxial tests and eventual effect of tri-axiality on these parameters is not taken into account.

The thermal calculations conducted here are stationary states between which thermal history is interpolated. The four computations of the creep damage show that the results are very sensitive to the wall temperatures especially to the thermal gradient. It is therefore necessary to have a good representation of temperatures to have access to damage. Of the four damage computations made, the one, where measured temperatures on the inner and outer surfaces are imposed, gives the results closest to the experimental values. If the computation is based only on the temperature of the external surface, no creep damage is predicted. This is in total disagreement with the results obtained using ANSYS code (Ref. [23]) where the time to rupture and the crack location are well predicted with this thermal state.

At present it is difficult to conclude on the validity of the numerical results, since, before any damage calculation, one must be sure of the thermal representation of the test. The present state of the SYSTUS code does not permit any investigation in this domain since a complete computation taking into account phenomena of convection, is not possible.

Finally, for the damage calculations, it will be necessary to be able to confirm the validity of the parameters used on tests other than the uniaxial tests, where stress triaxiality could have a non-negligible effect.

The report SAM - ARVI - D015 (Ref. [24]) deals in detail with all these aspects. The report also provides creep laws and parameter identification for the 16MND5 material.

C. 3.4 Lower Head Dynamic Loading

A systematic study of in-vessel fuel-coolant interactions and quantification of dynamic loadings and structural integrity of the AP600 reactor vessel in coremelt scenarios related to in-vessel retention was performed previously at CRSS, and published in the open literature. We used PM-ALPHA.L.3D code for premixing simulation and ESPROSE.m.3D for prediction of pressure transients and impulse on the vessel lower head. It was concluded that the resulting dynamic loads in relevant scenarios do not threat the AP600 vessel integrity.

The primary objective of the UCSB contribution to the ARVI project in this task is to revisit the modeling concept and simulation capability, and assess the risk significance of in-vessel steam explosion in light of up-to-date understanding and improved capabilities in PM-ALPHA and ESPROSE computer codes. We then performed a number of parametric calculations e.g. with different subcoolings of coolant in the vessel lower head, to evaluate pre-mixtures which are expected to be more readily explosive.

In general, based on results from these update and parametric calculations we found that the state of the art in the field of fuel-coolant interactions does not alter conclusions found for the AP600. However, it remains open whether such conclusions apply to high-power reactors. The main difficulty is not in the premixing and steam explosion calculations, but in the design-specific assessment of core degradation and subsequent core melt relocation pathways and characteristics.

C.4 Analysis development and validation of gap cooling

C.4.1 Model development to investigate corium coolability in gaps formed between oxidic corium and a metallic vessel.

Several experiments have been performed recently (Ref. [25], [26], [27], [27], [28], [29], and [30]) to investigate corium coolability in gaps formed between oxidic corium and a metallic vessel. These experiments have been performed in different geometries (vertical plates, hemispherical surfaces, etc.), at different pressures (between 1 and 100 bars) and with different fluids. The objective is to derive a CHF model to interpret and unify these results. Complementary to previous modelling efforts (Ref. [31], [32], and [33]), a model based on counter current flooding limited flow has been developed. The use of the formulation proposed by Kutateladze (Ref. [34]) proved to provide best-fit results for both vertical channels and hemispherical geometry

Vertical plane geometry:

Kutateladze approach: a~0.65-0.8 and b~1.79

$$\varphi_{CHF,vert,Kut} = \frac{\mathrm{mL'}\,\delta\left(g\sigma\Delta\rho\right)^{\frac{1}{4}}}{H}\frac{b^2\,\rho_v^{1/2}}{\left[1+a\left(\frac{\rho_v}{\rho_\ell}\right)^{1/4}\right]^2}$$

m = 1 for one side of plane heating

m = $\frac{1}{2}$ for two-side heating

H: height of the plate (m)

Hemispherical geometry

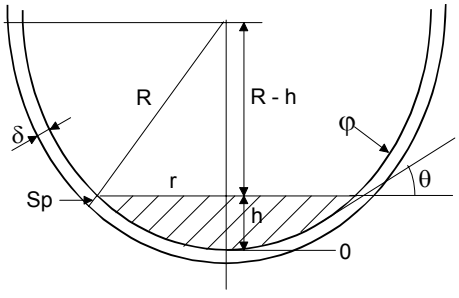

$$\varphi_{crit}(h)=L'\frac{\delta}{R}\left(\frac{2R}{h}-1\right)^{5/8}\left(\frac{h}{R}\right)^{\frac{1}{4}}(g\sigma\Delta\rho)^{1/4}\frac{b^2\rho_v^{1/2}}{\left[1+a\left(\frac{\rho_v}{\rho_\ell}\right)^{1/4}\right]^2}$$

δ : is the width of the gap (m)

ρ_l : density of liquid (kg/m^3)

ρ_v : density of vapour (kg/m^3)

g : gravity acceleration (m/s)

σ : surface tension (N/m)

L' is the latent heat of vaporisation for the coolant L, to which the sensible heat linked to subcooling has been added: $L' = L + C_p(T_{sat} - T_{water})$. C_p is the specific heat of liquid water.

The application of the model approach to the tests performed in plane geometry (Ref. [25]) shows that it is possible to explain the effects related

(i) to the number of heating surfaces,
(ii) to the height of the heating surface,
(iii) to the pressure,
(iv) to the gap size (for δ = < 5 mm or ~ 5 mm).

It is also shown that the experimental results obtained, in hemispherical geometry by (Ref. [28]) are compatible with those obtained by (Ref. [29] and [30]). The large differences in measured CHF are due to differences in pressure and differences in gap size. The comparison with the results obtained by (Ref. [29] and [30]) seems to indicate that models based on CCFL controlled CHF seem to be limited to gaps of less that 3 to 5 mm. Beyond this gap size, mechanisms other than CCFL might control the CHF. The deliverable D4.1.1 (Ref. [35]) corresponding to the Work Package 4.1. was issued in May 2001.

C.4.2 Validation of TOLBIAC thermal hydraulic severe accident code

C.4.2.1 The TOLBIAC code

The TOLBIAC code is devoted to the simulation of the behavior of a corium pool with natural convection within a structure, which may be the pressure vessel or a catcher, in order to study the behavior of the structure. The following main phenomena can therefore be calculated: metal-oxide stratification, residual power, free surface heat transfer (radiation, or heat transfer with water), wall ablation and crust formation. Its main characteristics are the use of a 3 fields equation system, in a 2D cylindrical or rectangular geometry. The two fluid model used in TOLBIAC is derived from the CEA thermo hydraulic code CATHARE. It is written in FORTRAN language and it is composed of about 100 000 instructions lines.

The 3 fields are the metal components, the oxide components and the gas.

- The metal liquid phase is a mixture of iron, zirconium, nickel and chromium, in proportions defined by the code user. It is characterized by its own volumetric fraction, temperature and velocity fields.
- The oxide liquid phase is characterized by its own temperature and velocity field. It is divided into light oxide issued from the ablation of the wall and

heavy oxide composed of uranium dioxide and zirconia, each one with its own volumetric fraction.

- The gas phase characterized by its volumetric fraction and velocity fields is a mixture of carbon dioxide and steam. Its temperature is supposed equal to the surrounding liquid temperature.

The model is therefore composed of four mass balance equations, three momentum balance equations and two energy balance equations. A diffusion term is included in the energy and momentum equations, taking into account viscosity and conductivity effects, but no peculiar turbulence model. The numerical method used in TOLBIAC is semi-implicit. It is used for transient regimes. The time step is limited by the current flow limitation: it is a relation between time step and space step. The hydraulic equations are discretized with a finite difference scheme on a spatial meshing, with the donnor cell method. The non-linear system of equations is solved with a Newton-Raphson iteration procedure. The closure laws of the system of equations (heat exchanges and friction terms) are correlations obtained from the literature or from experimental assessment. The physical properties of corium are not well known and are taken from literature. For validation purpose, simulants, for which the physical properties should be well known, are used. The wall temperatures are calculated by using conduction equations (either 1D or 2D). Temperature profile in the wall and ablation velocity are available. Crust formation is calculated at the wall and at the free surface by means of a heat balance in the crust with an assumption of steady state temperature profile in the crust.

C.4.2.2 Definition of the geometry

The validation for in-vessel configurations was made mainly with the BALI experimental results, simulating a homogeneous corium pool (Ref. [36] and [37]), or a metal layer (Ref. [12]). Other validations were previously conducted with the former single phase COPO experiments. The aim of this work is to assess the TOLBIAC code with COPO experiments P20 and P21 (Ref. [38]) and study the influence of heat transfer coefficients and interfacial shear stress between the two stratified liquids without crust at the interface. A paraffin layer is located above a water layer in a semicircular facility. The pool is heated by conducting current through the water (some uncertainties remain about the measurement of the power input) and the walls of the facility are cooled down thanks to a circulation of liquid nitrogen. In order to calculate the COPO experiment, some small developments were necessary in TOLBIAC. These developments were made to:

- Take into account the new experimental geometry.
- Take into account a new simulant: the paraffin oil, with its new physical properties obtained from data sent by FORTUM. Some uncertainties remain on these physical properties, especially on the solidification temperature and on the viscosity of the paraffin oil.
- Take into account the absence of crust at the interface, and calculate heat exchanges at the interface with an interfacial temperature instead of a solidification temperature.
- Take into account new heat exchange correlations for the parametric study.

A literature survey was made to define the friction modelling at the interface. Three different tendencies were observed.

- Some authors assume the continuity of tangential velocities between the two phases (Ref. [39] and [40]). This is modelled in TOLBIAC by assuming an infinite friction term for the horizontal velocities at the interface.
- Others (Ref. [41]) tend to think that at low velocities, in a oil-water stratified flow, the interfacial friction coefficient is assumed equal to the wall friction coefficient for water.
- In another simple approach, it can be considered that the configuration studied (liquid-liquid interface) can be modelled by a classical liquid-gas configuration. The two-phase flow literature is abundant in liquid-gas flow examples, but much less in liquid-liquid flows. The theories developed for stratified flows in horizontal pipes can also be used. Wallis proposes different correlations for the friction coefficient.

C.4.2.3 Parametric study

A reference calculation is defined. It shows significant differences between calculation and experiment: both heat fluxes and pool temperatures do not fit well.
The influence of some parameters on the results is then studied:

- The meshing of the pool.
- The interface friction modelling.
- The heat transfer correlations.
- The properties of the paraffin oil.
- The power input.

The study of these parameters shows that apart from the heat transfer correlations, the paraffin oil solidification temperature and the paraffin oil thermal conductivity, the other parameters don't influence the results in a large way. The modification of the heat transfer correlations gives a quite good heat flux repartition. The correlations giving the best results are the (Ref. [42]) or (Ref. [43]) correlations in the water layer, the (Ref. [44]) correlation for horizontal exchange in the paraffin layer and the (Ref. [45]) correlation at the lateral wall in front of the paraffin layer. However, using this set of correlations leads to temperatures of the water layer which are too high.
Decreasing the paraffin oil solidification temperature leads to an increase of the heat fluxes lost at the upper layer, but the temperature of this layer becomes too low.
With an increased paraffin thermal conductivity, correspondence between calculation and experiment is excellent for heat flux repartition. The temperature of the water is too high though and the paraffin becomes colder.
These results are summarised in Table IV and Figures 38, 39 and 40, using Kelkar correlations (Ref. [42]) in the water layer, Fishenden and Saunderscorrelation (Ref. [44]) for horizontal exchange in the paraffin layer and Churchill and Chu (Ref. [45]) correlation at the lateral wall in front of the paraffin layer (noted Kelkar).
The second calculation is made with a solidification temperature of the paraffin of –40°C instead of –9°C. The third one with an increased conductivity of the paraffin layer. The deliverable D4.2.1 corresponding to Work Package 4.2 is issued in October 2002 (Ref. [46]).

C.4.3 Application of ARVI and MVI data and models in system codes
Melt pool modelling

The objective of this work package is the development and application of simplified, fast running models for the corium behaviour in the core and the lower plenum which can be used in a core melt code like KESS or a system code like ATHLET-CD (the code system KESS is used as a test bed to develop modules for ATHLET-CD). A key subject concerning in-vessel melt retention is the melt-down and melt relocation process in the core region. This defines the conditions for the melt flow to the lower head, the interaction with residual water there and the resulting configurations in the lower head.

C.4.3.1 Melt pool modeling

Major questions in the frame of core degradation concern the melt accumulation in the core and the release modes to the lower head, i.e. essentially melt pool formation and failure modes. A simplified representative model for the thermal melt pool behavior has been developed for KESS and ATHLET-CD to determine the local distribution of heat fluxes from a melt pool to the surrounding crust. The model delineates three zones in a convecting melt pool, governed by different physical phenomena, namely a turbulent, well mixed upper layer, a thermally stratified lower zone and a lateral zone governed by boundary layer heat transfer. The main aim is to take into account geometrical influences of pool configurations developing in the core, as well as influences of filling height and superheat. This can only partly be done by correlations from specific experiments. Following the approach in (Ref. [47]), the model is based on a 1D convective heat balance in the pool centre, a boundary layer approach for the lateral heat transfer and an empirical correlation for the upwards heat transfer. It has been validated against data from BALI (Figure 41) and COPO experiments as well as classical correlations from literature. Additionally, a model for an overlying metal layer has been developed. It is similar to those of Theofanous (Ref. [48]) and of Villermaux (Ref. [49]) and has been coupled with the above model.
This model – with some further approximations – has been implemented in the module MESOCO-2D of KESS. MESOCO describes core degradation in late phases of this process. Calculations on melt accumulation, pool formation and melt release have been performed with this approach and correlation approaches for different pool shapes. No significant differences resulted until the beginning of the outflow. The geometrical form of the pool may thus be of minor importance. However, final conclusions need further checking.

C.4.3.2 Analysis of late phase core degradation

The melt accumulation in the core strongly depends on the scenario, especially on the water level development. The formation of large melt pools on a crust in the core requires a sufficient heat sink due to residual water. As a result, lateral crust failure and sideways release to the lower plenum from the top of the melt pool is then favoured. On the other hand, assuming a rapid decrease of the water level, i.e. a strong reduction of the lower heat sink, yielded a continuous downwards outflow of melt from the core, but with only minor melt accumulation and consequently small mass flow. Thus, in both cases, pool formation with sideways outflow at top and downwards melt flow without major melt accumulation, a rather gradual melt flow to the lower plenum is obtained. If, on the other hand, strong melt flows to the lower plenum could be excluded to a high degree, this yields a reduced potential for strong

steam explosions as well as an increased potential for the formation of (at least temporarily) coolable particulate debris in the lower head.
To include full feedback with the cooling water development, MESOCO-2D has been coupled with WABE-2D (Ref. [50]), the latter code describing the quenching and coolability of particulate debris or in general porous configurations. Further, both ceramic and metallic melting has been modelled in MESOCO, and the Zr/H_2O reaction has been included. The so combined code, MEWA-2D, has been implemented as a module in the system code ATHLET-CD. Thus the coupling to the thermohydraulics of the primary circuit is established.
A result of an ATHLET-CD calculation on core degradation including the MEWA-2D module is given in Figure 42. The calculation started with the water level at the top of the core. After boil-off the core begins to heat up. Regions in the core, which are strongly heated up and where melting has already reached a certain amount, are calculated by MEWA and can be seen at different times in Figure 42. The other core regions, still largely intact, are calculated by the models on the early phases of core degradation. With the increase of core degradation, the MEWA calculation regime extends as seen in Figure 42, until reaching the extend of the whole core. From the left to the right, the local porosity and the steam velocity, the metallic and the ceramic melt fractions including their velocities are shown. As can be seen from the plots in the middle column, first metallic melting and melt flow to colder regions occurs, with subsequent formation of a metallic crust and overlying metallic pool. Later-on, starting at about 4700 s ceramic melting begins, yielding a ceramic crust with a pool, mainly above the metallic one. The development of the water level is calculated by the ATHLET thermohydraulics, describing in principle the water and steam flows around the MEWA region, coupled to the water level in the downcomer, as well as by the thermohydraulics in MEWA, coupled to the ATHLET thermohydraulics and describing evaporation and water/steam flow in the MEWA region. The resulting water level is not visible in Figure 42, but is always close to the lower edge of the MEWA region, i.e., it is obvious that the water level determines the location of the melt pool strongly. Due to numerical problems the calculation stopped after about 5750 s, caused by lateral outflow from the metallic pool with resulting direct contact of the melt with the water below the crust. Further work is required to solve these problems and enable continued calculations on the core degradation and especially melt release processes. The melt release modes to the lower head determine the conditions there, and thus finally the conditions for in-vessel melt retention.
Some insight into trends can already be gained from the present calculation, but need further confirmation. Since the water level remains closely below the pool/crust region, a stable crust establishes and supports significant melt accumulation above. In general, this yields a trend to outflow of melt at the upper lateral edge of the pool. However, with the combination of metallic and ceramic pool this becomes now more complicated. On the one hand, the metallic precursor pool/crust system yields a barrier for the ceramic melt, thus supporting also ceramic pool formation. On the other hand, the precursor yields heatup in lower regions, which weakens the structures below the ceramic pool and may thus induce earlier failure, possibly also with downwards release. This may even be favoured by increased evaporation of water due to melt inflow from the metallic pool. Thus, with the combination of metallic and ceramic melt there may be counter-effects to the trends mentioned above from the earlier calculations. Further analyses are required for clarification.

C.4.3.3 Coolability of porous debris and gap cooling

The central aim of in-vessel melt retention is the long term coolability of the corium. Depending on the release modes from the core region, configurations with particulate debris can be expected in the remaining water in the lower head, if only partial melting of the core occurs (e.g. with subsequent re-establishment of water supply). This be possible with a larger amount of melt if intermediate water supply replaces evaporated water. Results of separate investigations with WABE-2D showed that the coolability of such particulate or porous debris is much better, compared to conclusions from classical 1D dryout heat flux considerations, if more realistic multi-dimensional configurations allowing sideways inflow of water are taken into account. Even for configurations including hindering effects, as e.g. stratified beds with smaller particles on the top or locally mixed multigrain configurations, as well as configurations with largely unfragmented parts ("cake"), a high potential of coolability could be shown (Ref. [51]).

As an additional feature, possible cooling contributions by thin gaps between cake parts of the debris and the vessel wall have been taken into account. Such thin gaps of thickness < 3 mm are not resolved within WABE but considered via a separate modelling. Assuming a gap with water access below a cake part, coolability is considered to correspond to the establishment of saturation temperature at the lower boundary. Setting this boundary condition in WABE, calculations for the whole situation including particulate debris around the cake as well as low porosity in the cake are performed. Assuming a completely dense cake the coolability is already limited by the heat conduction to the outer surface of the cake. If the cake is considered as solid with small porosities, cooling processes by heat conduction as well as water and steam flow through the porosities are taken into account, together with keeping the lower boundary at saturation by assuming gap cooling. Based on this, WABE calculates the overall cooling effects as well as the heat flux to the lower cake boundary, i.e. to the gap. The resulting heat flux to the gap from the WABE calculation is compared with CHF correlations for gaps yielding a limit to coolability. The CHF correlation given in (Ref. [52]) for hemispherical geometry has been chosen.

With a cake case similar to that considered in (Ref. [52]), here additionally with surrounding particulate debris, a temperature increase in the cake (assumed porosity of 0.05, hydraulic diameter 1.5 mm) results, which finally yields temperature rise up to melting. Thus, although a separate consideration yields a downwards heat flux below the gap CHF, coolability is not reached due to the limiting heat transfer to the cake surface. However, a final conclusion on the overall coolability could not be drawn yet for this case. If the "cake" is considered as composed of a melt pool, surrounded by crusts, the above pool model is to be applied (not yet done) to yield the heat fluxes at the boundaries. The higher heat flux to the top boundary of the pool due to convection would then remove the heat from the pool, but may then not be removable via the overlying particulate debris. The increased downwards heat fluxes may then also yield CHF problems with the gap.

However, assuming a higher porosity of 0.1 for the same cake, coolability can be reached, but only with an increased temperature of up to ~ 1900 °C. Gap cooling contributes here by two mechanisms. Firstly by keeping the lower boundary at saturation temperature, and secondly by enabling steam and even water penetration into a lower part of the cake, as can be seen from Figure 43. Since this water penetration occurs from the side of the gap, a condition for inflow (pressure

condition) as well as a condition of water supply via the gap, depending on friction, had also to be given, in addition to the CHF criterion connected to the saturation assumption. The produced steam can escape through the porous cake which yields in principle an increase of the CHF of the gap, because of the reduced steam back flow through the gap itself. Additionally the continuous steam flow through the porous cake enhances the cooling of this cake by heat transfer to the steam. Figure 43 shows the increase of corium temperature in the hot cake part until a limiting value.

C.5 Preliminary Design of IVMR SAM Scheme for VVER 440 NPP

C.5.1 Initial Conditions, Material Properties

The estimates in (Ref. [53]) resulted in relatively small amount of steel in the debris, between 16 and 32 tons. In the time of core plate penetration, substantial amount of water should exist below core plate and the debris would quench and cool down. Due to this effect, heating of the debris would not start earlier than after 2 hours from reactor shutdown (in the hypothetic large LOCA with ECC failure) and would last another 2 hours before creating a stable pool in the vessel bottom. The estimate of decay heat for steady state calculations is then about 10 MW at the time of attack (Ref. [53]) or maximum 1400 kW/m^3 in the case when its release purely in the oxide layer was assumed (Ref. [54]). An attempt was made to confirm these assumptions, the debris formation, pool composition and accident timing by MELCOR 1.8.4 analysis with a detailed core model (Ref. [55]). Though this calculation was basically confirming the assumptions concerning debris formation, no conclusion about the pool at the bottom could be made because the calculation always failed at a relatively early time, before core plate penetration. The reason was the impossibility to describe VVER-440 core correctly. The effort was therefore shifted to other project where MELCOR 1.8.5 (using more elaborate models, especially the supporting and non-supporting structures) will be used. Even such integral code calculation, if completed, is not able to predict the corium and metal distribution into layers, such codes assume single pool only. According to recent knowledge, it is improbable that all metal material (steel and unoxidized Zr) will form a top metal layer as assumed e.g. in the analyses (Ref. [56]). Reduction of UO_2 by metal Zr in the presence of steel and collection of steel with metal U at the bottom of the vessel is more probable. This, however, does not exclude possible appearance of thin metal layer on top of the pool from steel arriving at later time. The thin metal layer on top of the oxide pool is, because of its focusing effect, the weak point of the IVMR concept. For this reason, the analyses of vessel thermal load concentrated on cases with different top metal layer thickness. The analytical tools available are not able to describe the bottom metal layer, so it was accounted for by properties of the oxide pool, mainly higher conductivity.

C.5.2 Results of vessel wall thermal load analyses, discussion

It has been proved (Ref. [57]) that not reaching the critical heat flux (CHF) on the external wall surface is both sufficient and necessary condition for not failing (melting through) the vessel wall. For this reason, the analyses concentrated on the comparison of heat flux and critical heat flux, though temperature field and melted vessel wall thickness were also studied.

Three cases have been analysed with the VESSEL code, case A with thick top metal layer 0.36 m (result of combination of 16 tons of steel and unoxidised Zr) and cases B, C with 0.1 m deep metal layer. Cases B and C differed in using Churchill-Chu or Chawla-Chan correlation for heat transfer between metal layer and the vessel wall (Ref. [58]). For the thick metal layer case A, the CHF margin was sufficient, (figure 44), while for the thin metal layer, the CHF was exceeded, (figure 45). This is true also for case C, where the maximum heat flux was slightly lower. The depth of vessel wall melting for case A is shown in figure 46, in cases B and C the melt penetrated through in the area of contact with metallic layer. Heat transfer from the metal layer to the wall decreases with decreasing layer thickness, but the heat transfer area decreases much faster and focusing effect can be observed.

Several cases were analysed with the MVITA code assuming hemispherical bottom head with shape similar to VVER-440 torisphere, constant heat transfer coefficient 10000 W/(m^2K) on the external wall surface and time constant decay heat 10 MW/m^2 (Ref. [58]). Large thermal margin was found, as expected for cases with one layer or thick metal layer 0.36 m, (figures 47 and 48). For thin metal layer 0.1 m, the results were much more optimistic than those of VESSEL and CHF and wall penetration were not reached. In MVITA a substantial part of heat was transported longitudinally in the wall, as the increased conductivity was automatically applied also in longitudinal direction. The consequence is that the melt front propagates also in this direction. As a parametric study the increased conductivity was permitted in radial direction only by modifying the MVITA source code (line 10cm_mod in figure 48). In longitudinal direction the usual metal conductivity was used. In this case the wall melt down was deeper and the heat flux on the outer surface was higher but still below the critical heat flux. Unlike to the VESSEL code, detailed radiation model of the structures above the melt pool is missing in MVITA and gas with constant temperature is assumed here, the temperature of this gas was varied between 1250 and 1873 K (steel melting temperature). For the highest temperature, CHF margin was closely approached for thin metal layer without the assumption of increased conductivity. Several cases have been analysed in the real VVER-440 torispherical geometry with the MVITA code (Ref. [54]). They included mixed oxide and metal into single layer, separated metal in a thick layer and part of the steel forming thin layers 0.1 m and 0.02 m. For the metal layers, the effect of low emissivity was studied, it was changed from 0.45 to 0.2. One sensitivity study for the thick metal layer showed the effect of decay power distribution between the oxide and the metal layer, 10 % of decay power was released in the metal layer. In all other cases, all the decay heat was in the oxide layer. In all calculations, time variable decay heat was used, the curve was derived in (Ref. [53]). The decay heat decreased from 11.612 MW at the start of debris heatup assumed 2 hours after reactor shutdown, through 10.108 MW after 2 hours of heatup to 9.334 MW at 4 hours of heatup. The temperature above the debris for radiation calculation was 1500 K and the heat transfer coefficient from the vessel wall surface to the water was 10000 W/(m^2K) as in the cases with hemispherical bottom head. The results for thick metal layer are in figures 49 and 50, where case 2a is for the surface metal emissivity 0.2 and case 2b for power distribution between oxide and metal. The results for thin metal layers were much more optimistic than those of the VESSEL code, the focusing effect was not so strong to fail the vessel as can be seen from the CHF margin in figure 51, where the worst case 3b is for low metal surface emissivity 0.2. It should be noted, however, that the same problem with wall molten part modeling mentioned above was solved

only partly, by increasing the metal pool conductivity 10 times in both radial and axial directions. This means that the melt radial conductivity was almost 2 orders less than the Raleigh-Bénard conductivity. Also, in reality, the effective conductivity would be probably high only in the contact with the molten metal and not in the molten vessel part close to the oxide pool from which it is divided by crust. The wall attack would be thus stronger in the region of metal layer and smaller in that of oxide pool than indicated by MVITA. It was also found that the effect of surface emissivity is small and the decay power generated in the metal layer decreases the power in the oxide layer and tends to slightly decrease the wall attack, (figure 50). The main results of WP5 are that the in-vessel retention by external vessel cooling is a promising strategy for the VVER-440 reactor type giving usually large thermal safety margins. The focusing effect of a thin metal layer on top of the debris pool remains a problem of this concept, this was demonstrated by the calculation results. Some development of codes like MVITA would be needed for correct prediction of the limits connected with the focusing effect.

CONCLUSIONS

The FOREVER experiments, in WP.1, investigate the creep behaviour of a $1/10^{th}$ scaled reactor pressure vessel with and without penetration under prototypic thermal and pressure load. In the present studies, external vessel wall was elevated to a maximum temperature of ~950^0C and to a maximum pressure of 25 bar. The time of vessel failure, one of the primary results, depends primarily on the imposed maximum temperature from the thermal load. Failure time increases more than an hour, if the maximum temperature is reduced by ~30-40^0C. For the thermal load distribution imposed by melt pool convection the failure should occur at ~70^0 from the bottom of the vessel when lower head is fully filled with melt. Different situation is expected if lower head is partially filled. It was also observed that failure always occurs in the hot zone. In all the cases, the failure crack travelled circumferentially. Failure length in the American steel covers 27% of the vessel perimeter while the same in French reactor steel it is only 17%. More melt is discharged in a vessel made of the American reactor steel than that of the French reactor steel. Slightly higher creep strain (~3%) is observed at failure in the French reactor steel than those for the American Reactor steel. From the test data, it was found that maximum 16% total strain would be needed before the vessel failure occurs for vessels employing the French reactor steel. Major part of the total strain is creep and it is ~13%. Present experimental results provide substantial data on multi-axial creep behaviour of different reactor steels at high temperature and moderate pressure. The data can serve as a benchmark for validating the multi-axial creep models in the structural codes employed by the nuclear industry. The failure location is of greater interest in the EC-FOREVER experiments with penetrations, since there could be a competition between the failure at the penetration location (e.g. in the welding) and that in the vessel wall where the highest temperature are reached. Previously, the LHF tests had shown that the vessel failure location would be at a penetration for a uniformly heated vessel, while the EC-FOREVER tests showed that the vessel always failed where the wall temperature are the highest. It was found in the EC-FOREVER-3 and –3B tests that the failure occurred at ~70^0 above the bottom pole of the hemispherical lower had. The highest location of penetrations was 55^0 as it is in the prototypic Framatome PWR vessel and this location is not in the hot zone. We believe that a true test of the competition would be when the penetration is in the hot zone, which can occur for the case of a convecting melt pool filling lower head partially. In the

EC-FOREVER gap cooling tests, there is no vessel failure. However, maximum displacement at the time of water pouring is ~15 mm. After pouring the water, upper 6-7 cm deep part of the melt pool quenched but there is hardly any gap formation, which is detected from the experiment from the recorded temperature data of the vessel wall. It is confirmed that ~1 cm crust formation near the wall from cut open post-test vessel but there is no gap formed. From the heat flux calculations using the RELAP code it seems that the energy liberated in initial 100 seconds calculated from the melt pool temperature was 9.55 MJ and from water evaporation rate was 11.15 MJ. The imbalance, due to heat content of vessel and structures, is quite justified. The average initial heat flux obtained, 0.88 MW/m^2, is reasonable and comparable to values got in other experiments. The average heat flux over first 100 seconds, however is 0.38 MW/m^2.

In WP.2.1 the Stratified COPO-II experiments, run P20 and P21, using volumetrically heated water-zincsulfate solution in the lower layer and paraffin oil in the upper layer, were carried out. Both experiments were technically successful. The paraffin oil layer on top the heat generating layer clearly decreased the upward / downward power split of the facility comparing both to homogeneous pool COPO experiments and to stratified pool experiments with distilled water as the upper layer. Qualitatively, the results were in accordance with the smaller scale SIMECO experiments. Casting the heat transfer results in form of heat transfer coefficients or Nusselt numbers was an ambiguous task, since the effective freezing point of the paraffin oil (boundary temperature of the pool) is not a well defined parameter. Nevertheless, the general trend of the Nusselt number at the upper surface of the paraffin oil layer seemed to be consistent with previous COPO II data with distilled water as the upper layer. The data obtained is expected to be valuable for code validation purposes, in particular in comparison with previous stratified COPO II data and SIMECO data.

In BALI experiments from a zero dimension approach, calculated heat flux concentration factor for reactor geometry and for the selected reactor bounding case is about 2 for a 40 cm thick metallic layer (factor 1.5 between 2D and 3D geometry). Such a concentration factor leads to an elevated lateral heat flux about 1.6 MW/m^2, which is considered for in vessel retention as a maximum value regarding critical heat flux limits and residual vessel wall thickness.

In ULPU experiments, analysis of CHF results from the small-scale BETA experiments indicate that the surface morphology, aging, and chemistry are of paramount importance to the burnout mechanisms. Notably, CHF was found to increase, linearly, with the increase of nucleation site density – the latter parameter can be affected by water chemistry and surface treatment, and this open a new opportunity to the enhancement of the coolability limit.

In WP.3.1 evaluating the observations made in the experiments and in the calculations the following conclusions can be drawn:

- The creep process is only initiated by the combination of high temperatures (>600°C) and pressure (>1MPa), i.e., at low pressure and high temperature we observe only the reversible thermal expansion, because loads due to the dead-weight of the lower head and the melt pool are negligible, at high pressure and low temperature the material strength is high enough to keep the pressure load.

- If the creep process is initiated, the weak region is the hot focus area, where the highest local creep strain rate occurs, this leads to wall thinning, which accelerates the creep geometrically.
- The overall temperature level and the pressure level influence mainly the failure time, but not the failure position.
- Failure will occur at the position of highest temperatures. Additionally, there is a small influence of the vertical position of the focus region: closer to the cylinder it is more dangerous than at lower positions of the bottom head, this can be understood analyzing the simple vessel formulas for a cylinder and for a sphere.
- Contrary to the hot focus area a large "bowl"-shaped region at the lower head bottom center shows relatively high material strength due to the lower temperatures. This bowl keeps its shape and relocates only vertically downwards.

In WP.3.2 The goal of the post-test analyses, using the PASULA code, was to test tools for analysing the behaviour of the PWR pressure vessel in case of a severe accident. This goal was difficult to achieve, since the temperatures were not known accurately enough. One uncertainty was caused by unknown inelastic strain rate properties of 15Mo3 - German steel used in the cylindrical part of the vessel.
A failure was predicted by applying a strain based criterion. Most of the strains before failure are caused by primary stresses due to the pressure load. Primary stresses, which do not relax cause essentially a two-dimensional stress state. Critical effective strain of magnitude 0.3-0.6 depends on the sulphur content in the metal. Because the temperatures were inaccurate and inelastic deformation rate is very sensitive to temperature, it was not possible to calculate the critical strain from the experiments.
Inelastic deformation rate is very sensitive to temperature and a fairly small change in temperature changes significantly the deformations. For validating the calculation process it is important to determine the temperature distributions accurately. Otherwise it is impossible to validate the creep model and the failure criterion.
In case of crack formation the crack is initiated in the hottest area and the crack grows to the direction, in which the temperature gradient is smallest. In FOREVER experiments this direction was circumferential.

In WP.3.3 the present state of the SYSTUS code does not permit any investigation in this domain since a complete computation taking into account phenomena of convection, is not possible.

In WP.3, based on results from these update and parametric calculations we found that the state of the art in the field of fuel-coolant interactions does not alter conclusions found for the AP600. However, it remains open whether such conclusions apply to high-power reactors. The main difficulty is not in the premixing and steam explosion calculations, but in the design-specific assessment of core degradation and subsequent core melt relocation pathways and characteristics.

The limitations of gap coolability in real reactor conditions have been outlined by employing the CHF model. The conclusion is that for the situation similar to TMI-2 accident (see OECD document 1993) in which only ~20 tonnes of melt was deposited in the lower head (at 100 atm.), gaps of ~1mm are sufficient for cooling,

however, if the whole core mass is relocated, then the heat flux from the corium cannot be removed even when gap sizes, as large as 3 mm, are created.

Using adapted heat transfer correlations and paraffin oil properties leads to a heat flux distribution which fits well the experimental results. However, it seems difficult to fit both the heat distribution and the temperatures in the pool.
Due both to the uncertainties of the experiments and to the sensitivity of the calculations on the physical properties of paraffin oil, it seems difficult to assess the TOLBIAC code on experiments COPO P20 and P21.

In WP.4.3 is found that in-vessel retention requires long term coolability of the corium in the RPV. Configurations established in the lower head strongly depend on the melt accumulation in the core and subsequent melt release modes. Only gradual melt flows to the lower head may be assumed. But, this has to be further investigated. Precursor metallic melting and pool formation may yield counter-effects, favouring downward paths. For smaller melt flows the risk of strong steam explosions is smaller, and a more complete jet breakup can be expected. The resulting particulate debris has a high cooling potential if water can be fed into the vessel. Even cake parts with low porosity may be coolable if higher porosity regions or only gaps allow water access to the bottom boundary. Coolability can then be attained even with larger cakes, partly supported by upwards steam (and even water flow) through a low porosity cake and corresponding cooling. If in-vessel cooling should fail, time margins firstly until full pool formation and subsequently until vessel failure can in principle be calculated applying MEWA to the lower head, including the simplified model for the melt pool behaviour. Failure modes of the RPV and outflow modes and conditions depend on the integral behaviour. Different release modes from the core may yield different pre-heating and even RPV failure before pool formation. The modelling reached with MEWA in ATHLET-CD can in principle be applied to solve these questions. Concerning the melt outflow from the core, the remaining numerical problems must still be solved to calculate the further development. Applications of MEWA to the lower head have up to now been concentrated on the coolability questions, with some continued applications to melting and melt flow in dry regions. These calculations have to be continued to analyse the development until melt pool formation and RPV failure.

The conclusion from WP5 is that the in-vessel melt retention by external vessel cooling of VVER-440 reactor is normally connected with large thermal margin and defendable also from mechanical point of view. An occurrence of thin metal layer connected with focusing effect may challenge the concept. A correct prediction of the extent of the challenge needs further code development and could not be prepared now. The plant changes to allow the concept of cavity flooding are feasible.

REFERENCES

1. Ikonen, K., ‘Creep model fitting derived from REVISA creep, tensile and relaxation measurements’, Tech. Rep. MOSES-4/99’, VTT Energy, Finland, 27p., 1999.

2. Chu, T.Y., Pilch, M.M, Bentz, J.H., Ludwigsen, J.S, Lu, W-Y. and Humphries, L.L., 'Lower head failure experiments and analyses', *NUREG/CR-5582, SAND98-2047*,1998.
3. Chu, T.Y., Bentz, J.H., Humphries, L.L., Simpson, R.B., Koski, J.M. and Stevens, S.M., 'Quick-Look report for OLHF-1 experiment', *OECD Lower head failure project*, 2000.
4. Sehgal, B.R, Giri, A. and Karbojian, A., 'EC-FOREVER experiments on thermal and mechanical behaviour of a reactor pressure vessel during a severe accident. Technical Report: EC-FOREVER-4 test', *SAM-ARVI-D021, EC 5th EURATOM Framework Program*, Oct., 2002(b).
5. Willschütz, H.-G., E. Altstadt, F.-P Weiß, and B.R. Sehgal, 'Finite Element Pre- and Pos-test Calculations of the FOREVER-Experiments', *Jahrestagung Kerntechnik 2000*, Tagungsbericht S. 187-192, Bonn, Germany, May 2000b.
6. Theerthan, S., Giri, A, Karbojian, A. and Sehgal, B.R., 'EC-FOREVER experiments on thermal and mechanical behaviour of a reactor pressure vessel during a severe accident. Technical Report: EC-FOREVER-3 test', *SAM-ARVI-D016, EC 5th EURATOM Framework Program*, Feb., 2002.
7. Groeneveld, D.C., Cheng, S.C. and Doan, T, '1986 AECL-UO Critical Heat Flux Lookup Table', Heat Transfer Engineering, Volume 7, Numbers 1-2, 1986.
8. Bechta, S.V, 'Water boiling on the corium melt surface under VVER severe accident conditions', Nuclear Engineering and Design, vol. 195, pp. 45-56, 2000.
9. Bonnet J.M. and Villermaux C., 2001 BALI-Metal Test Reports: Focusing Effect Investigations, SAM-ARVI-D2.1.2.
10. Chawla T.C., Chan S.H., 1982, Heat transfer from vertical/inclined boundaries of heat generating boiling pools, Journal of Heat Transfer 104, 465 (1982).
11. Globe, S., Dropkin, D., 1959, Natural convection heat transfer in liquids confined by two horizontal plates and heated from below, Journal of Heat Transfer, pp 24-28.
12. Villermaux C., 1999, Modélisation physique et numérique de la convection naturelle dans une couche fluide de faible rapport d'aspect dans le cadre des études d'accidents graves de réacteurs à eau sous pression, Thèse de l'Institut National Polytechnique de Grenoble, présentée le 2 février 1999.
13. Ikonen, K.: *Creep Model Fitting Derived from REVISA Creep, Tensile and Relaxation Measurements*, Technical Report MOSES-4/99, VTT-Energy, Espoo, Finland, 1999.
14. J. Lemaitre, *A Course on Damage Mechanics*, ISBN 3-540-60980-6, 2nd edition Springer-Verlag Berlin, Heidelberg, New York, 1996.
15. E. Altstadt, Th. Moessner. *Extension of the ANSYS® creep and damage simulation capabilities*. Report, FZR-296, Forschungszentrum Rossendorf, Dresden, Germany, 2000.
16. ANSYS®, Programmer's Manual, ANSYS®, Inc., 2001.
17. Müller, G., Böhmert, J., 2001. *EC-FOREVER-2 Experiment Metallographic post test investigations of the pressure vessel material. Report*, Arbeitsbericht FZR/FWSM – 03/2001, Forschungszentrum Rossendorf, Dresden, Germany.
18. J.L. Rempe, S.A. Chávez, G.L. Thinnes, C.M. Allison, G.E. Korth, R.J. Witt, J.J. Sienicki, S.K. Wang, L.A. Stickler, C.H. Heath, S.D. Snow: *Light Water*

Reactor Lower Head Failure Analysis. Report NUREG/CR-5642, Idaho Falls, 1993.
19. Ikonen K., Large inelastic deformation analysis of steel pressure vessels at high temperature. Technical Research Centre of Finland. Doctoral thesis. VTT Publications 437. ISBN 951-38-5856-1. 141 p + App. 15 p.
20. K. Ikonen, Preliminary calculation of FOREVER penetration tests. VTT Energy, Espoo. October 2001. SAM-ARVI-D012, 22 p.
21. Ikonen K., FEM analysis of EC-FOREVER-3(B) test. VTT Processes, Espoo. December 2002. SAM-ARVI-D026, 39 p.
22. Ikonen K., FEM analysis of EC-FOREVER-4 test. VTT Processes, Espoo. December 2002. SAM-ARVI-D027, 20 p.
23. Theerthan A., Karbojian A. And Sehgal B.R., 'EC-FOREVER Experiment on Thermal and Mechanical Behavior of a Reactor Vessel during Severe Accident. Technical Report-1. EC-FOREVER-2 test', Report SAM-ARVI-D008, March 2001.
24. Devaux J., Mottet G., Bergheau J.M., Bhandari S. And Gilles P.,'Numerical Simulation of EC-FOREVER-2 Test', Report SAM-ARVI-D015, December 2001.
25. Asmolov V., Kobzar L., Nickulshin V., Strizhov V., 1998, Experimental study of heat transfer in the slotted channel at CTF facility OECD/CSNI Workshop on In-Vessel Core Debris Retention and Coolability, Garching, Germany, March 3-6, 1998.
26. Henry R.E., Hammersley R.J., 1996, Quenching of metal surfaces in a narrow annular gap, Fifth Int. Conf. on Simulation Methods in Nuclear Engineering, Sept 8-11, Montreal Canada.
27. Horner P., Zeisberger A., Mayinger F., 1999, Boiling and flow regimes in a gap with adjustable inclination and heating from the top, NURETH 9 San Francisco, California, Oct 3-8, 1999.
28. Jeong J.H., Park R.J., Kang K.H., Kim S.B., Kim H.D., 1998, Experimental study on CHF in a Hemispherical Narrow Gap, OECD/CSNI Workshop on In-Vessel Core Debris Retention and Coolability, Garching, Germany, March 3-6, 1998.
29. Köhler W., Schmidt H., Herbst O., Krätzer W., 1998a, Thermohydraulische Untersuchungen zur Debris/Wand-Wechselwirkung (DEBRIS), Abschlussbericht Project N° 150 1017, November 1998.
30. Köhler W., Schmidt H., Herbst O., Krätzer W., 1998b, Experiments on Heat Removal in a Gap between Debris Crust and RPV Wall, OECD/CSNI Workshop on In-Vessel Core Debris Retention and Coolability, Garching, Germany, March 3-6, 1998. Also in 1st European-Japanese Two-Phase Flow Group Meeting, 36th European Two-Phase Flow Group Meeting Portoroz 1-5 June. Also in 7th Conference on Nuclear Engineering Tokyo, Japan, April 19-23, 2000 ICONE 7012.
31. Murase M., Kohriyama T., Kawabe Y., Yoshida Y., Okano Y., 2001, Heat transfer models in narrow gaps ICONE 9 Meeting, 9th International conference on Nuclear Enginering,. Nice France, April 8-12
32. OECD document, 1993, Three Mile Island Reactor Pressure Vessel Investigation Project Proceedings from the OECD/NEA/NRC meeting Boston (USA) 20-22 October 1993.

33. Yang Z.L., Dinh T.N., Sehgal B.R., 1999, An analytical study of critical heat flux in a narrow gap, Multiphase Flow and Heat Transfer. Proc. of the Fourth International Symposium Aug. 22-24, 1999, Ki'an China.
34. Chung S.K., Liu L.P., Tien C.L., 1980, Flooding in two-phase counter current flows, II Experimental investigation, Physicochem. Hydrodyn. , vol. 1, pp 209-220.
35. Seiler J.M., 2001, Model for CHF in narrow gaps in vertical and hemispherical geometries, SAM-ARVI-D010.
36. Bernaz L., Bonnet J.M., Spindler B., Villermaux C., 1998a, Thermalhydraulic phenomena in corium pools: numerical simulation with TOLBIAC and experimental validation with BALI, Workshop on in-vessel core debris retention and coolability, Garching Germany, 3rd-6th March 1998.
37. Bernaz L., Bonnet J.M., Spindler B., Villermaux C., 1998b, Thermalhydraulic phenomena in corium pools: numerical simulation with TOLBIAC and experimental validation with BALI, Third International Conference on Multiphase Flow, ICMF98, Lyon, France, June 8-12, 1998.
38. Kymäläinen O., 2002, COPO experiments, stratified pool tests with paraffin oil in the upper layer tests P20 and P21, note Fortum Nuclear Services Ltd, Finland– May 2002.
39. Cartellier A., 2001, Cours d'écoulements diphasiques, DEA MFT/DEA énergétique physique/ENSHMG, janvier 2001.
40. Koster Jean N., Prakash A., Fujita D., 1992, Benard and Marangoni convection in immiscible layers, ASME 28th National Heat transfer conference, August 1992, San Diego.
41. Angeli P. , Hewitt G.F., 1998, Pressure gradient in horizontal liquid-liquid flows, international journal of Multiphase Flow, (24), pp 1183-1203.
42. Kelkar K.M., Patankar S.V., 1993, Turbulence model for melt pool natural convection heat transfer, ANS Reactor Safety meeting, Oct 25-28 1993, Washington DC.
43. Mayinger F., Jahn F., Reinecke H., Steinberner U., 1976, Examination of thermohydraulic processes and heat transfer in a core melt, BMFT RS 48/1, Hanover, Germany.
44. Fishenden M., Saunders O.A., 1950 cited by McAdams W.H., 1959, Heat transmission, Mc Graw Hill.
45. Churchill S.W., Chu H.H.S.,1975, Correlating equations for laminar and turbulent free convection from a vertical pipe, Int. J. Heat and Mass Transfer, vol 18, pp 1323-1328.
46. Vandroux S., 2002, Assessment of the TOLBIAC code on the COPO stratified pool tests P20 and P21, SAM-ARVI-D024.
47. Bonnet, J. M.: An Integral Model for the Calculation of Heat Flux Distribution in a Pool with Internal Heat Generation, Proc. NURETH-7, Saratoga, USA, September 1995.
48. Theofanous, T.G. et al.: In-vessel coolability and retention of a core melt, DOE/ID-10460, Vols. 1 and 2 (1996) [also Nucl. Engrg. Des., 169, 1-48 (1997)].
49. Villermaux, C.: Modélisation physique et numérique de la convection naturelle dans une couche de fluide de faible rapport d'aspect dans le cadre des études d'accidents graves de réacteurs à eau sous pression, Ph.D. thesis, Institut National Polytechnique de Grenoble, February 1999.

50. Schmidt, W., Bürger, M. and Widmann, W.: Investigations of Constitutive Laws and 2D Effects on Debris Coolability, 2nd Conference on Computer Methods for Engineering in Porous Media Flow and Transport, Besançon, France, July 10-13, 2000.
51. Bürger, M. et al.: Ausbau und Verifikation der Spätphasenmodelle und des Gesamtmodells zum Kernschmelzen in KESS und ATHLET-CD, Universität Stuttgart, IKE 2-145, Mai 2001
52. Seiler, J.M.: Model for CHF in narrow gaps in vertical and hemispherical geometries, CEA Grenoble, SAM-ARVI-D10 (SETEX/LTEM/01-251), May 2001.
53. Dienstbier : Estimation Of Debris Mass And Heat In The VVER-440 Reactor Vessel Bottom Head. SAM-ARVI-D007. October 2000.
54. J. Dienstbier : Analysis of In-Vessel Retention Scheme for VVER 440/213 Reactors. SAM-ARVI-D023. September 2002.
55. J. Dienstbier, J. Duspiva, P. Vokáč : Detailed model of VVER-440 reactor core damage using the MELCOR code (in Czech). ÚJV 11667-T. October 2001.
56. O. Kymäläinen, H. Toumisto, T.G. Theofanous: In-vessel retention of corium at the Loviisa plant. *Nuclear Engineering and Design 169 (1997) p:109-130.*
57. T.G. Theofanous, C. Liu, S. Additon, S. Angelini, O. Kymäläinen, T. Salamssi : In vessel coolability and retention of a core melt. *Nuclear Engineering and Design 169 (1997) p.1-48.*
58. P. Kostka, R. Taubner, Zs. Téchy : Assessment of In-Vessel Melt Retention for VVER-440/213 Reactors. SAM-ARVI-D028. November 2002.

TABLES

Table I: Sequence of water injection into vessel.

Time (sec)	Event
00	Point of reference of data (dataset – 37685.0 s).
06	Heater off – All three valves were opened – water feed to vessel started. The water injected was about 5 Lit.
17	Water and melt contact
115	About 3 Lit of water is injected
385	About 2.8 Lit of water injected
495	About 3 Lit of water injected
945	About 2.5 Lit of water injected
1980	About 3 Lit of water injected
3520	About 5 Lit of water injected. The last injection.

Table II: Geometrical details used in RELAP model for FOREVER analysis

Hydrodynamic Component (No of volumes) (Ref to Fig 2.)	**Flow Area (m^2)**	**Flow length (m)**	**Hyd. Dia (m)**
506 – Vessel (snglvol)	0.11009347	0.535	0.3744
507 (Pipe with 4 vol)	50.2655E-06	.065, 103.3 × 3	0.008
508 (Pipe with 4 vol)	50.2655E-06	-0.485, 113.3 × 3	0.008

509 (Pipe with 4 vol)	50.2655E-06	-0.535, 101 × 3	0.008
561, 562 and 563 – On-off Valves.	35.2564E-06		0.0067
510 (Pipe with 4 vol)	50.2655E-06	0.4 × 2, -0.45 × 2	0.008
511 (Pipe with 4 vol)	50.2655E-06	0.31 × 2, -0.2 × 2	0.008
512 (Pipe with 4 vol)	50.2655E-06	0.375 × 2, -0.2 × 2	0.008
100 (Pipe with 4 vol)	1.9635E-03	0.25 × 4	0.05
101 (Pipe with 4 vol)	0.4909E-03	0.25 × 2, 0.35 × 2	0.025
102 (Pipe with 4 vol)	1.9635E-03	0.25 × 4	0.05
103 (Pipe with 4 vol)	0.4909E-03	0.25 × 2, 0.35 × 2	0.025
551, 552, 553, 151, 152, 153, 154, 155 are Junctions. (sngljun)			

Table III: Summary of the main results.

	P20	***P10***	**P21.1**	**P21.2**	***P9***
Total cooling power (kW)	5.72	*9.2*	6.57	7.26	*8.8*
Cooling power of the curved boundary next to lower layer (%)	76.5	*48.9*	95.2	84.1	*55.7*
Cooling power of the side boundary next to upper layer (%)	7.3	*9.9*	4.8	3.9	*6.8*
Cooling power of the upper boundary (%)	16.2	*41.2*	-	12.0	*37.5*
Average heat flux at the curved boundary next to lower layer (kW/m^2)	20.0	*20.3*	26.7	26.1	*19.7*
Average heat flux at the side boundary next to upper layer (kW/m^2)	5.3	*11.9*	7.0	6.4	*12.2*
Average heat flux at the upper boundary (kW/m^2)	4.9	*21.4*	-	4.6	*19.2*

Table IV: Summarised results.

	Water average temperature [°C]	Paraffin average temperature [°C]	Water lateral heat flux [kW]	Paraffin lateral heat flux [kW]	Paraffin upper heat flux [kW]
COPO	**50**	**34.4**	**4.38**	**0.42**	**0.93**
Reference Kelkar	78.5	31.8	4.65	0.33	0.73
Tsol = -40°C	75.8	9	4.48	0.39	0.85
$\lambda = 0.3$	73.4	26.4	4.35	0.42	0.94

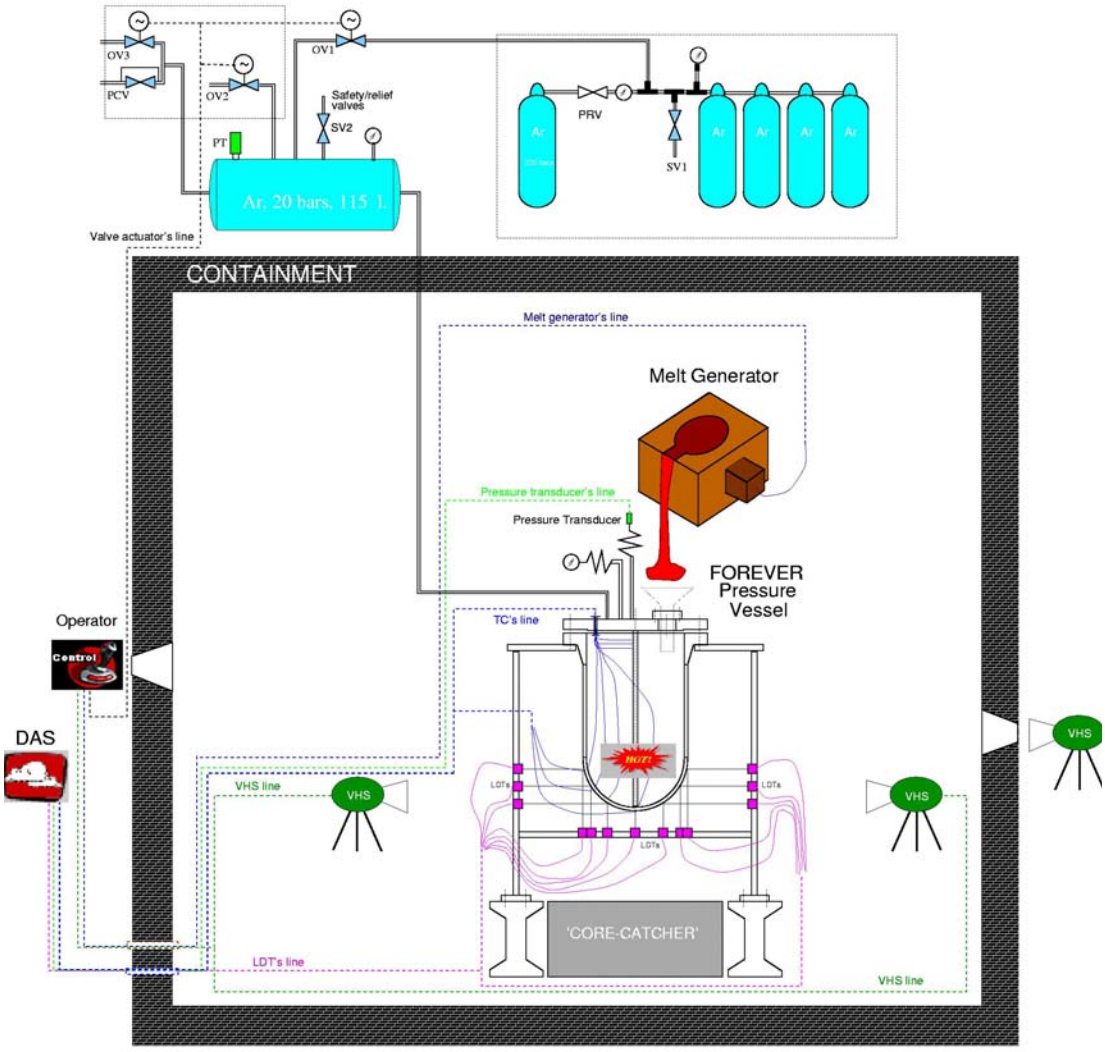

Figure 1: Schematic of the facility arrangement inside the containment.

Figure 2: Post-test view of the failure site in EC-FOREVER-2 test.

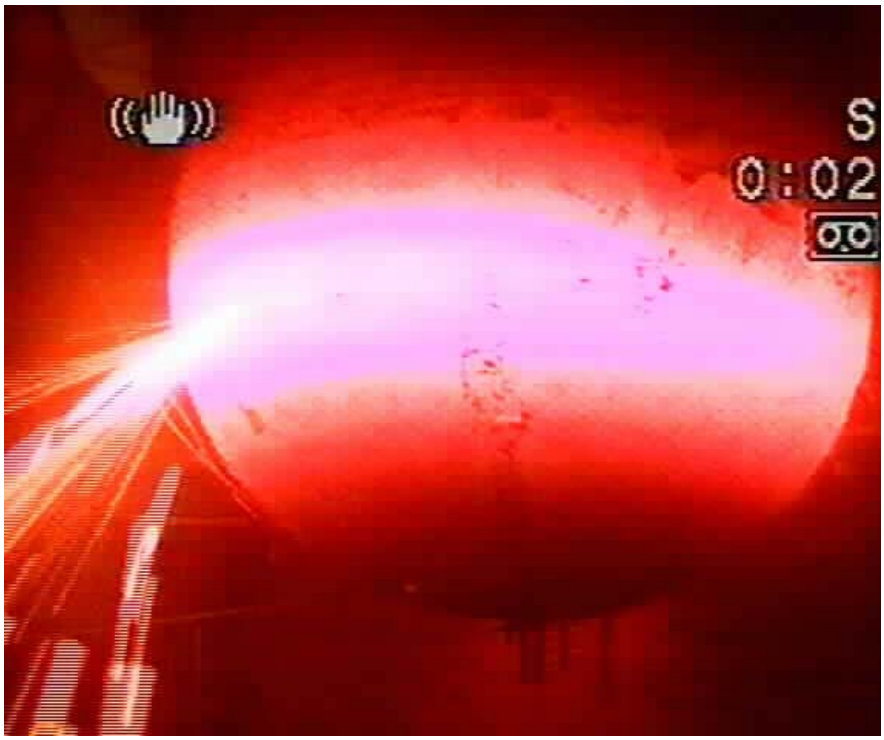

Figure 3: Vessel during failure in EC-FOREVER-3(B) Experiment.

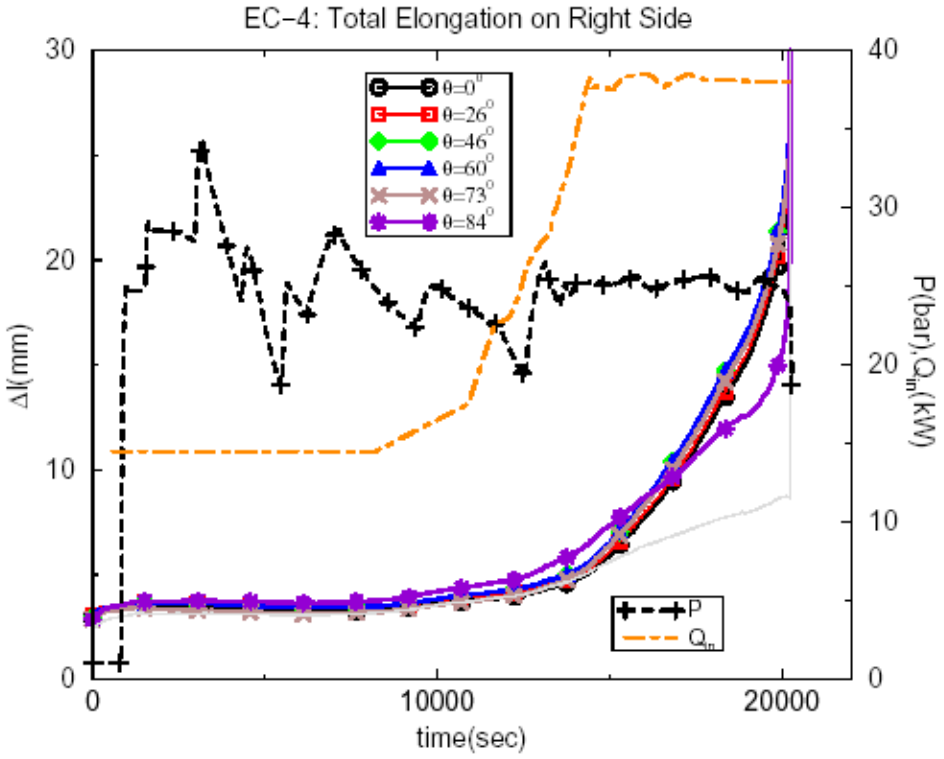

Figure 4: Time histories of displacement of the external vessel wall(right side), time histories of pressurization inside the vessel and time histories of heat input to the melt in EC-FOREVER-4.

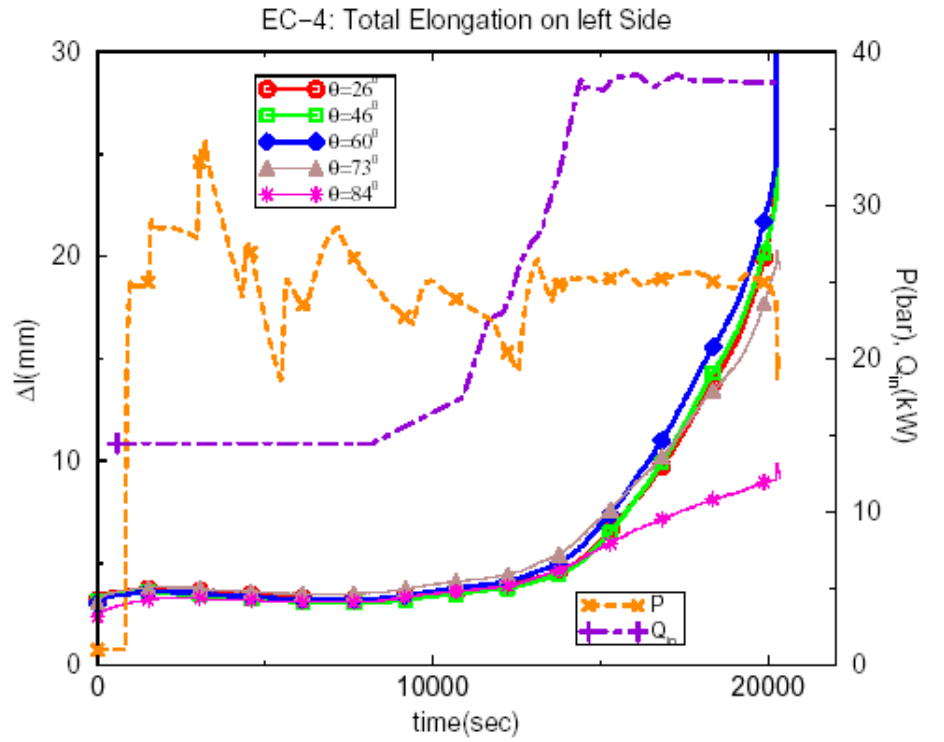

Figure 5: Time histories of displacement of the external vessel wall (left side), time histories of pressurization inside the vessel and time histories of heat input to the melt in EC-FOREVER-4.

Figure 6: Failure site of the vessel in EC-FOREVER-4 experiment.

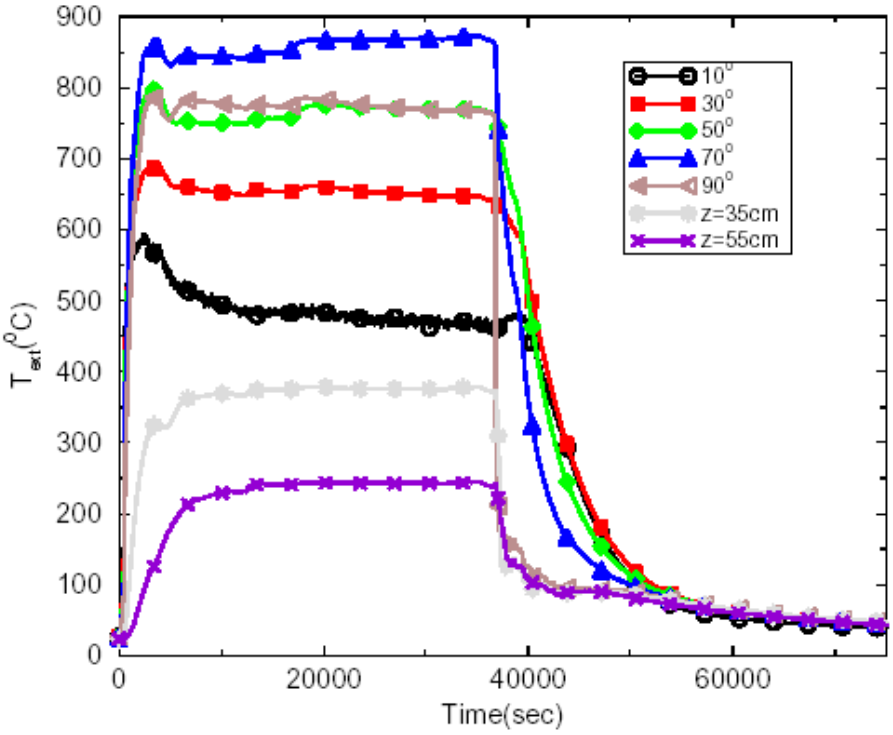

Figure 7: Time history of external wall temperatures on the right side in EC-FOREVER-5 experiment.

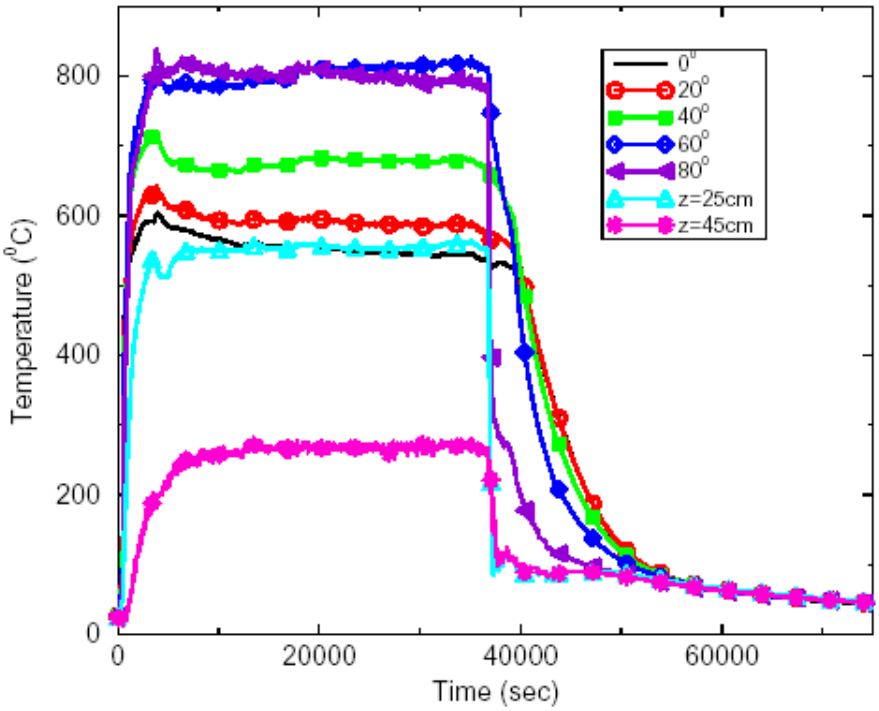

Figure 8: Time history of external wall temperatures on the left side in EC-FOEVER-5 experiment.

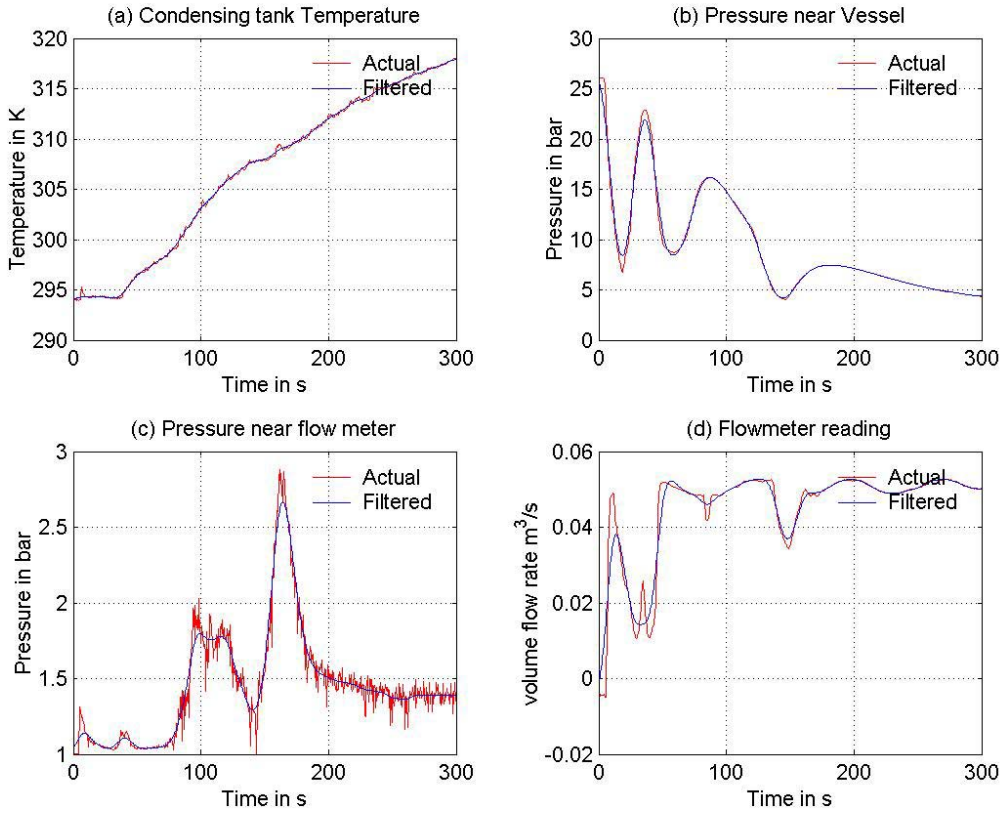

Figure 9: Experimental data (filtered and non filtered)

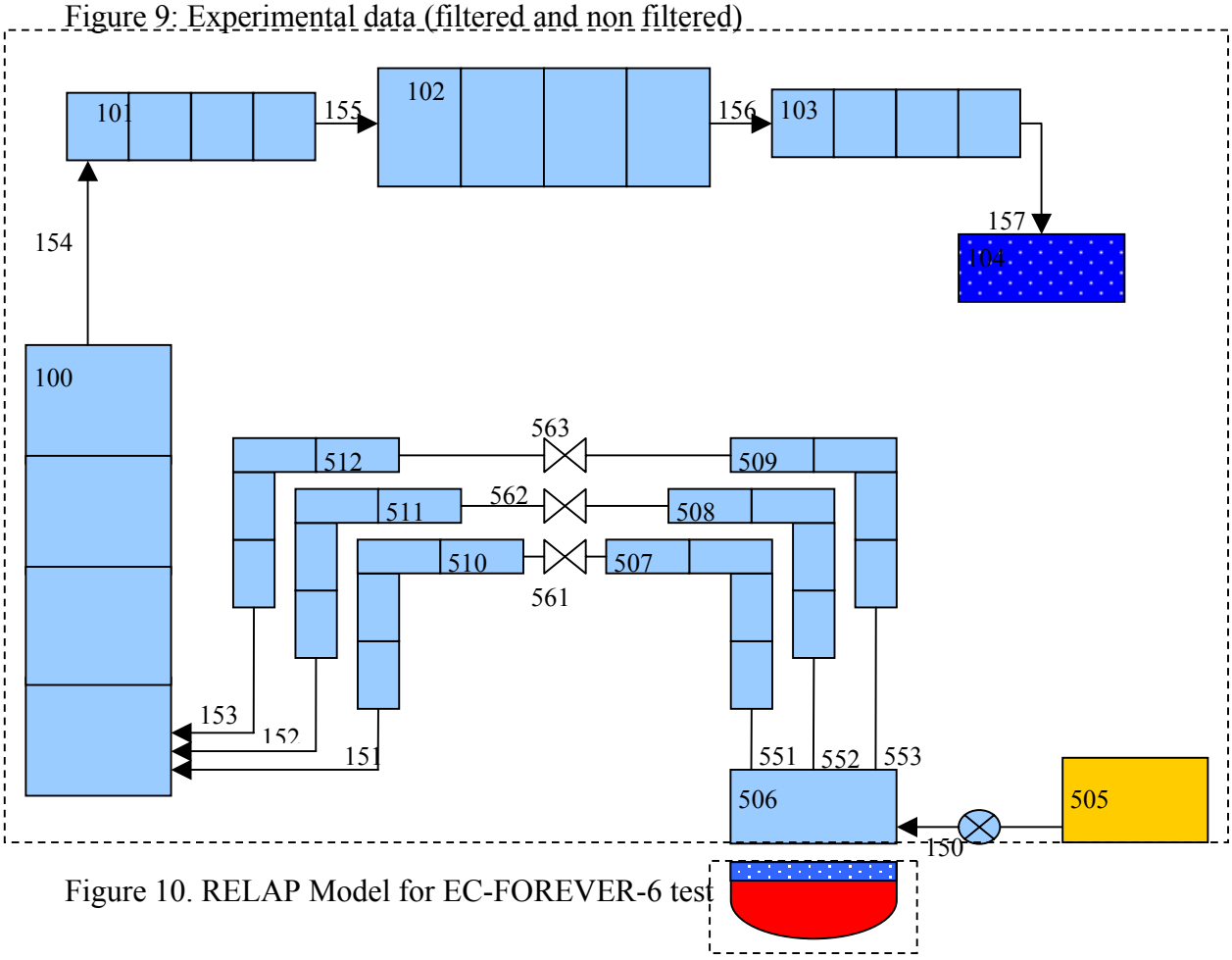

Figure 10. RELAP Model for EC-FOREVER-6 test

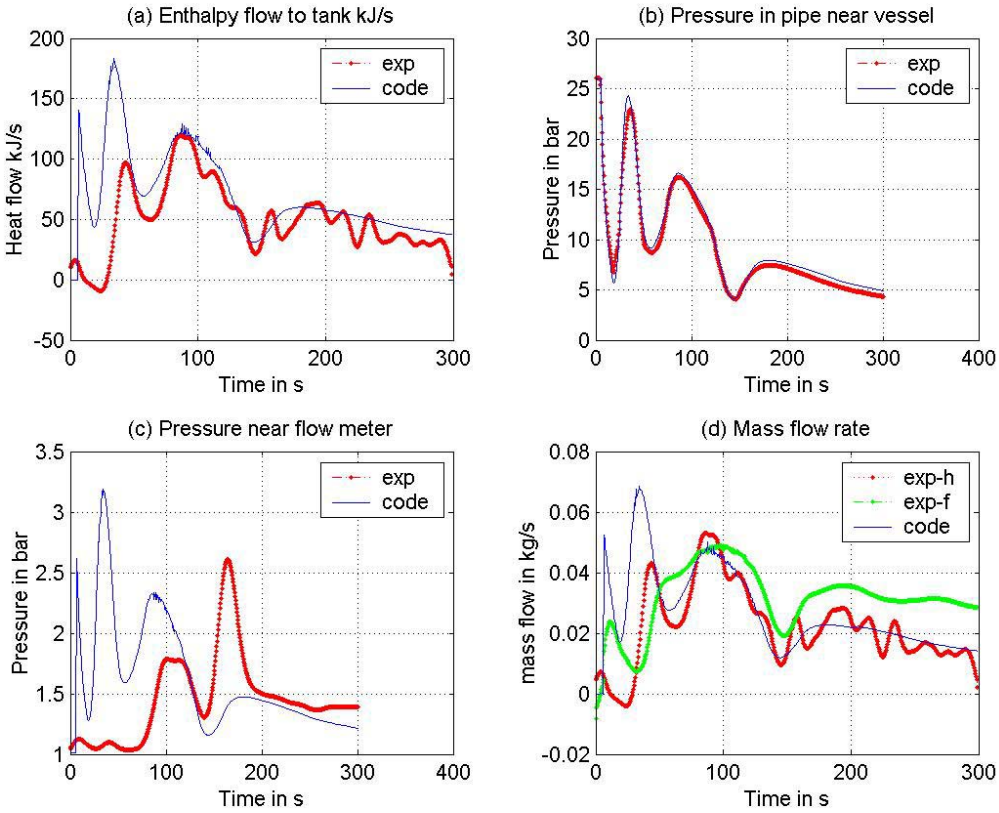

Figure 11: Experimental and code results comparison

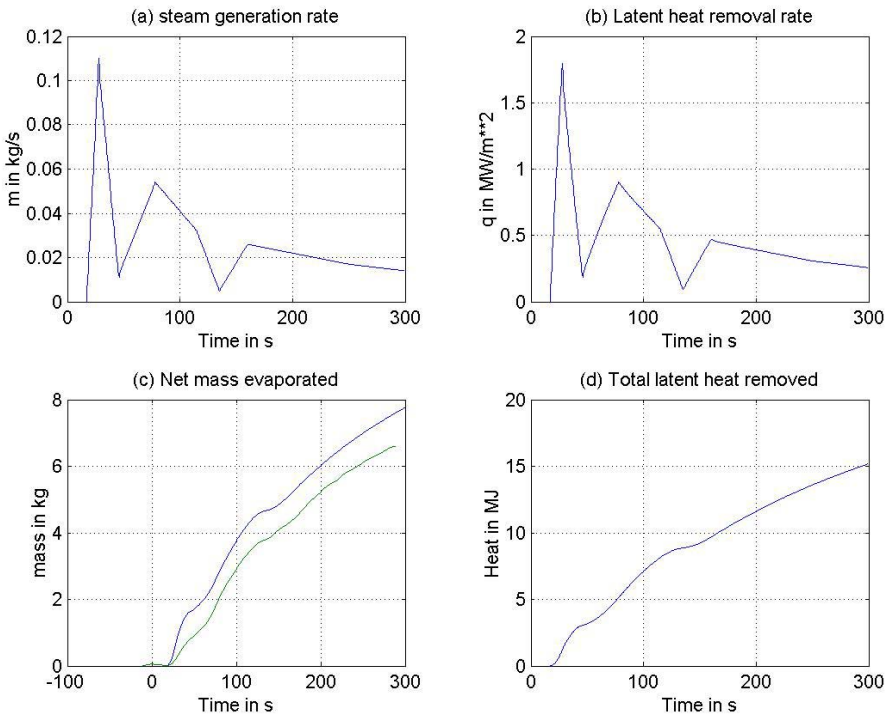

Figure 12: Heat flux and mass generation rates.

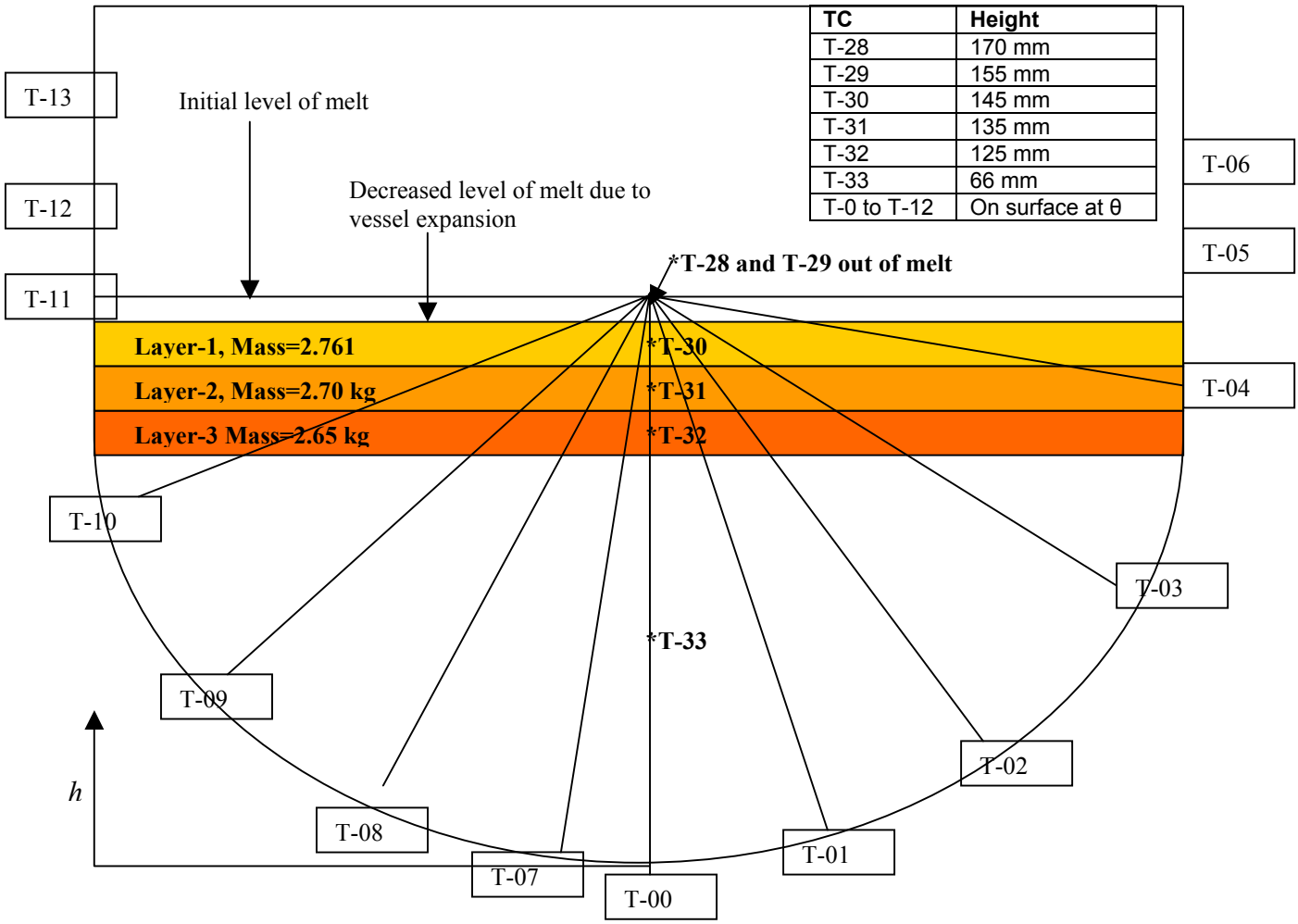

TC	Height
T-28	170 mm
T-29	155 mm
T-30	145 mm
T-31	135 mm
T-32	125 mm
T-33	66 mm
T-0 to T-12	On surface at θ

Figure 13 Thermocouple locations after vessel expansion

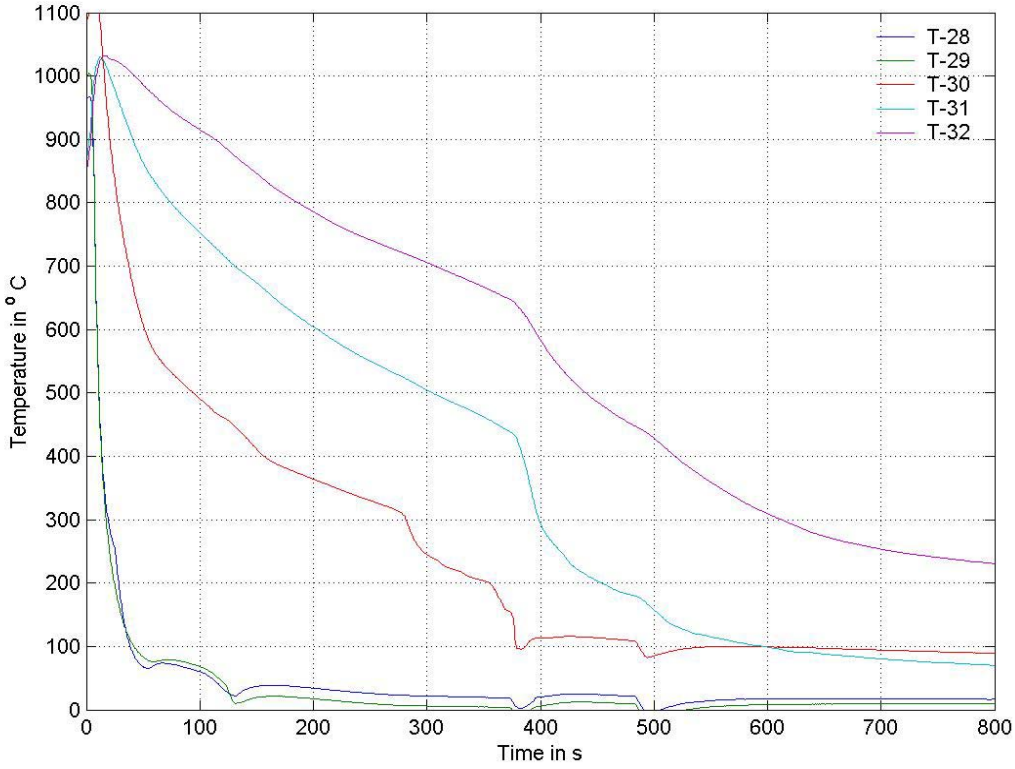

Figure 14: Melt centerline temperature variation for initial 800 seconds.

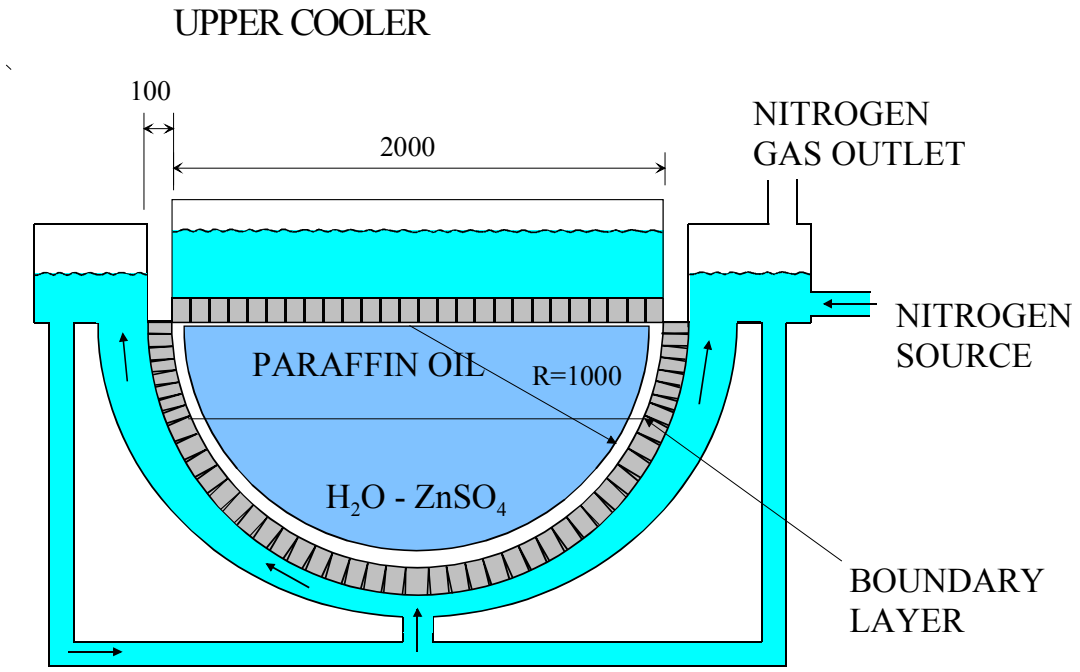

Figure 15: A schematic of the COPO facility.

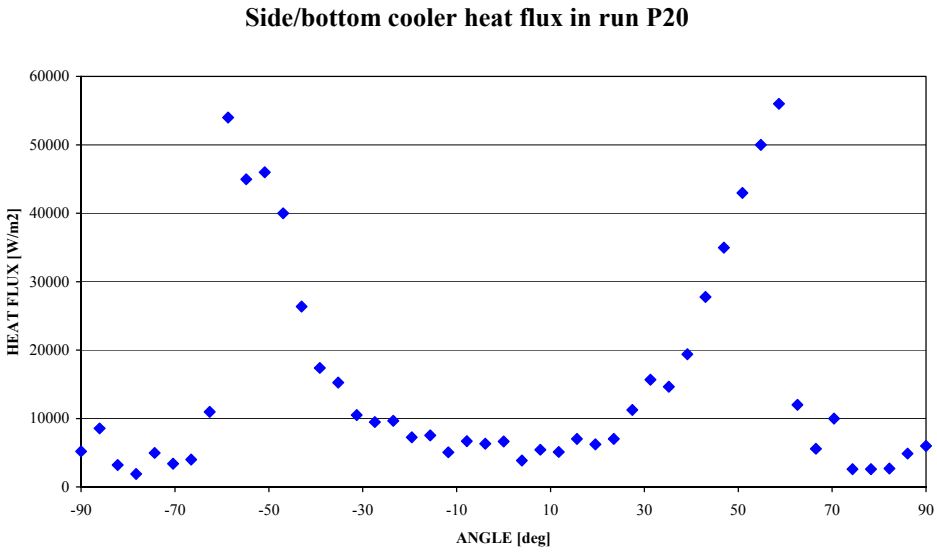

Figure 16. The heat flux profile at the curved boundary in the test P20.

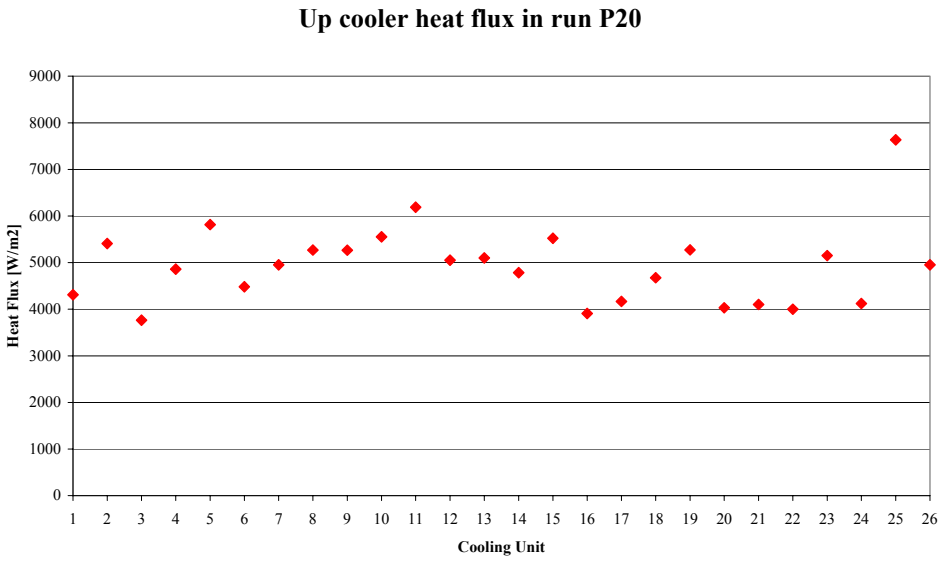

Figure 17. The heat flux profile at the upper boundary in the test P20.

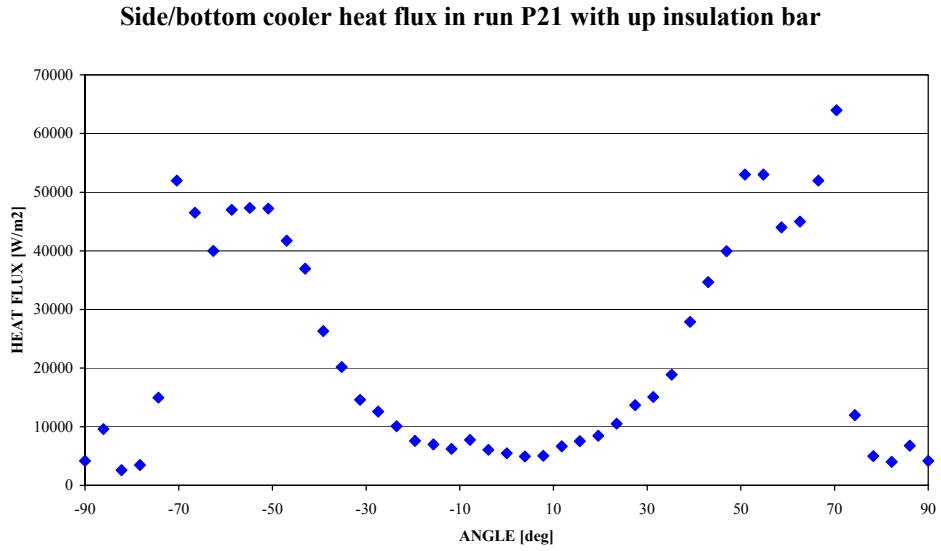

Figure 18. The heat flux profile at the curved boundary in the test P21.1.

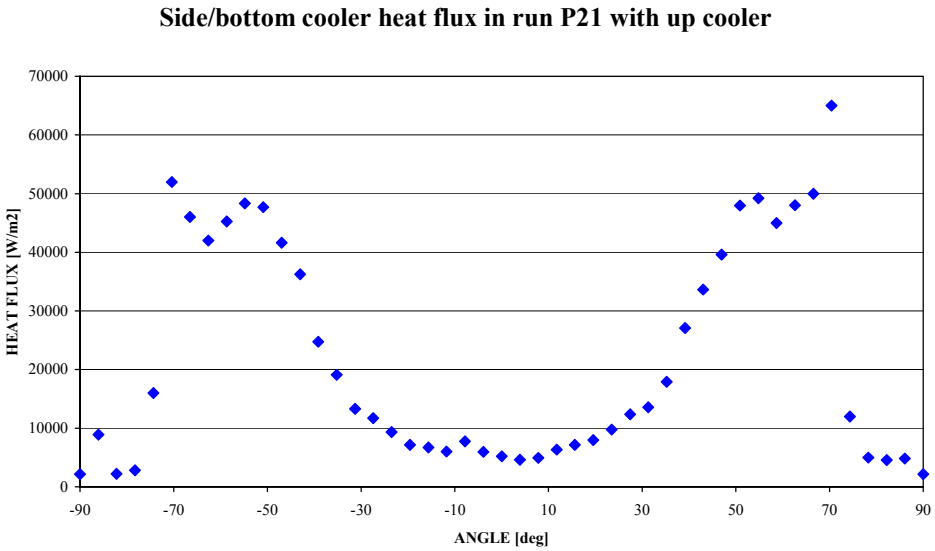

Figure 19. The heat flux profile at the curved boundary in the test P21.2.

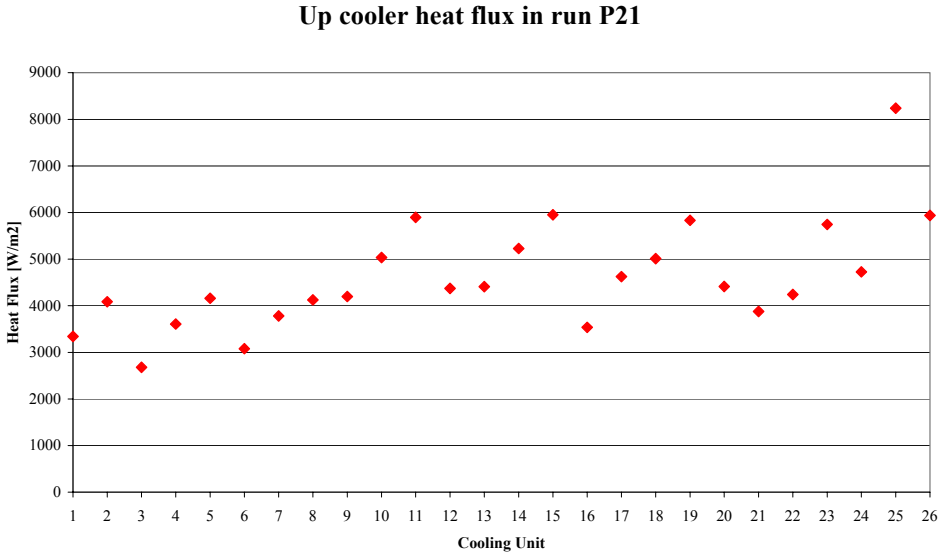

Figure 20. The heat flux profile at the upper boundary in the test P21.2.

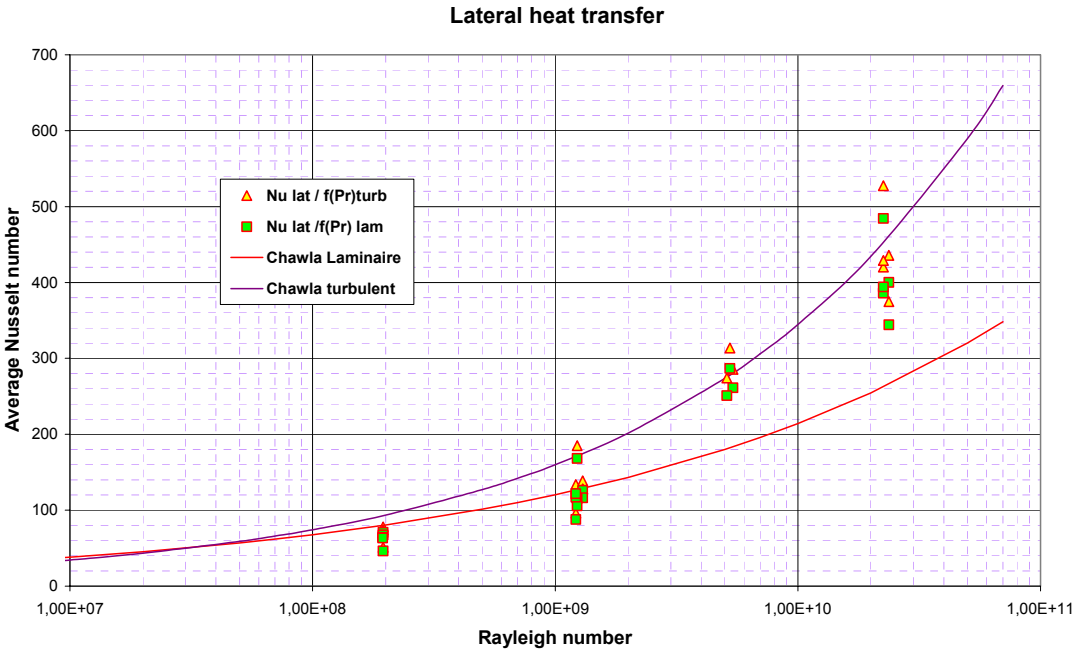

Figure 21: BALI-metal average lateral heat transfer: experiment and Chawla correlations.

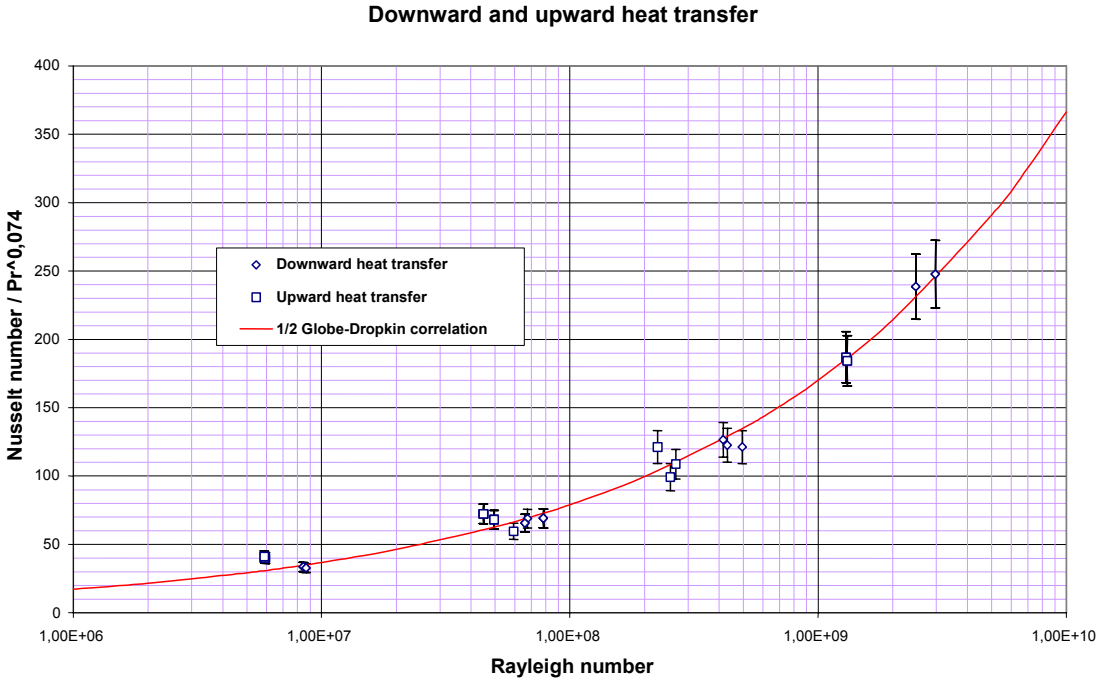

Figure 22: BALI-metal average downward and upward heat transfer: experiment and Globe and Dropkin correlation

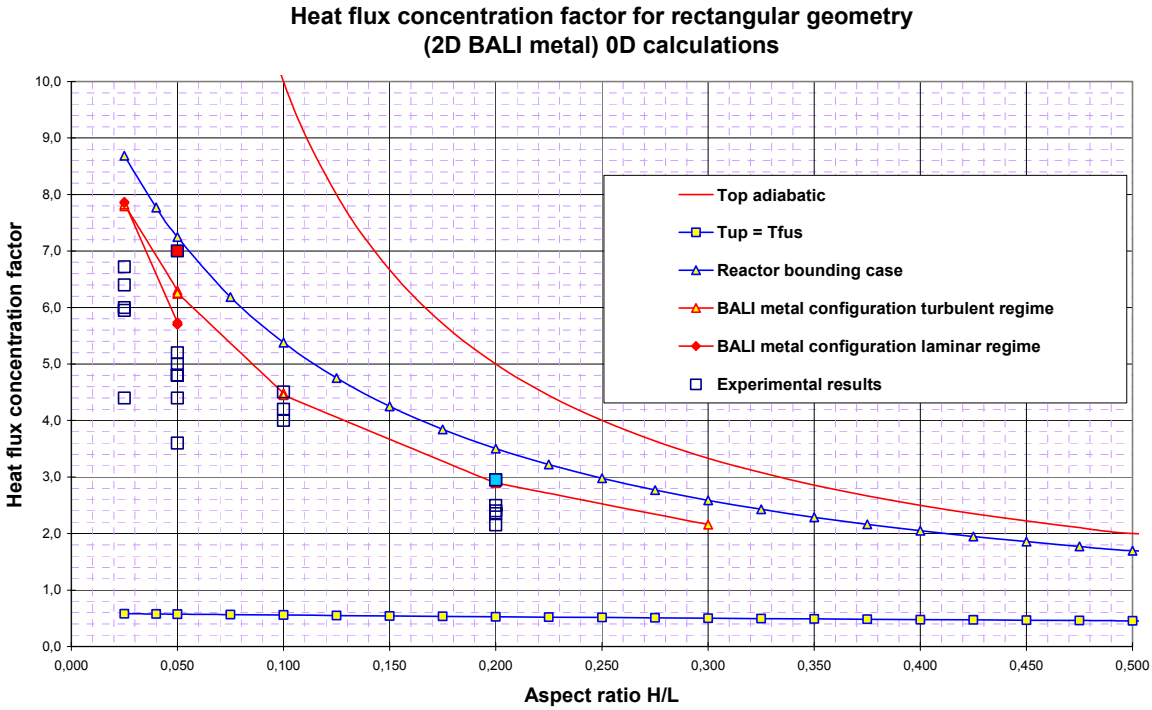

Figure 23: BALI-metal concentration factor in 2D geometry

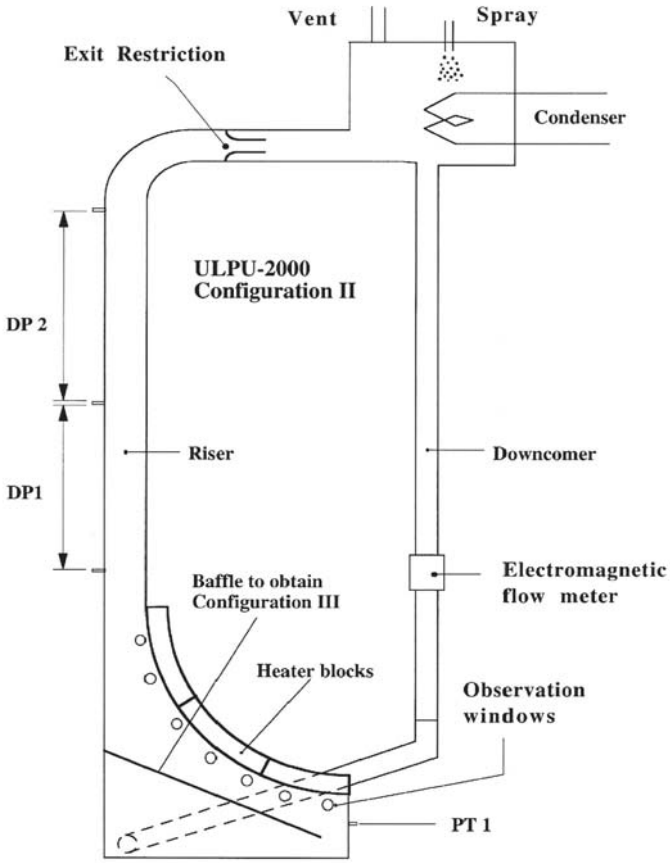

Figure 24: A schematic of the ULPU-2000 facility. The exit restriction is 4" in diameter.

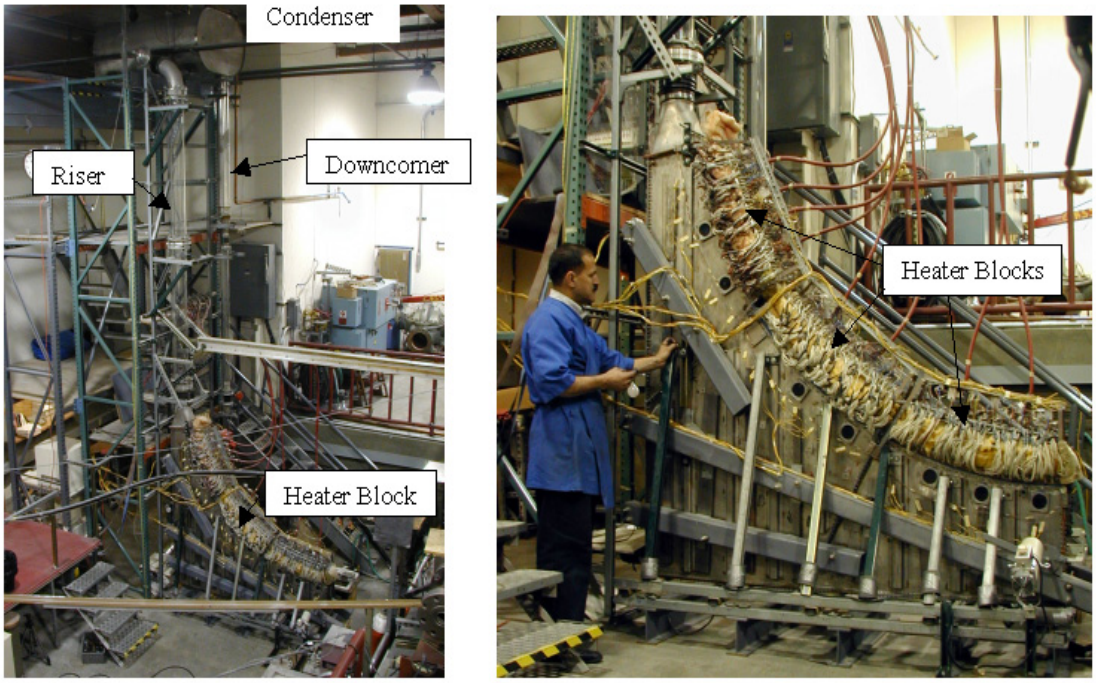

Figure 25: An overall view of the ULPU facility as it exists toda

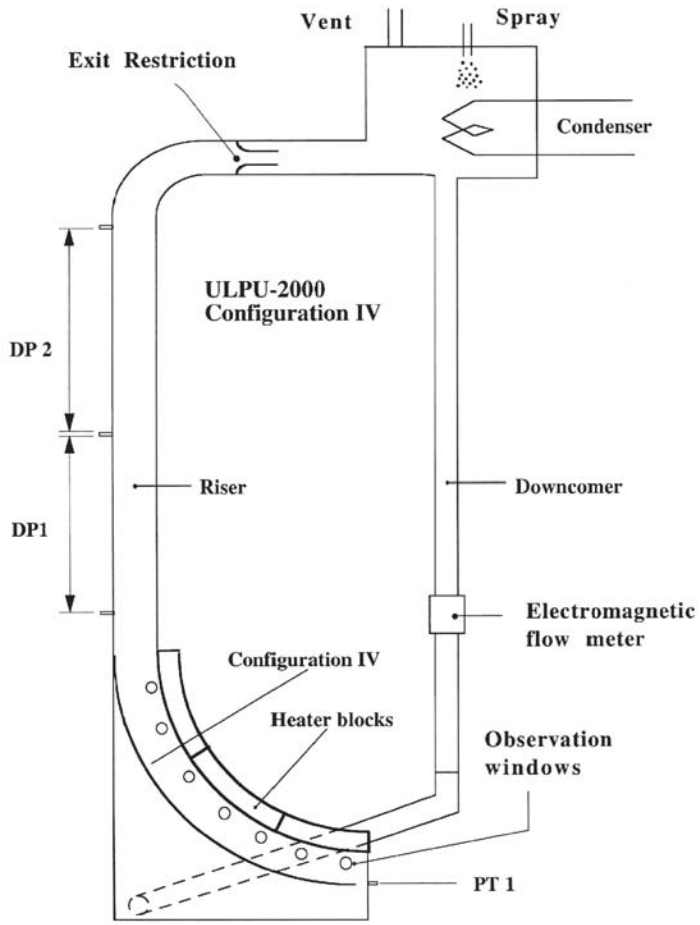

Figure 26: Schematic of the ULPU-2000 Configuration IV.

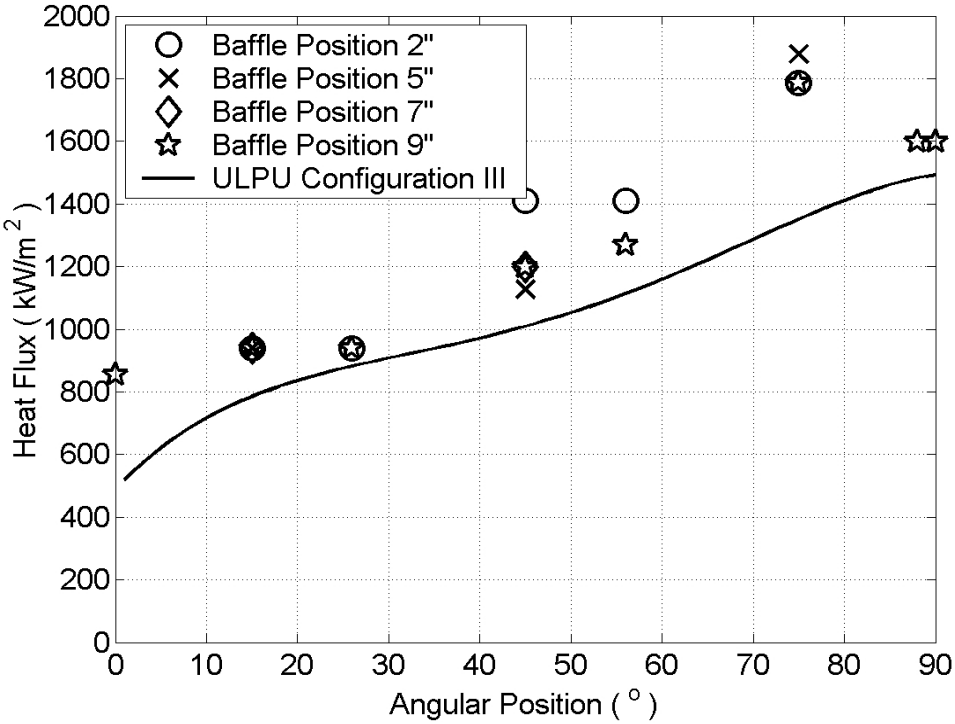

Figure 27: Critical heat fluxes as measured in ULPU-2000 Configuration IV.

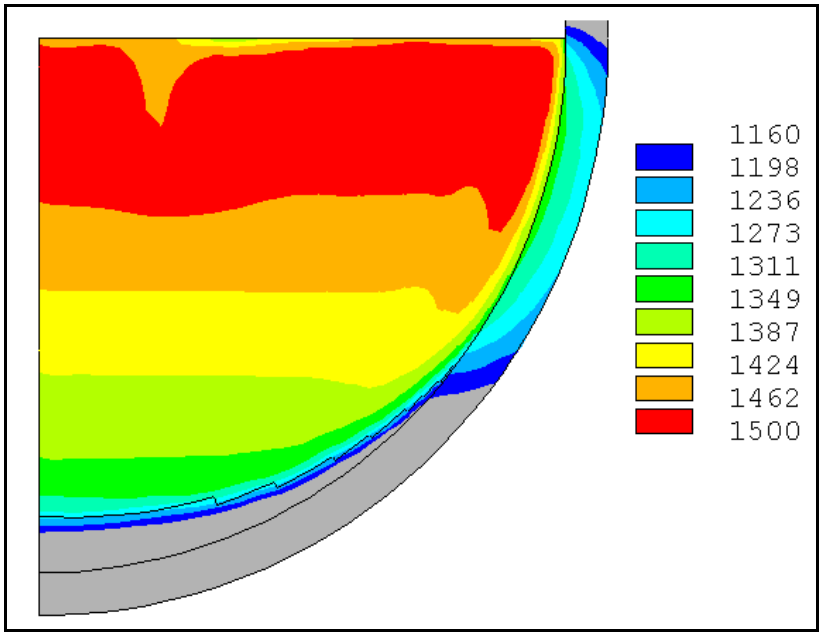

Figure 28: Calculated temperature field (T in [K]).

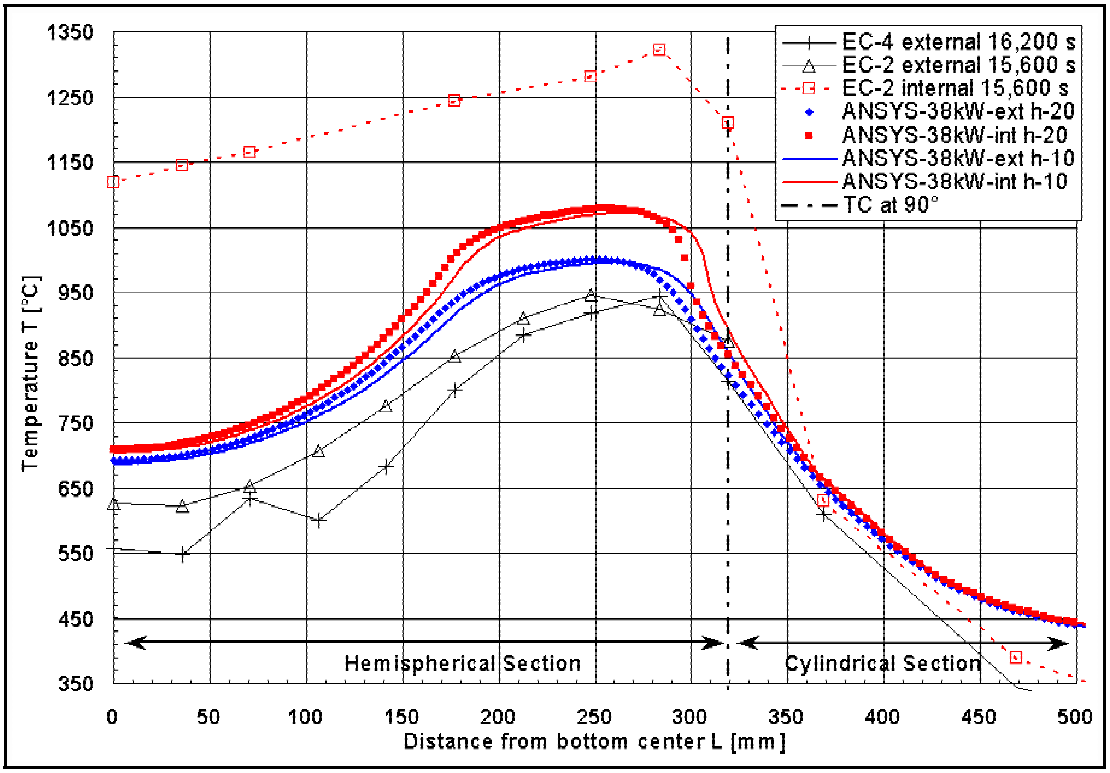

Figure 29: Temperatures along the vessel wall inside or outside starting from the lower head south pole to the welding line and the cylindrical part. Comparison of EC-2 and EC-4 with different melt level heights in the ANSYS calculations (10 mm or 20 mm below welding line).

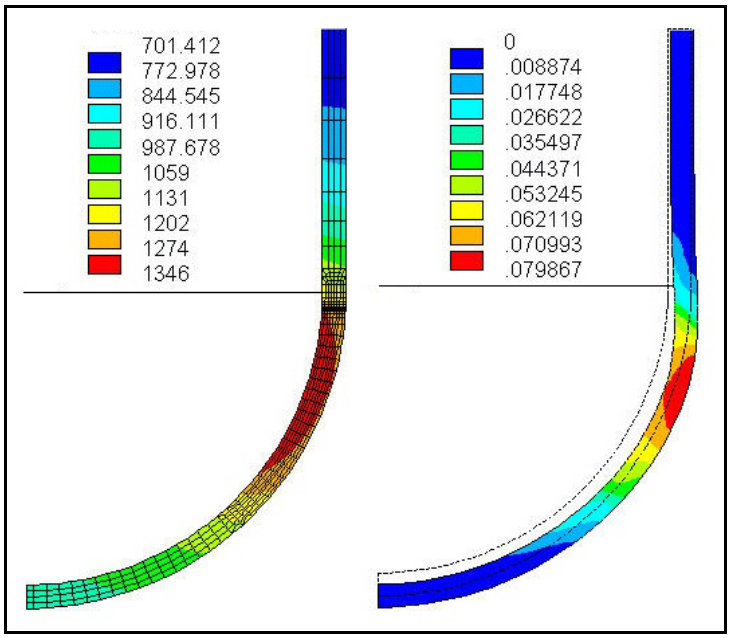

Figure 30: Temperature field (left side, max. 1346 K) and local creep strain (right side, max. 7.99%) after t=1 h in the calculation (38 kW, 25 bar).

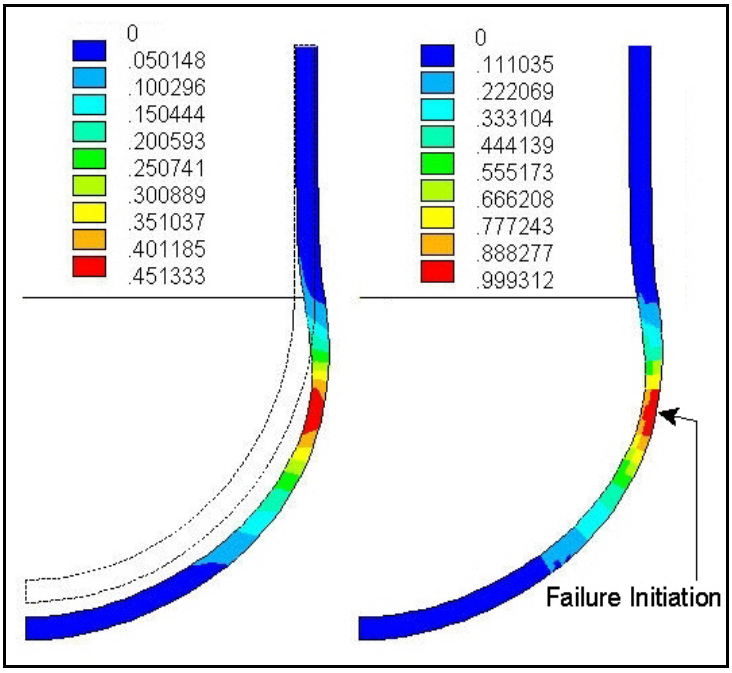

Figure 31: Local creep strain (left side, max. 45.13%) and damage (right side, max. 0.9993) at the calculated rupture begin after t=4:05 h (38 kW, 25 bar). The expected crack initiation position is indicated.

Figure 32: Micrograph of a polished, non-etched sample just above the final crack position (ca. 50 mm below the welding line; left side: wall inside; right side: wall outside). Dark areas indicate voids: creep pores and cracks.

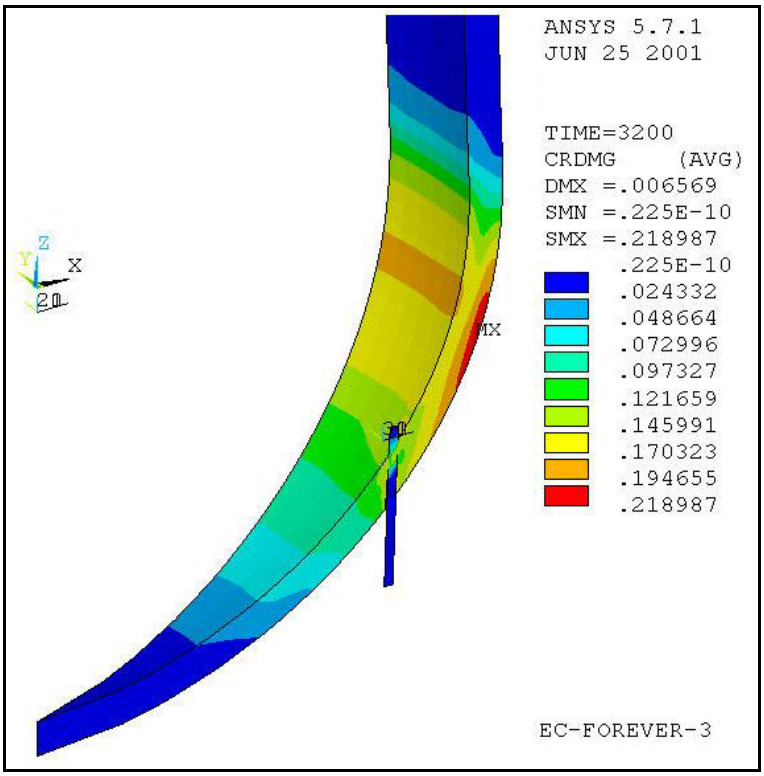

Figure 33: Damage plot after a pressure load of 25 bar over 3200 s.

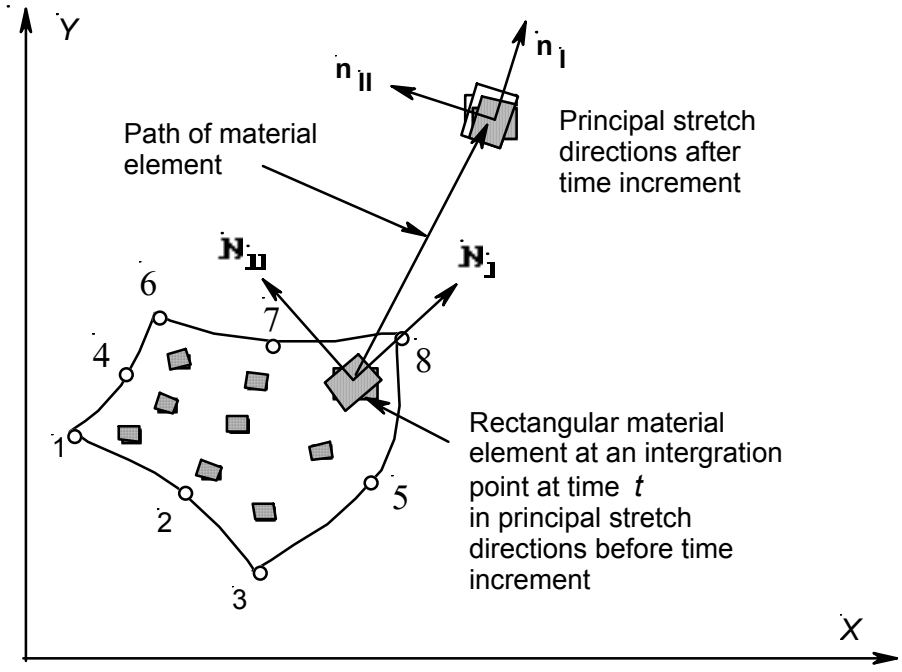

Figure 34: Illustration of principal stretch directions in a 2D case.

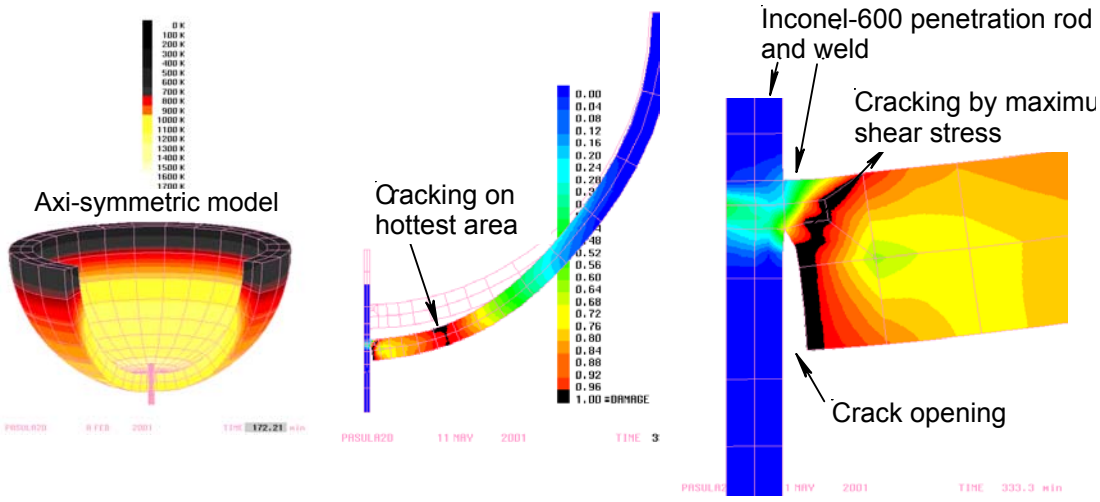

Figure 35: Pre-analysis of FOREVER penetration 1:10 test by axisymmetric FEM model.

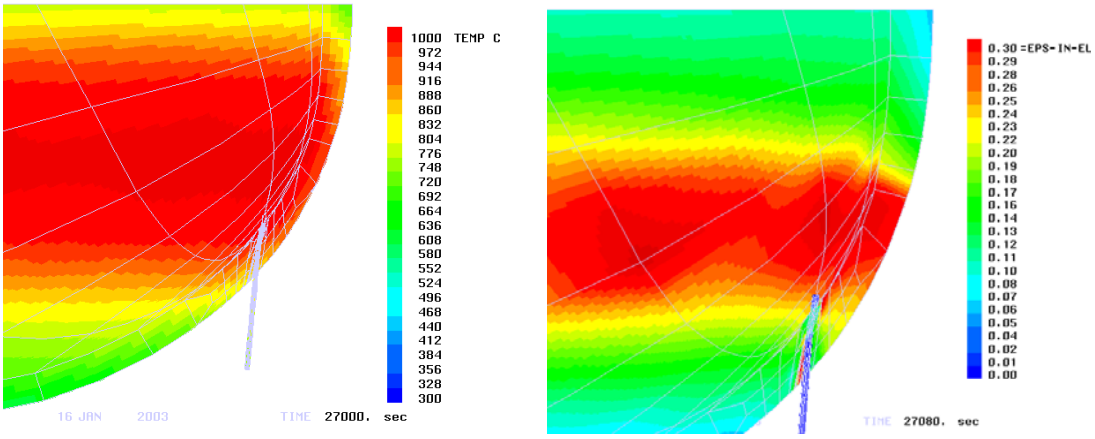

Figure 36: Temperature distribution and calculated inelastic strain distribution of the EC-FOREVER-3(B) test.

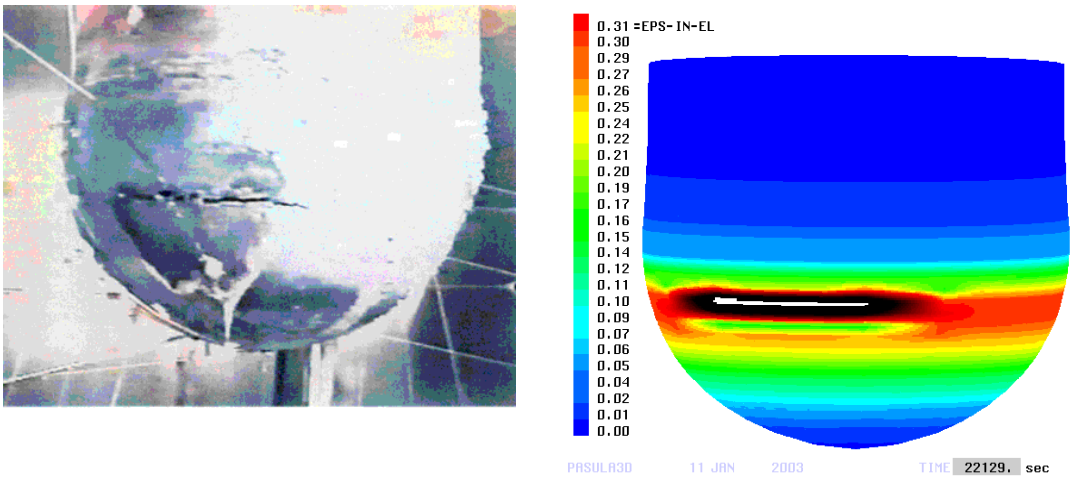

Figure 37: Photograph of the EU-FOREVER-3(B) experiment and calculated leak opening (shown by white colour).

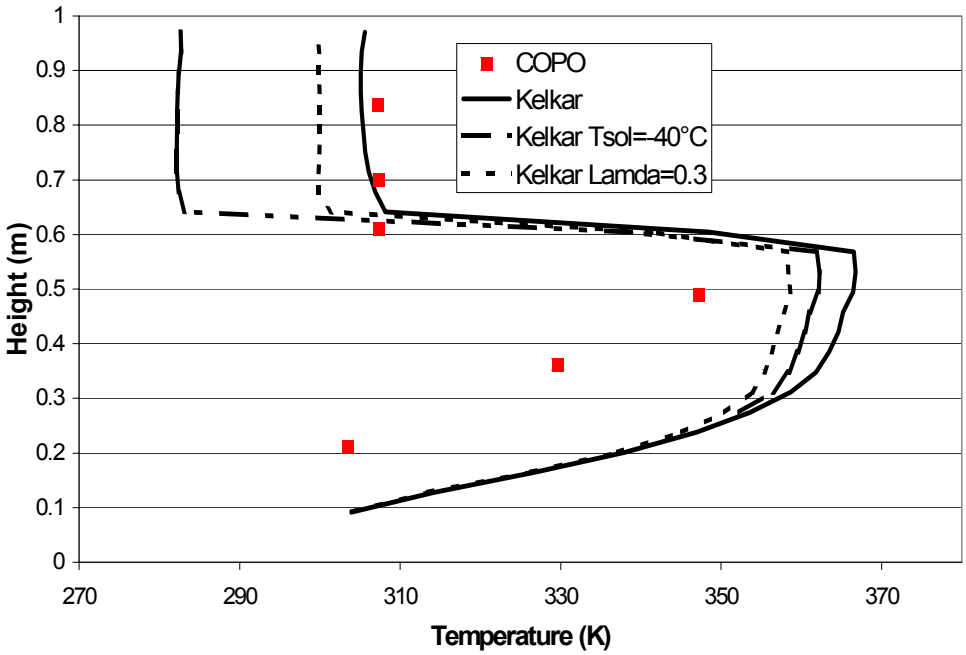

Figure 38: Temperature at 0.47m from the axis.

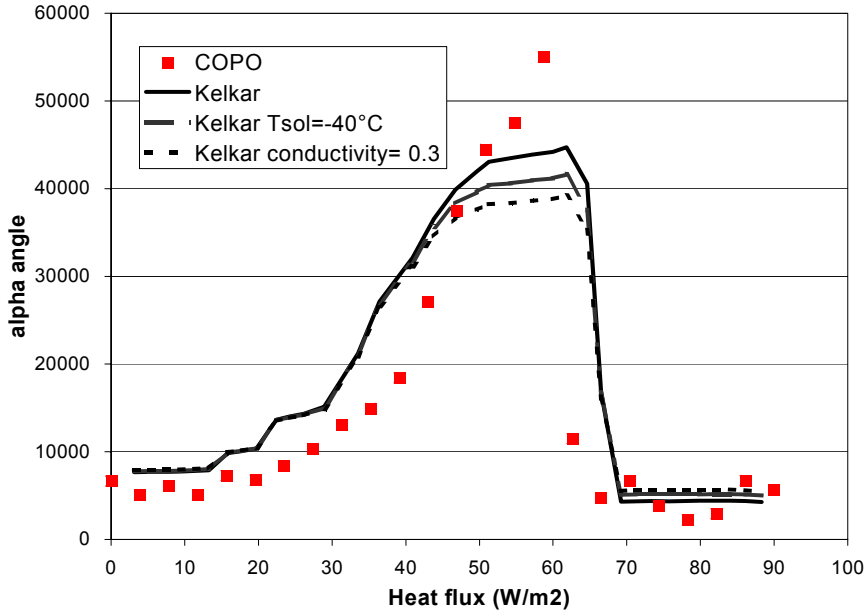

Figure 39: Lateral heat flux

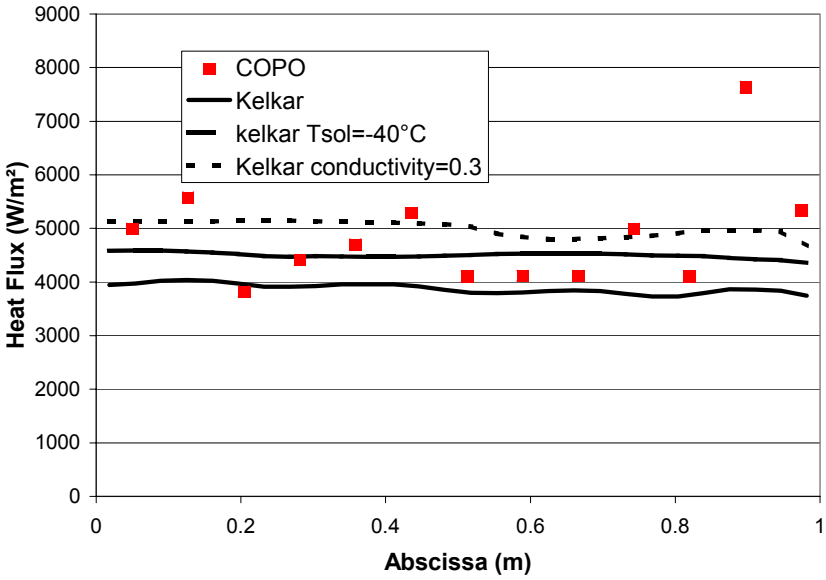

Figure 40:Upper heat flux

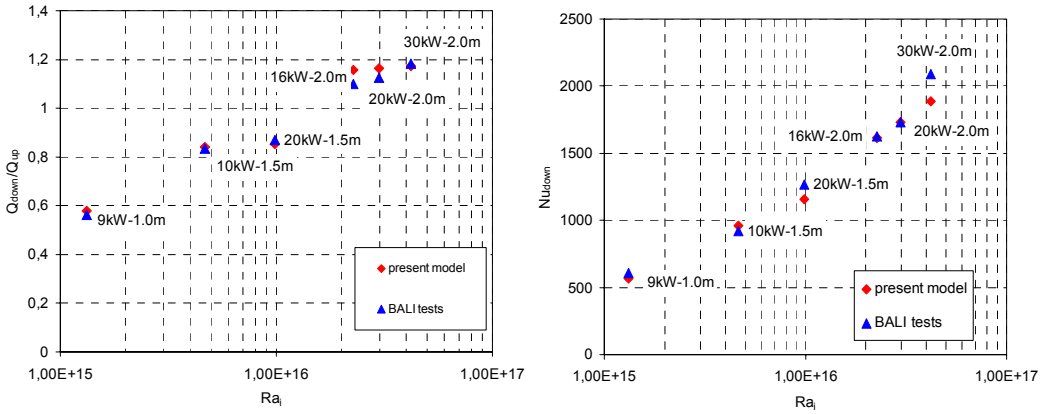

Figure 41: Comparison of MESOCO melt pool model results with BALI experiments for downwards /upwards heat flux split and average downwards Nusselt number. The numbers at the data points give the heating power and the maximum depth of the melt pool.

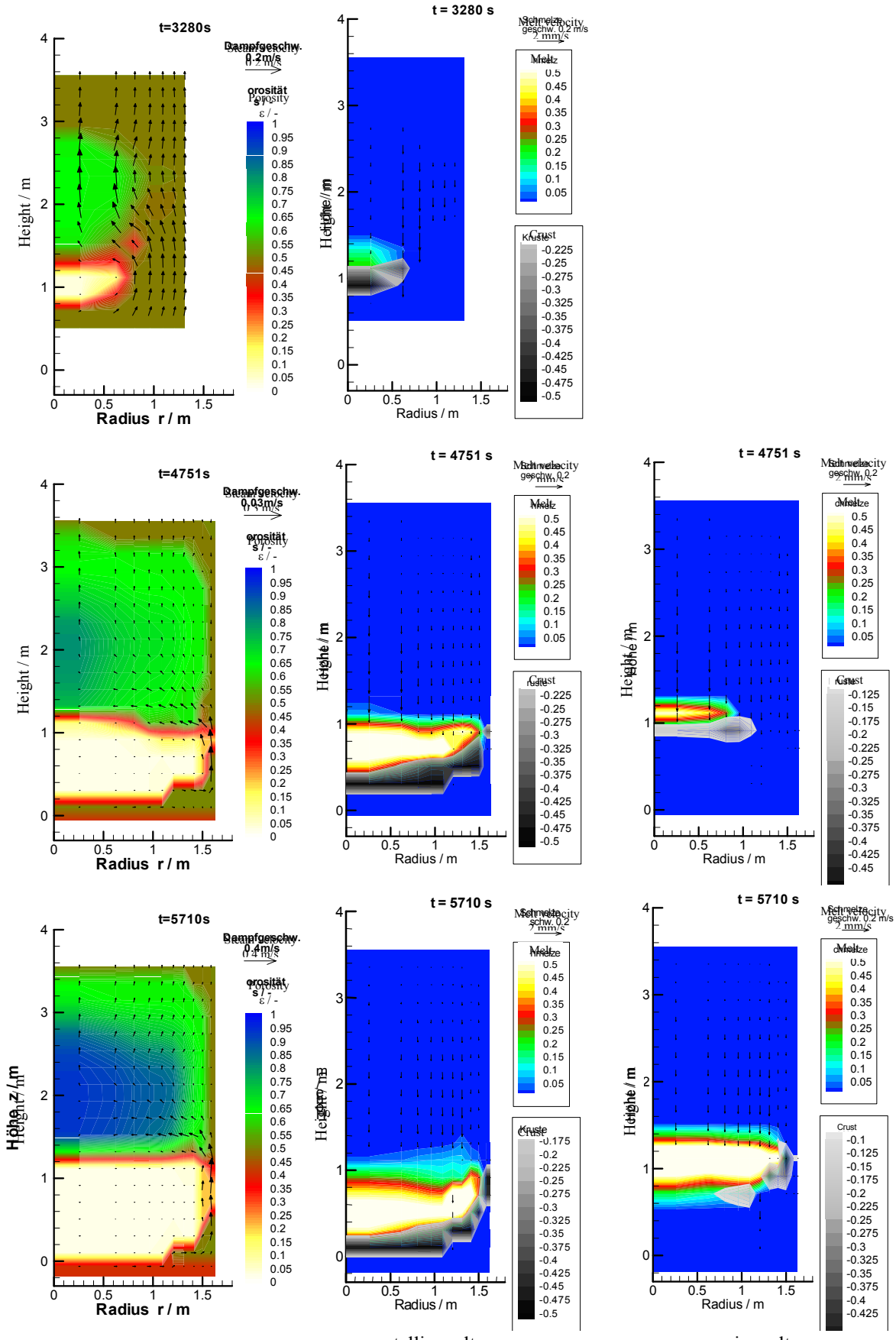

Figure 42: ATHLET-CD calculation on core melting: start of calculation from intact core, water level at the upper edge, no water supply (the colours indicate the porosity in the left column, volume parts of metallic U-O-Zr phases in the middle column, ceramic UO_2-ZrO_2 phases in the right column, crust volume parts are given by negative numbers for technical reasons).

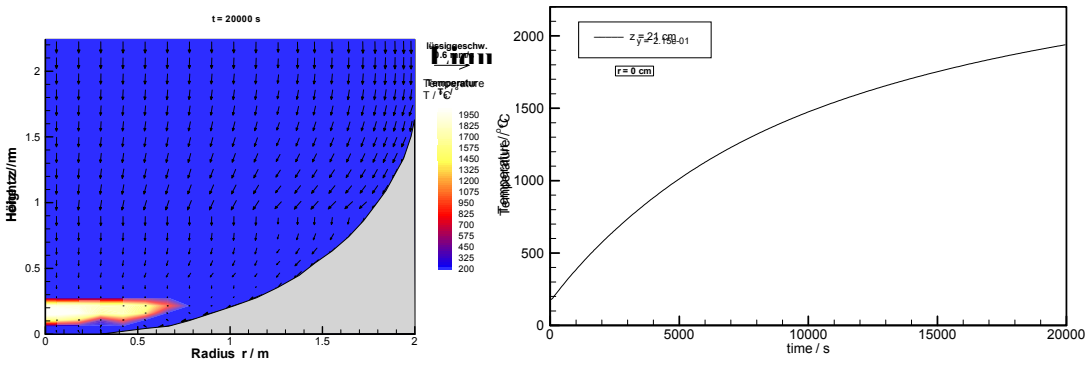

System pressure: 10 bar
porosity 0.4
particle dia. 3 mm
Power: 1 MW/m^3

Cake: height 0.4 m
porosity 0.1
particle dia. 1.5 mm

Figure 43: Coolability of a densified region (cake) with overlying particulate debris via water inflow through a lateral gap.

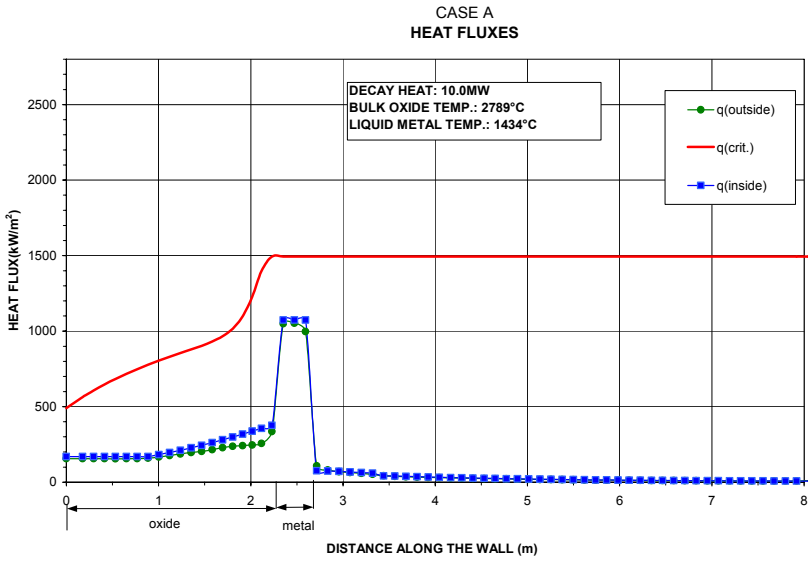

Figure 44: Heat fluxes, case A

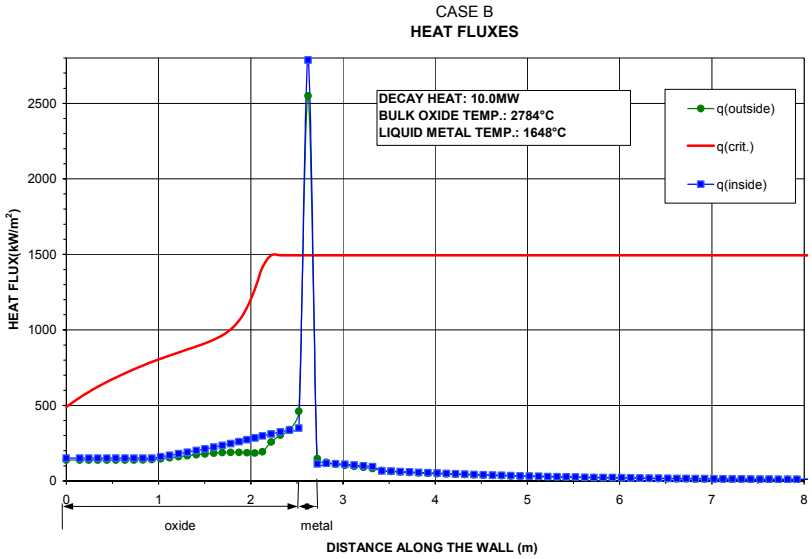

Figure 45: Heat fluxes, case B

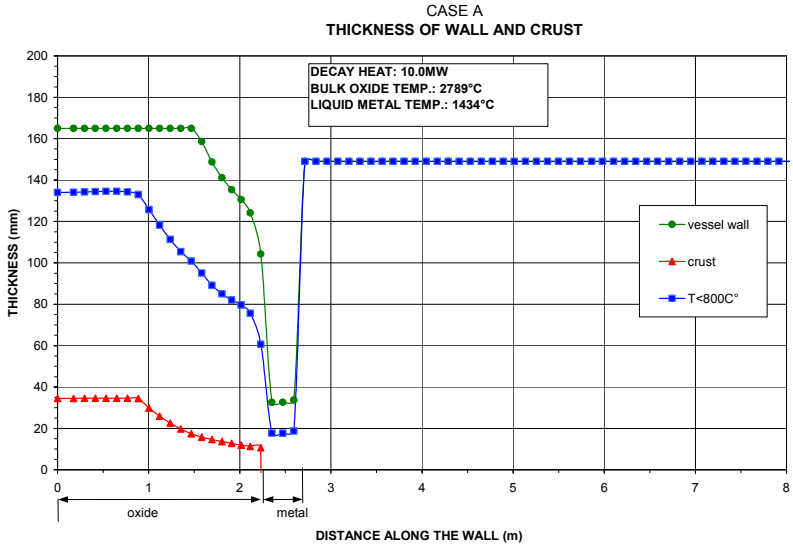

Figure 46: Thickness of wall and crust, case A

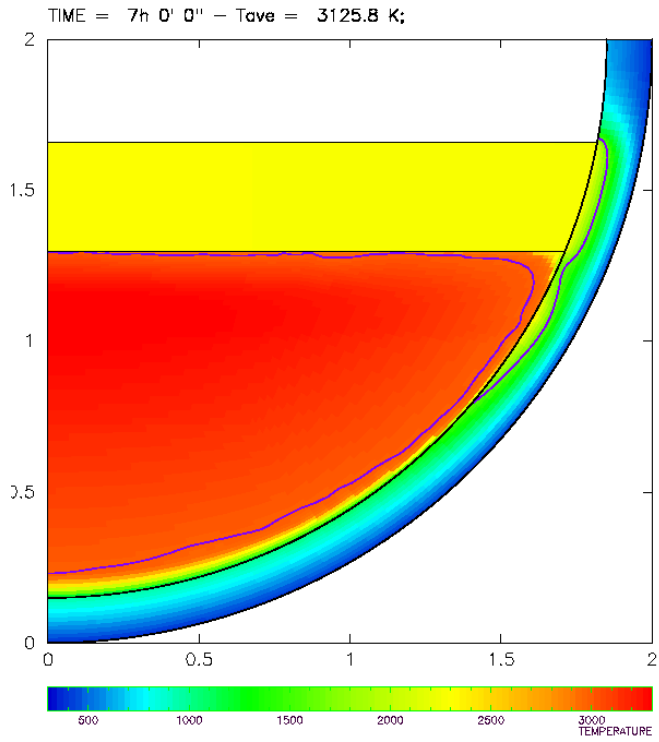

Figure 47: Temperature distribution in bottom head calculated by MVITA, hemispherical head.

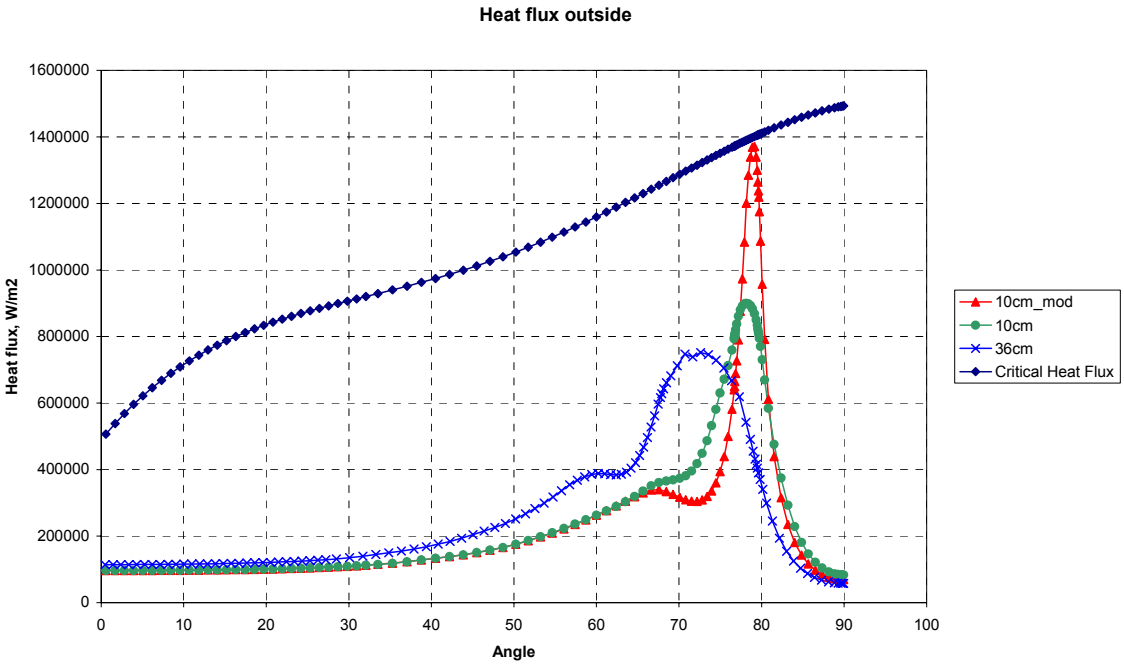

Figure 48: Heat flux on the vessel outer surface calculated by MVITA, hemispherical head.

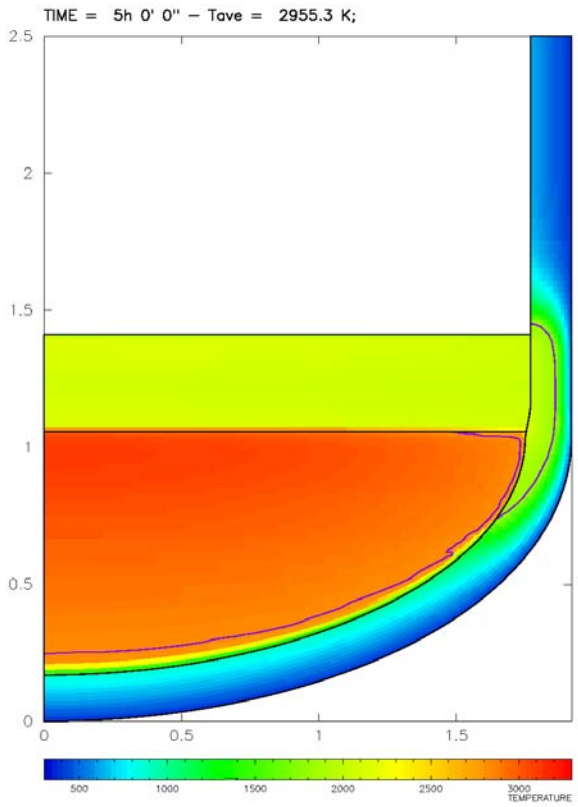

Figure 49: Temperature distribution in bottom head calculated by MVITA, torispherical head.

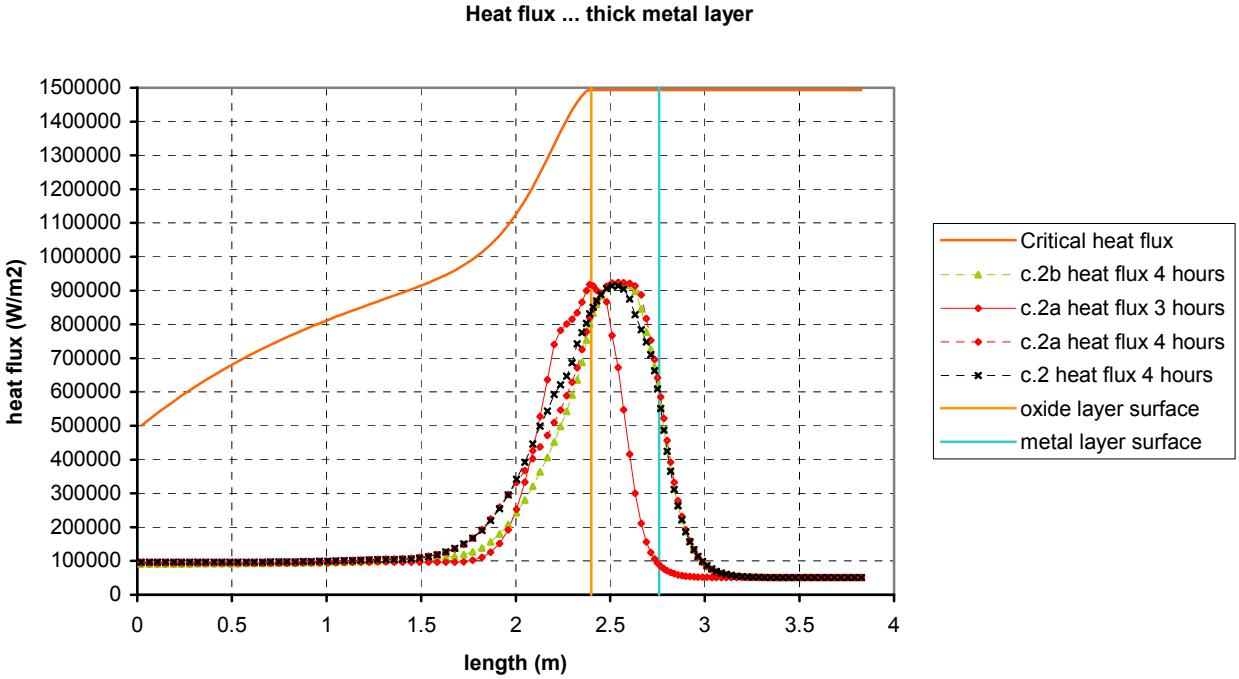

Figure 50: Heat flux on the vessel outer surface calculated by MVITA, torispherical head, thick metal layer

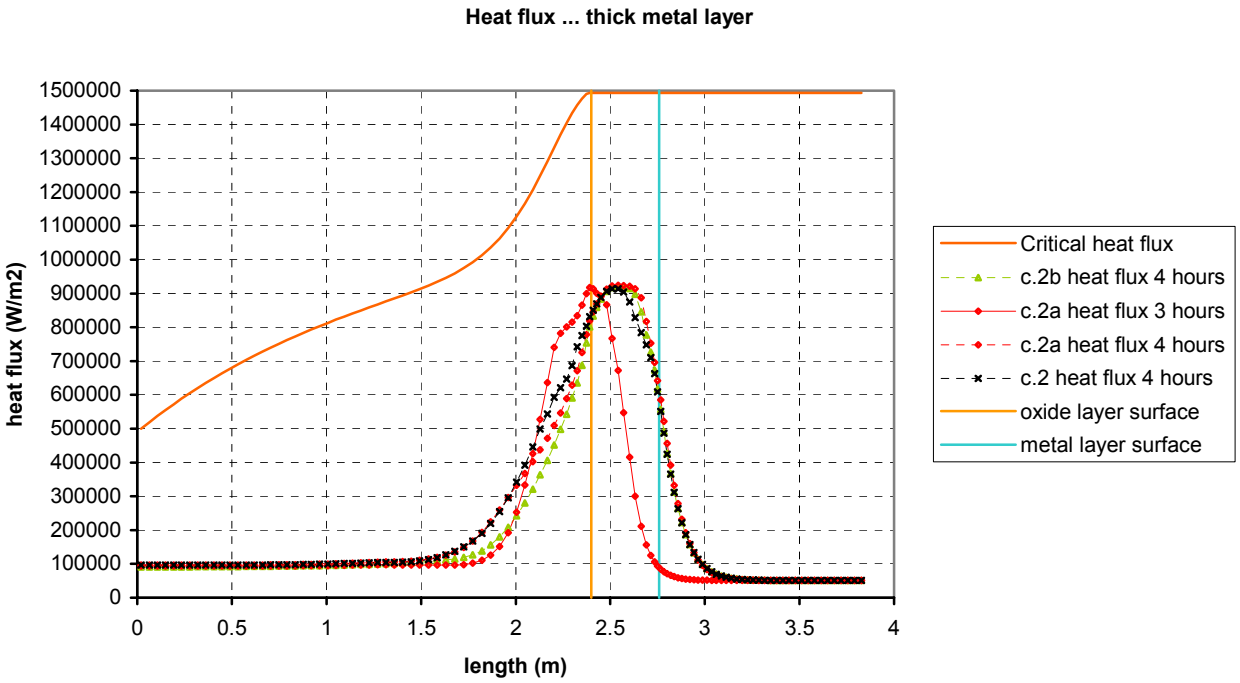

Figure 51: Heat flux on the vessel outer surface calculated by MVITA, torisphercial head, thin metal layer 0.1 m .